Thesis presented to the Instituto Tecnológico de Aeronáutica, in partial fulfillment of the requirements for the degree of Doctor of Science in the Graduate Program of Physics, Field of Nuclear Physics.

Isabella Aparecida Marzola

CONFINEMENT AND DARK MATTER EFFECTS IN AN EQUIPARTICLE QUARK MODEL.

Thesis approved in its final version by signatories below:

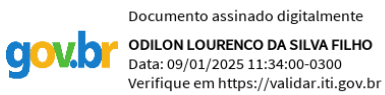

Prof. Dr. Odilon Lourenço da Silva Filho

Advisor

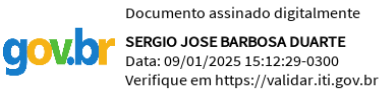

Prof. Dr. Sérgio José Barbosa Duarte

Co-advisor

Campo Montenegro
São José dos Campos, SP - Brazil
2024

Cataloging-in Publication Data
Documentation and Information Division

Marzola, Isabella Aparecida
Confinement and dark matter effects in an equiparticle quark model. / Isabella Aparecida Marzola.
São José dos Campos, 2024.
79f.

Thesis of Doctor of Science – Course of Physics. Area of Nuclear Physics – Instituto Tecnológico de Aeronáutica, 2024. Advisor: Prof. Dr. Odilon Lourenço da Silva Filho. Co-advisor: Prof. Dr. Sérgio José Barbosa Duarte.

I. Instituto Tecnológico de Aeronáutica. II. Title.

BIBLIOGRAPHIC REFERENCE

MARZOLA, Isabella Aparecida. **Confinement and dark matter effects in an equiparticle quark model.**. 2024. 79f. Thesis of Doctor of Science – Instituto Tecnológico de Aeronáutica, São José dos Campos.

CESSION OF RIGHTS

CONFINEMENT AND DARK MATTER EFFECTS IN AN EQUIPARTICLE QUARK MODEL.

Isabella Aparecida Marzola

Thesis Committee Composition:

Prof. Dr.	Pedro José Pompeia	President	-	ITA
Prof. Dr.	Odilon Lourenço da Silva Filho	Advisor	-	ITA
Prof. Dr.	Sérgio José Barbosa Duarte	Co-advisor	-	CBPF
Prof. Dr.	Franciole da Cunha Marinho		-	ITA
Prof. Dr.	Débora Peres Menezes	External member	-	UFSC
Prof. Dr.	Dyana Cristine Duarte	External member	-	UFSM

ITA

To the child who always wondered about the mysteries of the sky and who, as she grew up, never stopped wondering.

Acknowledgments

There are not enough words to thank all the people involved in this process. Having the privilege of being my parents' daughter was certainly a determining factor in me having enough courage and strength to continue moving forward, due to their support throughout my life and academic career. In addition to them, the beginning of this journey was quite challenging because of the pandemic we faced and for almost 2 years of my doctorate I was living by myself and I had to be my own support, so it's worth to do a personal recognition here. I also need to address thanks to all my friends who have been by my side throughout this time, both my old friends and the ones that I was able to meet along the way here in the institution and in the city, and in particular, I would like to thank Elisa who accepted me with open arms into her house for us to live in together, which contributed for a very beautiful friendship between us. Finally, I would very much like to thank my supervisors: my teacher and advisor Odilon for always being very calm, mature and understanding to face the challenges that appeared along the way, my co-supervisor Sérgio for always being very kind to me and also to the teachers with whom I had the pleasure of learning a lot here at ITA and CBPF.

Portuguese version:

Não existem palavras suficientes para agradecer todas as pessoas envolvidas nesse processo do doutorado. Ter o privilégio de ser filha dos meus pais com certeza foi um fator determinante para eu ter coragem e força o suficiente para continuar seguindo em frente, isso devido ao apoio deles ao longo de toda minha vida e carreira acadêmica. Para além deles, o início dessa jornada foi bastante desafiador por causa da pandemia que enfrentamos e durante quase 2 anos de doutorado eu estive morando sozinha e tendo que ser meu próprio suporte, então vale aqui um reconhecimento pessoal de mim para eu mesma. E não há como não agradecer aos amigos que estiveram ao meu lado durante todo esse tempo, tanto os amigos antigos quanto os que o doutorado e que a cidade de São José dos Campos puderam me proporcionar, e em especial, queria agradecer a Elisa que me aceitou de braços abertos na casa dela para morarmos juntas e que permitiu que isso se tornasse uma amizade muito bonita entre nós. Por último, gostaria muito de agradecer aos meus orientadores: ao meu professor e orientador Odilon por sempre ter tido muita calma, maturidade e compreensão para enfrentar os desafios que foram aparecendo ao

longo do caminho, ao meu co-orientador Sérgio por ter sido sempre muito amável comigo e também aos professores com quem tive o prazer de aprender muito aqui no ITA e no CBPF.

"A new scientific truth does not triumph by convincing its opponents and making them see the light, but rather because its opponents eventually die, and a new generation grows up that is familiar with it."
— Max Planck

Abstract

In order to study quark matter under extreme conditions, such as high density and zero temperature, that are usually associated with compact objects (e.g strange stars), we explore two different scenarios throughout this work. In the first scenario, we introduce the traced Polyakov loop into a thermodynamic consistent model with density-dependent quark masses ($m'_{u,d,s}$). This implementation is responsible for the effects of quark confinement/deconfinement phase transition. By applying realistic values for the current quark masses, provided by the Particle Data Group, and by replacing the constants of the interacting part of $m'_{u,d,s}$ by functions of Φ, the symmetric and stellar quark matter systems become capable of achieving a first-order phase transition structure, with Φ being the order parameter. This improved model shows that the system goes towards a similar chiral symmetry restoration behavior due to the emergence of a deconfined phase. Following, we perform an analysis concerning the mass-radius profiles of quark stars, where we can verify that the results found for the new model satisfy recent astrophysical observational data coming from the LIGO and Virgo Collaboration, and the NICER mission concerning the millisecond pulsars PSR J0030+0451, and PSR J0740+6620. The second scenario concerns the study of strange stars admixed with dark matter. Here we restrict ourselves into describing the "visible" matter through the previously mentioned quark model, but without the Polyakov loop. The dark sector is introduced into the system by two approaches: the fermionic and the bosonic one, where we investigate the predictions of both models. For the fermionic model, a spin 1/2 dark particle is considered, and for the bosonic model, the particle is a dark scalar meson. In both models, there is the presence of a repulsive vector interaction, which is responsible for avoiding the collapse of the star due to the lack of degeneracy pressure in the bosonic model. Our findings for the two new systems suggest that stable strange star configurations are consistent with data from PSR J0030+0451, PSR J0740+6620, NICER, and HESS J1731-347. Additionally, we identify stars with dark matter halo configurations for lower dark particle masses.

Contents

1 Introduction

Since the dawn of mankind, humans have always been curious about the environment that surrounds them, especially about the nature of matter since the atom's idea emergence (the smallest, solid, and indivisible portion of matter). Even nowadays with the consensus of the hadrons atomic structure being composed of quarks and gluons, we continue to look for explanations about the microscopic world. Today, the Standard Model of Particles (SM) (Tanabashi *et al.* 2018), which is based on the formalism of Quantum Field Theory (QFT), is the one responsible for describing the most basic building blocks of all known matter. One of the areas covered by the model concerns strongly interacting particles and is called "Quantum Chromodynamics" (QCD) (Weinberg 1973; Fritzsch *et al.* 1973; Huang 1992).

1.1 The Quantum Chromodynamics (QCD)

Around the 60's and 70's, the American physicists Gell-man and Zweig made a proposal that hadrons would be constituted by even more elementary particles, the quarks (Griffiths 2008), in which these particles could arise in different types called "flavors" carrying one of the three "color charge", namely, red, green or blue (in analogy to the primary colors of light, although there is no connection with color in the usual sense). These color charges are the basis of quantum chromodynamics and play the same role as electric charges in quantum electrodynamics (QED).

In QED, the quantum field theory of the electromagnetic force studies the electromagnetic interactions of charged particles by assuming that the photons, best known as the "particles" of light, are the mediators of these interactions. Here, there is only one type of electric charge, which can be positive or negative (anti-charge). By analogy, in QCD, the mediators of the strong interaction between quarks are the gluons. In Fig. 1.1, the color charge of the quarks is displayed. Particles that are color neutral, such as baryons, are built by three quarks each of a different color, and a mixture of the three colors produces a neutral particle. Mesons, on the other hand, are composed only of two quarks (in pairs of quarks and anti-quarks, their antimatter counterparts), and they are also color-neutral,

but through the neutralization of the anti-color of the anti-quark with the color of the quark.

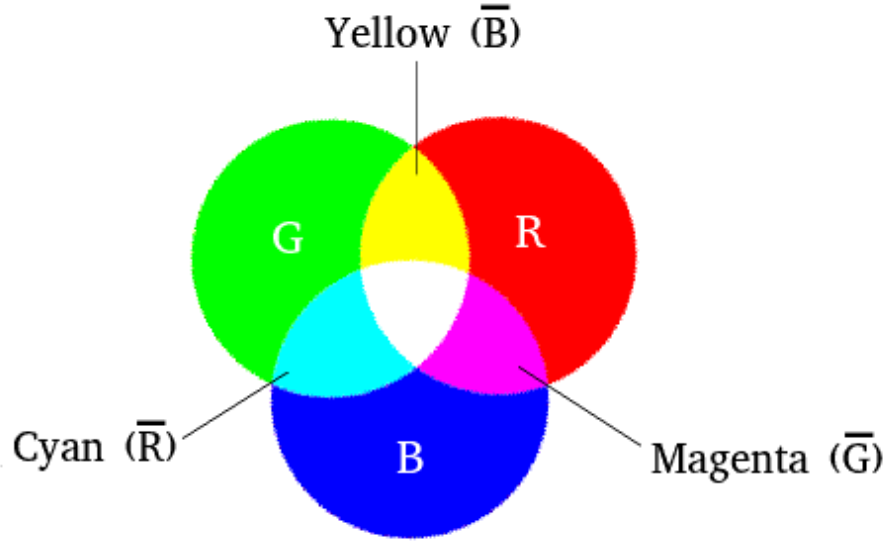

FIGURE 1.1 – Diagram of quark composition of baryons. The RGB colors, i.e., red (R), green (G), and blue (B) are associated with quarks, while cyan, magenta, and yellow are associated with anti-quarks. The white region is associated with a baryon.

The gluons can also carry color charges, and for all interactions between the three colors of quarks to exist there must be eight gluons. In QED, the photon carriers are electrically neutral and the force is described as the inverse square of the distance between the charges, which means that it becomes weaker when the distance increases. For QCD, that is not the case, because the nature of the strong force is observed at short ranges, being limited by a distance about 10^{-15} m (shorter than the diameter of an atomic nucleus), where apparently quarks cannot be separated, since they have been observed only inside hadrons (baryons and mesons). If one tries to knock a quark out of a proton, for example, the sufficient energy invested will only create a quark-antiquark pair, i.e. a meson. This happens because gluons can interact among themselves through their color charges, preventing the charges involved from being pulled apart. However, if the distance between quarks is very short, the asymptotic freedom can be achieved (ultraviolet region, at high energy). This means that when quarks get very close together, the force that contains them inside the hadrons becomes weaker, which would allow them to move freely. This is the definition of asymptotic freedom.

In QCD, matter composed of quarks and gluons is studied at extreme conditions, such as temperature and density, where it is known that there are, at least, two different states of matter: the hadronic phase where quarks and gluons are confined inside hadrons, and the quark-gluon plasma (QGP) where they are free. Inside compact stars, such as

neutron stars (or quark or hybrid stars), it is believed that QGP can be found, as well it may have existed in the early universe moments after the Big Bang, with temperature and density being extremely high. In terrestrial experiments, such as the Relativistic Heavy Ion Collider (RHIC) and the Large Hadron Collider (LHC) (Harris e Müller 1996; Emerick *et al.* 2012; Gunion e Vogt 1997; Singh 1993; Braun-Munzinger e Stachel 2007), propitious conditions are created to investigate the QGP. In Fig. 1.2 we can identify the different regions studied by QCD: hadrons concern the region at ordinary temperature and density; and by increasing the temperature to the critical point or the density until quarks are very close to each other that hadrons will dissolve themselves into quarks, we have the regions concerning quark matter. Here, different phase transitions happen, according to temperature and density conditions. There is, in fact, a wide discussion about the location of the critical point, known as the connection between a first-order phase transition of quark matter (as the one that occurs with water) and the crossover, the phase transition where there is no discontinuities. Besides, there is the region where matter can exhibit superconductivity (Alford *et al.* 2008), the one where it may present the quarkyonic phase (Mclerran 2009), and the region where neutron stars are found: at zero temperature and high densities.

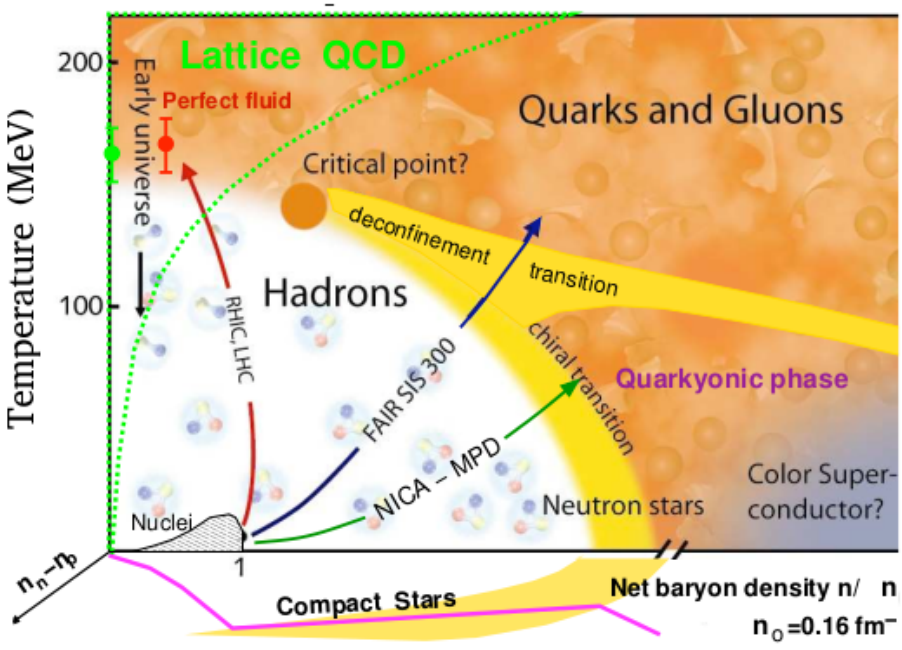

FIGURE 1.2 – Schematic phase diagram of QCD (Menezes 2016).

As we can see, it is not simple to study QCD and its particularities. In fact, infinite nuclear matter, finite nuclei, or even stellar matter should be described directly by this theory. However, due to the non-perturbative nature of the QCD infrared region, this

is not a trivial task to be implemented. Because of that, different approaches are used, such as the lattice calculations (Kogut 1979; Kogut 1983). The Lattice Quantum Chromodynamics (LQCD) is based on numerical simulations done usually by Monte Carlo methods to investigate the lower region of the QCD phase diagram, at the high temperature and low chemical potential (or density) regime. Although being a powerful tool, LQCD has some problems, such as the need to extrapolate their results to grid spacing tending to zero, the "signal problem" (Muroya *et al.* 2003), where standard Monte Carlo methods may become inefficient or even infeasible due to difficulties in sampling configurations because of certain systems where the action becomes complex. Another problem faced by this method involves the algorithm, in which auto-correlation and convergence challenges appear due to the sample gauge configurations (Duane *et al.* 1987); and there is also the need of increasingly advanced machines to perform the calculations, which are very costly from a computational point of view. Another method to study the infrared region is the application of the Dyson-Schwinger equations, which are an infinite set of coupled integral equations for Green's functions built in Euclidean space (Roberts e Williams 1994; Alkofer e Smekal 2001). Solving them requires truncating this infinite series in a way that captures the essential physics while remaining computationally feasible.

Therefore, it is clear that these methods are not capable of describing QCD completely, which leads us to look for other methods, such as the effective/ phenomenological quark/gluons models, developed in order to present as many similarities with QCD as possible. In that direction, many models were constructed and improved over the years as, for instance, the Massachusetts Institute of Technology (MIT) bag model (Chodos *et al.* 1974; Chodos *et al.* 1974), in which the building block particles are submitted to a confining potential mathematically represented by a "bag" constant. Or, as another example, the Nambu-Jona-Lasino (NJL) model (Nambu e Jona-Lasinio 1961; Nambu e Jona-Lasinio 1961), where the dynamical breaking of chiral symmetry is taken into account. In addition to these, some effective models consider the quark masses as dependent on density and/or temperature (PlÜmer *et al.* 1984; Fowler *et al.* 1981). However, it was verified a very relevant issue in these kinds of models: the lack of thermodynamic consistency. Basically, this violation emerges because the pressure at a density corresponding to the minimum of the energy per baryon is not vanishing as it should be. In order to fix this problem, the equiparticle (EQP) model was proposed in 2014 (Xia *et al.* 2014), in which the authors establish a suitable expression for the density-dependent equivalent quark masses, along with the direct connection between the quark Fermi momentum, at $T = 0$ regime, with an effective chemical potential instead of the real one. The concept introduced for the effective chemical potential is also useful at finite temperature regimes because it allows us to explore regimes where we can not use direct simulation due to the already explained sign problem, and it also provides a means

to validate theoretical models against numerical simulations and experimental data.

With the solution for the thermodynamic inconsistency, the EQP model was applied to describe strange stars. These stars would be composed of strange matter, with the concept being proposed by Bodmer (Bodmer 1971), where the strange matter would be the true ground state of matter instead of hadrons, claiming that quark matter could have lower energy per baryon than a normal nucleus (^{56}Fe). The strange stars' existence itself was proposed by Witten (Witten 1984), who considered stable strange matter as composed of quarks up, down, and strange. Combined, the authors' idea was called the Bodmer-Witten conjecture/hypothesis, and a final experimental/observational probe is not available yet.

In order to test many effective hadronic (LourenÇo *et al.* 2019; LourenÇo *et al.* 2020; Souza *et al.* 2020) and quark models, such as the EQP model, new astrophysical data that have arisen over the last years are been used. Among them, there is the recent detection, made by the LIGO and Virgo Collaboration (Abbott *et al.* 2017; Abbott *et al.* 2018; Abbott *et al.* 2020), of gravitational waves coming from a binary system with its respective electromagnetic counterparts also detected by many observatories (Abbott *et al.* 2017), the measurements from the x-ray telescope installed on the International Space Station, named as the NASA's Neutron star Interior Composition Explorer (NICER), regarding the massive millisecond pulsars PSR J0030+0451 (Riley *et al.* 2019; Miller *et al.* 2019) and PSR J0740+6620 (Riley *et al.* 2021; Miller *et al.* 2021), and also the measurement of HESS J1731-347 (DOROSHENKO *et al.* 2022), which is the first simultaneous measurement of mass, radius, and surface temperature of a compact star.

The compact stars present in our universe have been an interest to scientists because of their complex structure and dynamics which many areas of physics can be applied, such as quantum field theory, general relativity, thermodynamics, etc. Since these objects are extremely dense, the usual matter conditions are pushed to their extremes, which makes them environments full of possibilities where other enigmatic ingredients can be added to the system. Along with strange quark matter, dark matter (DM) (Bertone e Hooper 2018; Arbey e Mahmoudi 2021; Salucci 2019) is a possible candidate to maybe coexist inside compact objects. The existence of DM is supported by different evidence across various fields of astrophysics and cosmology. Among them, there is the analysis of galactic rotation curves, where the rotational velocities of stars and gas in galaxies remain constant at large distances from the galactic center, rather than decreasing as expected from visible matter alone (Rubin Vera C. 1970). There is also the use of gravitational lensing methods (Koopmans e Treu 2003; Massey *et al.* 2010) that are responsible, for example, for mapping the distribution of mass in galaxy clusters and large-scale structures (Clowe *et al.* 2006). These methods have found

that around 80% to 90% of the galaxy cluster masses are composed of DM, and only the remaining 10% to 20% are due to ordinary matter. The studies of cosmic microwave background (CMB) provide a snapshot of the early universe with measurements of its temperature fluctuations (anisotropies) that also suggest the presence of DM (Adams *et al.* 1998; Pierpaoli 2004; Padmanabhan e Finkbeiner 2005; Aghanim *et al.* 2016; Hu e Dodelson 2002; Hu *et al.* 1997). Therefore, according to theoretical models, observations, and data from various cosmic surveys, it is a consensus that our current universe is composed of 68% of dark energy, 27% of dark matter, and only 5% of ordinary matter. In compact stars, theories are saying that the star's gravitational pull can capture DM particles, which allows dark matter to accumulate inside the star (due to the high density and gravitational fields (Kouvaris e Tinyakov 2010)). The DM particles could also annihilate their antiparticles producing high-energy particles, since they are the same. This process could potentially change the luminosity and surface temperature of the star by providing additional heat (Bertone *et al.* 2005).

In this work, we study strong interaction systems at high-density regions and zero temperature regimes through two different approaches. The first one consists of implementing the confinement/deconfinement phase transition phenomenology (PTP) into the EQP model. For this part of the thesis, we divide the chapters as follows: in the next chapter we introduce the original EQP model, where the thermodynamic consistency criterion is established, and the equations of state and quark masses are developed through its formalism. Also, the symmetric and stellar matter systems that will be further investigated are presented, and the criterion for the strange matter to be stable is discussed in more detail with the model stability windows being presented by using recent values of the current quark masses provided by the Particle Data Group (PDG) (Workman e Others 2022).

In sequence, in chapter 3, we introduce the improved EQP model, called Polyakov equiparticle model (PEQP), where we follow the procedure performed in (Mattos *et al.* 2019; Mattos *et al.* 2021; Mattos *et al.* 2021) and describe the PTP through the inclusion of the traced Polyakov loop (Φ) by making the free parameters of the model suitable functions of Φ. We show that the new improved model exhibits a first-order phase transition structure, and we discuss the results when we consider the symmetric matter case. This structure is also observed for the stellar matter case, in which we present and discuss its particularities as well as the results found when applying the new model for describing strange stars, where they are confronted by the aforementioned astrophysical observational data.

For the second part of the thesis, in chapter 4, we focus on exploring the possibility of strange stars' existence admixed with two different types of dark matter, namely, fermionic and bosonic. The procedure done here follows the two-fluid approach, which considers only gravitational interactions between DM and quark matter. Therefore, in this chapter

we will develop the formalism concerning each type of DM mentioned, with its equations of state being presented, as well as the dark mass equations, and in the sequence, the results and analysis are investigated and discussed. Finally, we present our final remarks about the work and some future perspectives.

2 Equiparticle model

For a long time, the fundamental state of matter was considered to be composed only of quarks up and down, which is the case for the matter found here on Earth. However, in the seventies, a new proposition stated that the absolutely stable fundamental state of matter would be strange quark matter (SQM), which is the matter composed of quarks up, down, and strange. That is called the Bodmer-Witten Hypothesis (Bodmer 1971; Witten 1984) and, since then, it has been responsible for the development of different kinds of phenomenological effective models concerning SQM. One of these models was chosen for our study, the equiparticle model (EQP). This model was proposed in 2014 (Xia *et al.* 2014) as a model that is density and/or temperature-dependent to investigate strange quark matter assuming that the quark masses are density-dependent, as well as to correct the lack of thermodynamic consistency found in other models of the same type (Fowler *et al.* 1981; Zhang e Su 2002). This chapter presents the EQP model in its original form with all its features: thermodynamic consistency, equations of state (EOS), quark masses scaling, and the stability window for symmetric and stellar matter.

2.1 Thermodynamic consistency

Let's begin by assuming a thermodynamic system of interacting particles given by quarks up (u), down (d), and strange (s), and the leptons represented by electrons (e). The thermodynamic consistency formalism of this system begins by deriving the fundamental equation of standard thermodynamics, which leads to

$$d\overline{E} = Td\overline{S} - PdV + \sum_i \mu_i d\overline{N_i}, \tag{2.1}$$

where $\overline{E}$ = internal energy, T = temperature, $\overline{S}$ = entropy, P = pressure, V = volume, μ_i = chemical potential of particle i, and $\overline{N_i}$ = i particle number. This equation represents the three different ways in which it is possible to increase the system's internal energy, i.e., heat transfer, doing work, and particle exchange. Once you add heat to a system, the heat energy contributes to the random motion and vibration of the particles within the

system, raising its overall internal energy. The same will happen when work is done: if you change the volume of the system or if you apply force the energy will be transferred into the system. In the case of particle exchange, it is possible to increase the system's internal energy through endothermic reactions, where the energy from the surroundings is absorbed into the system. Following, we apply Eq. (2.1) with the one for the Helmholtz free energy ($\overline{F} = \overline{E} - T\overline{S}$), and obtain

$$d\overline{F} = -\overline{S}dT - PdV + \sum_i \mu_i d\overline{N_i}. \tag{2.2}$$

Because we are dealing with an isotropic system with homogeneously distributed particles, we define the following quantities: the energy density as $\epsilon = \overline{E}/V$, the free energy density as $F = \overline{F}/V$, the entropy density as $S = \overline{S}/V$, and the particle number density as $\rho_i = \overline{N_i}/V$. From the free energy density and the particle number density we have that

$$\overline{F} = FV \rightarrow d\overline{F} = dFV + FdV, \tag{2.3}$$

$$\overline{N_i} = \rho_i V \rightarrow d\overline{N_i} = d\rho_i V + \rho_i dV, \tag{2.4}$$

which is substituted into Eq. (2.2), resulting in

$$dFV + FdV = -\overline{S}dT - PdV + \sum_i \mu_i (d\rho_i V + \rho_i dV)$$

$$dF = -SdT + \left(-P - F + \sum_i \mu_i \rho_i\right)\frac{dV}{V} + \sum_i \mu_i d\rho_i. \tag{2.5}$$

Since the system is considered to be infinitely large, it becomes size-independent, assuming an asymptotic behavior. Therefore, the correspondent term of volume can be disregarded, leaving us with

$$dF = -SdT + \sum_i \mu_i d\rho_i. \tag{2.6}$$

If we choose the energy density F as the characteristic quantity, the Eq. (2.5) indicates that T, $\{\rho_i\}$, and V will be the independent state variables of the system, and once known, they allow us to obtain all the other thermodynamic quantities:

$$S = \left.\frac{dF}{dT}\right|_{\{\rho_k\}}, \qquad \mu_i = \left.\frac{dF}{d\rho_i}\right|_{T,\ \{\rho_{k\neq i}\}}, \qquad \text{and} \qquad P = -F + \sum_i \mu_i \rho_i. \tag{2.7}$$

From the entropy density (S) and the chemical potential (μ_i) equations, we can cal-

culate

$$\frac{dS}{d\rho_i} = \frac{d}{d\rho_i}\left(\frac{dF}{dT}\right)\bigg|_{\{\rho_k\}} \qquad \text{and} \qquad \frac{d\mu_i}{dT} = \frac{d}{dT}\left(\frac{dF}{d\rho_i}\right)\bigg|_{T,\ \{\rho_{k\neq i}\}}, \tag{2.8}$$

and because the second-order mixed partial derivatives of an arbitrary analytic function are equal to each other, that is, $\partial^2 F/\partial\rho_i\partial T = \partial^2 F/\partial T\partial\rho_i$, we can obtain the Cauchy conditions for the right-hand side of Eq. (2.6) to be integrable, which are given by

$$\Delta_i \equiv \frac{dS}{d\rho_i}\bigg|_{T,\ \{\rho_{k\neq i}\}} - \frac{d\mu_i}{dT}\bigg|_{T,\ \{\rho_k\}} = 0, \tag{2.9}$$

$$\Delta_{ij} \equiv \frac{d\mu_i}{d\rho_j}\bigg|_{T,\ \{\rho_{k\neq j}\}} - \frac{d\mu_j}{d\rho_i}\bigg|_{T,\ \{\rho_{k\neq i}\}} = 0, \qquad \text{(i, j = u, d, s)}. \tag{2.10}$$

As we can see, Eq. (2.6) is a temperature and density-dependent function. Defining $\rho_b = \rho \equiv \sum_q \rho_q/3$ (q = u, d, s) and $\nu = \mu_u + \mu_d + \mu_s$, for a given temperature T, we have that $dF/d\rho = \sum_i \mu_i d\rho_i/d\rho$. By applying the conditions of chemical equilibrium ($\mu_u + \mu_e = \mu_d = \mu_s$), charge neutrality ($2\rho_u/3 - \rho_d/3 - \rho_s/3 - \rho_e = 0$), and baryon number conservation ($\rho_u/3 + \rho_d/3 + \rho_s/3 = \rho_b$), we obtain

$$\begin{aligned}
\rho\frac{dF}{d\rho} &= \rho\left[\sum_q \mu_q\frac{d\rho_q}{d\rho} + \mu_e\frac{d\rho_e}{d\rho}\right] = \rho\left[\nu\sum_q\frac{d\rho_q}{d\rho} - \mu_e\frac{d\rho_u}{d\rho} + \mu_e\frac{d\rho_e}{d\rho}\right] = \\
&= \rho\left[\nu\frac{d}{d\rho}\left(\sum_q \rho_q\right) - \mu_e\frac{d}{d\rho}(\rho_u - \rho_e)\right] = \rho(3\nu - \mu_e) = \\
&= \nu\sum_q \rho_q - \mu_e\rho = \sum_q \mu_q\rho_q + \mu_e\rho_u - \mu_e\rho = \\
&= \sum_i \mu_i\rho_i - \mu_e\rho_e + \mu_e\rho_u - \mu_e\rho = \sum_i \mu_i\rho_i + \mu_e(\rho_u - \rho_e - \rho) = \\
&= \sum_i \mu_i\rho_i, \qquad (i = u, d, s, e).
\end{aligned} \tag{2.11}$$

Applying this result in the pressure expression in Eq. (2.7), we obtain $P = -F + \rho dF/d\rho$. By considering that

$$\rho^2\frac{d}{d\rho}\left(\frac{F}{\rho}\right)_T = \rho^2\left[\frac{1}{\rho}\frac{dF}{d\rho} - \frac{F}{\rho^2}\right] = \rho\frac{dF}{d\rho} - F, \tag{2.12}$$

we finally have that

$$P = \rho^2 \frac{d}{d\rho}\left(\frac{F}{\rho}\right)_T \quad \Rightarrow \quad \Delta = P - \rho^2 \frac{d}{d\rho}\left(\frac{F}{\rho}\right)_T = 0. \tag{2.13}$$

This equation tells us that the pressure must be zero at the free-energy minimum (or at the energy minimum at zero temperature), which is coherent with the thermodynamics since the free-energy minimum is a mechanically stable state of a system. Although Eq. (2.13) was found considering stellar matter (by the inclusion of the electrons), it is possible to obtain the same result when considering symmetric matter (where there is only quarks u, d, s) by applying the chemical equilibrium condition ($\mu_u = \mu_d = \mu_s = \mu$) into $dF/d\rho = \sum_i \mu_i d\rho_i/d\rho$, resulting in

$$\rho \frac{dF}{d\rho} = \rho\mu \frac{d}{d\rho}\left(\sum_q \rho_q\right) = 3\rho\mu = \sum_i \mu_i \rho_i, \qquad (i = u, d, s, e). \tag{2.14}$$

Therefore, this formalism allows us to establish that Eqs. (2.9), (2.10) and (2.13) are the necessary criteria for strange matter to be thermodynamically consistent for symmetric and stellar cases.

2.2 Equations of state

From the free energy density equation we can start the formalism to obtain the equations of state (EOS) of the system:

$$F = \Omega_0(T, \{\mu_i^*\}, \{m_i\}) + \sum_i \mu_i^* \rho_i, \tag{2.15}$$

where Ω_0 = effective thermodynamic potential, T = temperature, μ_i^* = effective chemical potential with i (i = u, d, s quarks), m_i = effective particles mass and ρ_i = particle number density. The effective thermodynamic potential is introduced as the quantity that allows the heat and particle exchange in the system this is why it is a function that depends on the temperature, the effective chemical potentials, and the effective particle masses. Concerning the effective chemical potentials μ_i^*, they are chosen as effective to guarantee the thermodynamic consistency of the system. For the effective particle masses, it is considered effective because it will have a dependency on the baryonic density:

$$m_i = m_{i0} + m_I, \tag{2.16}$$

with m_{i0} = the current mass of the i quark and m_I is the density dependent quantity. This equation will be fully derived in the next section since it does not influence the formalism of the EOS. The characteristic function will be the free energy density, with the temperature T, the volume V, and the particle number density ρ_i as its independent state variables. The effective chemical potential will be connected to the independent state variables through the particle number density as follows:

$$\rho_i = -\frac{\partial}{\partial \mu_i^*}\Omega_0(T, \{\mu_i^*\}, \{m_i\}). \tag{2.17}$$

The other thermodynamic quantities of interest can be obtained from the derivative of Eq. (2.15):

$$dF = d\Omega_0 + \sum_i \rho_i d\mu_i^* + \sum_i \mu_i^* d\rho_i, \tag{2.18}$$

where,

$$d\Omega_0 = \frac{\partial \Omega_0}{\partial T}dT + \sum_i \frac{\partial \Omega_0}{\partial \mu_i^*}d\mu_i^* + \sum_i \frac{\partial \Omega_0}{\partial m_i}dm_i, \tag{2.19}$$

with

$$dm_i = \frac{\partial m_i}{\partial T}dT + \sum_j \frac{\partial m_i}{\partial \rho_j}d\rho_j. \tag{2.20}$$

Applying Eqs. (2.17), (2.19) and (2.20) in Eq. (2.18), we have that

$$dF = \left(\frac{\partial \Omega_0}{\partial T} + \sum_i \frac{\partial \Omega_0}{\partial m_i}\frac{\partial m_i}{\partial T}\right)dT + \sum_i \left(\mu_i^* + \sum_j \frac{\partial \Omega_0}{\partial m_j}\frac{\partial m_j}{\partial \rho_i}\right)d\rho_i. \tag{2.21}$$

Comparing Eq. (2.21) with Eq. (2.6), to ensure that the free-energy density of the model will be in agreement with the one derived in the previous section, we result with the entropy density as being

$$S = -\left(\frac{\partial \Omega_0}{\partial T} + \sum_i \frac{\partial \Omega_0}{\partial m_i}\frac{\partial m_i}{\partial T}\right), \tag{2.22}$$

and the real chemical potential results to be connected with the effective one as

$$\mu_i = \mu_i^* + \sum_j \frac{\partial \Omega_0}{\partial m_j}\frac{\partial m_j}{\partial \rho_i}. \tag{2.23}$$

For the equations of state, the pressure is calculated by the substitution of Eqs. (2.15) and (2.23) in Eq. (2.7):

$$P = -\Omega_0 + \sum_i (\mu_i - \mu_i^*)\rho_i = -\Omega_0 + \sum_{i,j} \frac{\partial \Omega_0}{\partial m_j}\rho_i \frac{\partial m_j}{\partial \rho_i}, \tag{2.24}$$

and the energy density through the substitution of Eqs. (2.15) and (2.22) in $\epsilon = F + TS$, so

$$\epsilon = \Omega_0 - \sum_i \mu_i^* \frac{\partial \Omega_0}{\partial \mu_i^*} - T\left(\frac{\partial \Omega_0}{\partial T} + \sum_i \frac{\partial \Omega_0}{\partial m_i}\frac{\partial m_i}{\partial T}\right). \tag{2.25}$$

The real grand-canonical thermodynamic potential density is obtained from

$$\Omega = F - \sum_i \mu_i \rho_i = \Omega_0 - \sum_{i,j} \frac{\partial \Omega_0}{\partial m_j}\rho_i \frac{\partial m_j}{\partial \rho_i},$$

with Ω_0, given by (Peng *et al.* 2000), as being

$$\Omega_0 = -\sum_i \frac{\gamma T}{2\pi^2}\int_0^\infty ln[1 + e^{-\beta(\sqrt{k^2+m_i^2}-\mu_i^*)}]k^2 dk, \tag{2.26}$$

where γ = degeneracy factor (for quarks it is given by spin and color of the quarks involved, in this case is 2_{spin} x 3_{color} = 6), and β = inverse of the temperature, since $k_b = 1$ in natural units. For zero temperature, we obtain that:

$$\Omega_0 = -\sum_i \frac{\gamma}{24\pi^2}\left[\mu_i^* k_{Fi}\left(k_{Fi}^2 - \frac{3}{2}m_i^2\right) + \frac{3}{2}m_i^4 \ln\frac{\mu_i^* + k_{Fi}}{m_i}\right], \tag{2.27}$$

with k_{Fi} = particle i Fermi momentum, which is given by $k_{Fi} = \sqrt{\mu_i^{*2} - m_i^2}$. Moreover, Ω can be obtained from the pressure as $\Omega = -P$.

Although the model is already constructed to be thermodynamically consistent, we can verify its consistency from other two different viewpoints. The first one consists of taking the derivative of $-\Omega_0$ concerning μ_i^* and comparing it to the particle number density given by $\rho_i = \gamma k_{Fi}^3/6\pi^2$, in which the results are equivalent. This relation is consistent with the ones from fundamental thermodynamics, in other words, $\rho_i = -\partial\Omega_0/\partial\mu_i^* = \partial P/\partial\mu_i$. The second verification concerns the energy density, where we simply apply the following relation:

$$P + \epsilon = \mu\rho \quad \Rightarrow \quad \sum_i P_i + \sum_i \epsilon_i = \sum_i \mu_i \rho_i \qquad (i = u, d, s, e). \tag{2.28}$$

2.3 Quark masses

The quark masses can be obtained by considering a density-dependent part on it, written as

$$m_i = m_{i0} + m_I, \tag{2.29}$$

where m_{i0} ($i = u$, d, s) is the current mass of the i quark and m_I is its density dependent part. In order to determine m_I, as done in (Peng 2005), a Laurent series expansion is applied to the Fermi momentum, and the leading term is taken in both directions:

$$m_I = \frac{a_{-1}}{k_F} + a_1 k_F, \quad \text{with} \quad k_F = \left(\frac{1}{N_f} \sum_i k_{Fi}^3 \right)^{1/3}, \tag{2.30}$$

where k_{Fi} = Fermi momentum of the quark i and N_f = quark flavor number. The Fermi momentum is connected to the baryonic density by

$$\rho_b = \sum_i \frac{\rho_i}{3} = \left(\sum_i \frac{1}{3\pi^2} k_{Fi}^3 \right) . \frac{N_f}{N_f} = \frac{N_f}{3\pi^2} k_F^3. \quad \Rightarrow \quad k_F = \left(\frac{3\pi^2}{N_f} \rho_b \right)^{1/3}. \tag{2.31}$$

At the limit where the Fermi momentum (or the density) approaches to zero, at lower density, the first term of Eq. (2.30) dominates. This implies that $m_I = a_{-1}/k_F = D/\rho_b^{1/3}$, where D is known as a lower energy free parameter (Wen *et al.* 2005). At higher density, the second term of Eq. (2.30) dominates, so $m_I = a_1 k_F = C\rho_B^{1/3}$, where C is a second dimensionless adjustable parameter. Therefore, the final equation for the quark masses is given by

$$m_i = m_{i0} + \frac{D}{\rho_b^{1/3}} + C\rho_b^{1/3}. \tag{2.32}$$

2.4 Symmetric and stellar matter

Since we are studying symmetric and stellar matter in this work, we need to describe its properties properly. Beginning with symmetric matter we must address here that we are establishing that only the chemical potentials of the quarks are equal, meaning that their masses and densities are different from each other, which is a different description when discussing hadronic models. Therefore, symmetric matter must obey the following condition: $\mu_u = \mu_d = \mu_s \equiv \mu$. Because the model is carefully treated to be thermodynamic consistent, it introduces the concept of effective chemical potentials, so an equivalent relationship for them is given by $\mu_u^* = \mu_d^* = \mu_s^*$. This can be found by checking Eq. (2.23) where the real and effective chemical potentials only differ by the latter term, which is

the same for every quark flavor.

For the EOS itself, Eqs. (2.24) and (2.25) must be written in terms of the zero-temperature regime. The pressure is given by

$$P = -\Omega_0 + \rho_b \frac{\partial m_I}{\partial \rho_b} \frac{\partial \Omega_0}{\partial m_I}, \tag{2.33}$$

with its derivatives being

$$\frac{\partial m_I}{\partial \rho_b} = -\frac{D}{3\rho_b^{4/3}} + \frac{C}{3\rho_b^{2/3}}, \quad \text{and} \quad \frac{\partial \Omega_0}{\partial m_I} = \sum_i \frac{\gamma m_i}{4\pi^2} \left[\mu_i^* k_{Fi} - m_i^2 \ln \frac{\mu_i^* + k_{Fi}}{m_i} \right], \tag{2.34}$$

and for the energy density, we have

$$\epsilon = \Omega_0 - \sum_i \mu_i^* \frac{\partial \Omega_0}{\partial \mu_i^*}. \tag{2.35}$$

Alternatively, the energy density can be evaluated from the sum of the i quark energy densities ($\epsilon = \sum_i \epsilon_i$), where ϵ_i is given in (Wen *et al.* 2005) as

$$\epsilon_i = \frac{\gamma}{2\pi^2} \int_0^{k_{Fi}} k^2 \sqrt{k^2 + m_i^2} dk = \frac{\gamma}{16\pi^2} \left[\mu_i^* k_{Fi} (2\mu_i^{*2} - m_i^2) - m_i^4 ln \left(\frac{\mu_i^* + k_{Fi}}{m_i} \right) \right]. \tag{2.36}$$

In the case of stellar matter, we are dealing with zero temperature and high-density regime to be able to describe pure quark or hybrid stars (Schertler *et al.* 1999; Ranea-Sandoval *et al.* 2 Hanauske *et al.* 2001; Menezes *et al.* 2006; Lenzi *et al.* 2010; Drago e Pagliara 2020; Pereira *et al.* 20 Ferreira *et al.* 2020). This implies that beta equilibrium and charge neutrality are the main conditions present in these systems. The first one happens after the Urca process (Lattimer *et al.* 1991; Yakovlev *et al.* 2001), when neutrinos are emitted during the cooling process of compact stars, with the loss of their initial energy. Once neutrinos are no longer in the system, beta equilibrium comes along represented by the chemical potentials of the particles as $\mu_u + \mu_e = \mu_d = \mu_s$. From the same procedure done for symmetric matter, this expression can be written in terms of the effective chemical potentials as $\mu_u^* + \mu_e = \mu_d^* = \mu_s^*$. Since the presence of leptons (electrons) is responsible for weak interactions, such as $d, s \leftrightarrow u + e + \bar{\nu}_e$, they play no role in strong interactions. That is why its chemical potential remains the same in the beta-equilibrium condition. The second condition refers to the fact that compact stars are electrically neutral objects, requiring that $\frac{2}{3}\rho_u - \frac{1}{3}\rho_d - \frac{1}{3}\rho_s - \rho_e = 0$. Finally, the total energy density (ε) and pressure (p) of stellar matter are found by implementing the leptons contribution. By assuming only

mass-less electrons, these expressions read as

$$\varepsilon = \epsilon + \frac{\mu_e^4}{4\pi^2}, \quad \text{and} \quad p = P + \frac{\mu_e^4}{12\pi^2}, \tag{2.37}$$

with $\mu_e = (3\pi^2\rho_e)^{1/3}$, and P and ϵ are given by Eqs (2.33) and the sum of (2.36) for the three quarks, respectively.

2.5 Stability windows

Following what Bodmer-Witten hypothesis states, phenomenological effective models as the one presented here need to fulfill the conditions that guarantee the stability of SQM, which is done by confronting it with nuclear matter. With the conditions being established, a stability window is constructed to represent the stable regions of each type of matter. We start by taking a large set of values for the C and $\sqrt{D}$ parameters and running it through the EQP model algorithm, where the minimum of the energy per baryon, namely, $(E/A)_{\rm min} = (\mathcal{E}/\rho_b)_{\rm min}$ where $\mathcal{E} = \epsilon$ (ε) for symmetric (stellar) matter, is evaluated and classified according to the following criteria:

(i) SQM is stable when $(E/A)_{\rm min} \leqslant 930$ MeV. In other words, when the minimum of energy per baryon is lower than the binding energy of ^{56}Fe (because iron is the element with the most stable nucleus found in nature).

(ii) SQM is said to be metastable when 930 MeV $< (E/A)_{\rm min} \leqslant 939$ MeV, which is the value of the nucleon mass.

(iii) SQM will be unstable when $(E/A)_{\rm min} > 939$ MeV.

Besides fulfilling these criteria, SQM will only be stable if the two-flavor quark matter (2QM) is unstable for the same set of C and $\sqrt{D}$ parameters, because there is no matter found in nature, neither in terrestrial experiments, where quarks u and d are deconfined, which means that 2QM must satisfy the condition of $(E/A)_{\rm min} > 930$ MeV.

In order to model symmetric and stellar matter similar to what it is believed to be in nature, the quark current masses used here are the ones provided by PDG (Workman e Others 2022), which are $m_{u0} = 2.16^{+0.49}_{-0.26}$ MeV, $m_{d0} = 4.67^{+0.48}_{-0.17}$ MeV and $m_{s0} = 93.4^{+8.6}_{-3.4}$ MeV. The stability windows were constructed based on these values, where, for symmetric matter, we applied $m_{u0} = 1.90$ MeV, $m_{d0} = 4.67$ MeV, and $m_{s0} = 93.4$ MeV, and for stellar matter: $m_{u0} = 2.16$ MeV, $m_{d0} = 5.15$ MeV, and $m_{s0} = 90$ MeV. This choice was also made based on the analysis performed in (Backes *et al.* 2021), where we were not so rigorous with the values of quarks current mass at that time.

Proceeding with our first results, the stability window for symmetric matter is shown

in Fig. 2.1. The green region is the one of our interest because it represents where SQM is stable. Below this area, the blue region corresponds to where the 2QM is stable, being a forbidden region for SQM to happen. Above the stable region of SQM, the meta-stability region is in orange, and the unstable one is in red.

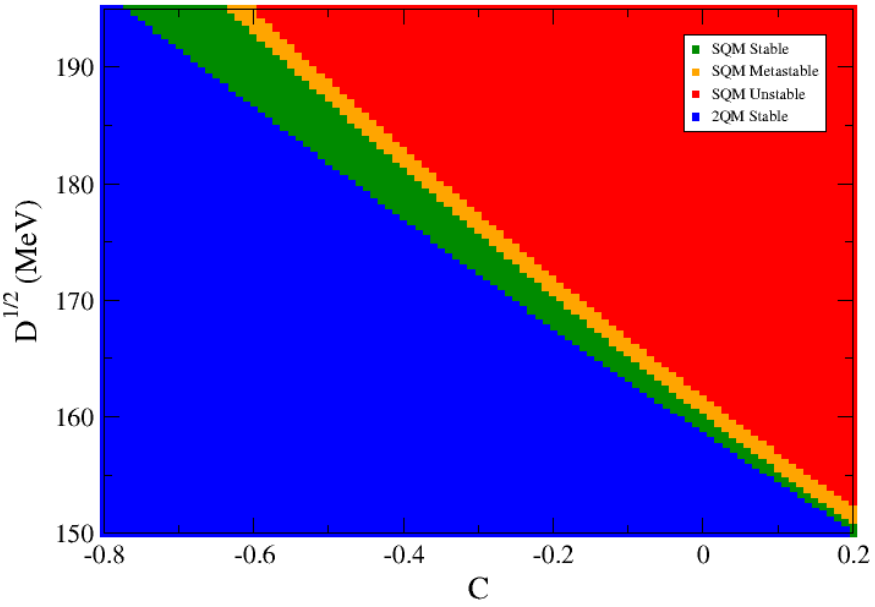

FIGURE 2.1 – Stability window for symmetric matter: EQP model.

Concerning the stability window for stellar matter, the lower region continues to be forbidden for SQM, since 2QM would be stable here, as shown in blue in Fig. 2.2. The region where SQM is stable is again shown in green, with the meta-stable and unstable ones being above it in orange and red, respectively. From the figure, it is also possible to notice a white region where there are no solutions for either 2QM or SQM.

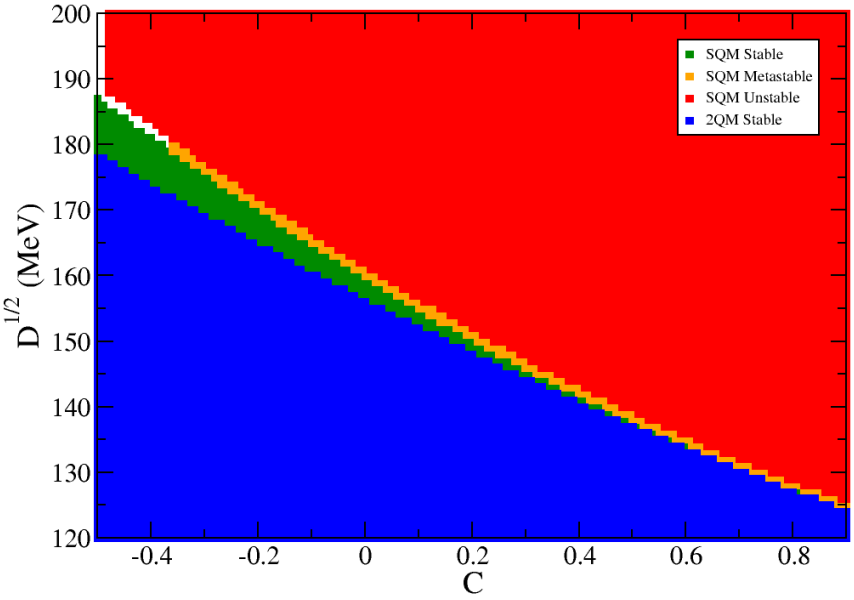

FIGURE 2.2 – Stability window for stellar matter: EQP model.

For comparison purposes, it is possible to notice that the symmetric stability window includes higher values of $\sqrt{D}$ and lower values of C than the one for stellar matter. The stellar stability window, on the opposite, allows higher values for C, which have an important role when we model compact stars because it provides higher values of maximum masses for these objects. One can also pay attention that the stable and meta-stable regions of stellar matter are significantly thinner than the ones of symmetric matter. Such differences can be explained by the presence of electrons in the system and the impact they have on matter stability.

3 Polyakov equiparticle model

Phenomenological effective quark models were developed to describe different phenomena of the QCD theory, in which the EQP model is included. Although these models investigate SQM with an interesting approach, some of them do not consider the prediction of a possible quark deconfinement at very short distances, which is an important characteristic of strong interaction. In models like the MIT bag model (Chodos *et al.* 1974; Chodos *et al.* 1974), quarks remain confined in a called "bag", where a constant term is implemented in the pressure equation representing its effects. In the Nambu-Jona-Lasinio (NJL) model (Nambu e Jona-Lasinio 1961; Nambu e Jona-Lasinio 1961; Klevansky 1992; Buballa 2005; Vogl e Weise 1991; Hatsuda e Kunihiro 1994), only the chiral transition is described, with quarks interacting only when they are in contact with each other. In order to introduce the dynamics of quark deconfinement in the NJL model at finite temperature, a first proposal was done in Ref. (Fukushima 2004) resulting in the Polyakov-Nambu-Jona-Lasinio (PNJL) model (Ratti *et al.* 2006; Rößner *et al.* 2007; Ratti *et al.* 2007; Fukushima 2008; Dexheimer e Schramm 2010; Dexheimer *et al.* 2021; RÖßner 2009). However, at zero temperature regime, the PNJL model fails to describe the dynamic of confinement/deconfinement transition, which is corrected by the PNJL0 model (Mattos *et al.* 2019; Mattos *et al.* 2021). In this chapter, we are going to present the Polyakov equiparticle (PEQP) model, which is a version of the EQP model with the implementation of the Polyakov loop, inspired by the PNJL0 model. This new model will be now useful through the investigation of SQM phase transition at zero temperature without losing its original thermodynamic consistency.

3.1 The Polyakov loop

The deconfinement dynamics of quarks will be incorporated in the EQP model through the inclusion of the traced Polyakov loop (Φ) (Polyakov 1978; Susskind 1979; Svetitsky e Yaffe 1982; Svetitsky 1986), which plays the role of an order parameter for deconfinement in the absence of dynamical quarks at the heavy quark limit (Fukushima 2004). In order to understand the relation between the Polyakov loop

and the effects of deconfinement let's take a step back into history. In 1974, Wilson proposed a model to describe the confinement of quarks where massive quarks would be coupled with a gauge field (with strength "g") (Wilson 1974). For a weak coupling, the quarks would be unbound because of the weak coupling in which the gauge field acts like a normal free zero-mass field. On the other hand, for strong coupling, the quarks are bound since the gauge field is massive. Throughout his work, the author develops the formalism to find this binding mechanism between quarks, and in summary, he finds what is called the "Wilson loop", which is written in Euclidean space as

$$W(x,y) = \mathcal{P}\exp\left[i\int_x^y dx^\mu A_\mu\right], \tag{3.1}$$

where A_μ = gluonic field and $\mathcal{P}$ = path order in an imaginary time (τ). If the integral reaches the same spatial position $\vec{x}$ at two different Euclidean times, let's say $\tau = 0$ and $\tau = \beta$, the loop found is given by the operator $\hat{L}(\vec{x})$ as

$$\hat{L}(\vec{x}) = \mathcal{P}\exp\left[ig\int_0^\beta d\tau A_4(\vec{x},\tau)\right], \tag{3.2}$$

with $A_4 = iA_0$, which is the Euclidean temporal component of the A_μ field associated with the gluons, and $\beta = 1/T$ is the temperature inverse. The formalism associated with imaginary time is applied when quantum field theory (QFT) is treated at finite temperature and is constructed through Wick's rotation, which is a powerful tool since it allows the rotation of the time axis into the pure imagination direction (Reinhardt 1996). In a more effective way, as $t \to it_E$ the Euclidean versions of the functional integrals are being generated. In (3.2), when $\beta \to it$, the integrals are now over t_E with the limits $t_E = 0$ and $t_E = t$ instead of $\tau = 0$ and $\tau = \beta$. This implementation guarantees the connection between QFT at zero temperature and the quantum statistical mechanics.

The interpretation that $\hat{L}$ is a loop comes from the fact that it is calculated in the same point of space connected by different times (0 and β). If we take the trace of this operator we will find the Polyakov loop itself, which reads as

$$\Phi \equiv \left\langle \frac{1}{N_f} Tr[\hat{L}] \right\rangle = \left\langle \frac{1}{3} Tr\left[exp\left(i\int_0^\beta d\tau A_4\right)\right]\right\rangle, \tag{3.3}$$

with N_f being the quarks flavor number. Here, Φ becomes a direct measure of the quark's confinement, since the quark's free energy F_q is connected to Φ through $\Phi = e^{F_q/T}$ (McLerran e Svetitsky 1981). Given that the divergence of the free energy is linked to systems where quarks are confined, it is possible to represent this phenomenon for

specific values of Φ as follows

$$\Phi = e^{-F/T} = \begin{cases} 0, & F \to \infty \quad \text{and} \quad T \quad \text{finite} \quad \text{(confinement)}, \\ 1, & F \quad \text{finite} \quad \text{and} \quad T \to \infty \quad \text{(deconfinement)}. \end{cases} \tag{3.4}$$

Therefore, at finite temperature, the systems where the free energy diverges lead to total confinement, and for the opposite, in systems where the temperature tends to infinity and the free energy is finite, i.e. $\Phi \neq 0$, deconfinement takes place. At the limit of extremely high temperatures, the asymptotic freedom is expected to occur and quarks will be deconfined at $\Phi = 1$. In fact, confinement is directly related to center symmetry (Weiss 1982; Holland e Wiese 2000).

Center symmetry is an important concept in gauge theories and the study of confinement because it refers to the symmetry related to the global transformations of the gauge group that do not affect the local gauge invariance of the theory, i. e. these transformations leave the physical observables invariant but change the configuration of the fields (Polyakov 1977). In the confined phase, the expectation value of the Polyakov loop $\left\langle \hat{L} \right\rangle$ is zero, indicating that the center symmetry is unbroken. However, in the deconfined phase, $\left\langle \hat{L} \right\rangle$ is nonzero, which implies that center symmetry is spontaneously broken leading to the emergence of distinct phases.

For example, if we take an invariant gauge system only with bosonic fields, like QCD containing only gluons, the gluonic field can be described by A_μ that transforms as $A_\mu \to A'_\mu = U(A_\mu + i\partial_\mu)U^\dagger$, with U being a local gauge transformation. At finite temperature, A_μ and A'_μ must satisfy the periodicity condition (Kapusta J. I.; Gale 2011) given by

$$A_\mu(0) = A_\mu(\beta) \qquad \text{and} \tag{3.5}$$

$$A'_\mu(0) = A'_\mu(\beta). \tag{3.6}$$

In order to verify Eq. (3.6), one can admit that U also obeys the periodicity condition of $U(0) = U(\beta)$ and by applying Eq. (3.5) we have that $A'_\mu(0) = U(0)(A_\mu(0) + i\partial_\mu)U^\dagger(0) = U(\beta)(A_\mu(\beta) + i\partial_\mu)U^\dagger(\beta) = A'_\mu(\beta)$. We can also probe this relation, by taking $U(0) = zU(\beta)$ with $z = e^{2\pi ik/N_c}$ ($k = 1, 2, 3, ...$ and N_c is the color number), as follows:

$$A'_\mu(0) = U(0)(A_\mu(0) + i\partial_\mu)U^\dagger(0) = zU(\beta)(A_\mu(\beta) + i\partial_\mu)z^*U^\dagger(\beta) \tag{3.7}$$

$$= e^{2\pi ik/N_c}e^{-2\pi ik/N_c}U(\beta)(A_\mu(\beta) + i\partial_\mu)U^\dagger(\beta) \tag{3.8}$$

$$= U(\beta)(A_\mu(\beta) + i\partial_\mu)U^\dagger(\beta) = A'_\mu(\beta). \tag{3.9}$$

Once the periodic and antiperiodic boundary conditions are satisfied, as a direct con-

sequence, we have that $\Phi = z\Phi$, which means that Φ is no longer an invariant quantity and can only be verified if $\Phi = 0$. As already discussed, this case represents the confined phase and once $\Phi \neq 0$, the center symmetry is spontaneously broken (Φ becomes the order parameter for the confinement/ deconfinement phase transition). With the inclusion of quarks in the system, the fermionic field transforms as $\Psi \to \Psi' = U\Psi$, and in order satisfy the anti-periodicity conditions (Kapusta e Gale 2006) given by:

$$\Psi(0) = -\Psi(\beta) \qquad \text{and} \tag{3.10}$$

$$\Psi'(0) = -\Psi'(\beta), \tag{3.11}$$

the necessary gauge transformation leads to $\Psi'(0) = U(0)\Psi(0) = -zU(\beta)\Psi(\beta) = -z\Psi'(\beta) \neq -\Psi'(\beta)$. This result indicates that center symmetry is explicitly broken by fermionic fields, always leading to $\Phi \neq 0$. Hence, Φ is defined as an approximate order parameter for the quarks phase transition.

3.2 The Polyakov potential

For a system defined as an effective gas of gluons, its equations of state must agree with the lattice QCD calculations in the pure gluon sector (PGS) at finite temperatures. Therefore, the grand-canonical thermodynamic potential, also called Polyakov potential, $\Omega_{PGS} \equiv \mathcal{U}(\Phi, \Phi^*, T)$, is introduced to describe the PGS and its first order phase transition when Φ jumps from 0 to a finite value (at a given temperature T_0). In the literature, $\mathcal{U}(\Phi, \Phi^*, T)$ has different forms, such as RTW05 (Ratti *et al.* 2006), RRW06 (Ratti *et al.* 2007; Rößner *et al.* 2007) and FUKU08 (Fukushima 2008), which are given, respectively, by ($\Phi = \Phi^*$):

$$\frac{\mathcal{U}_{RTW05}}{T^4} = -\frac{b_2(T)}{2}\Phi^2 - \frac{b_3}{3}\Phi^3 + \frac{b_4}{4}\Phi^4, \tag{3.12}$$

$$\frac{\mathcal{U}_{RRW06}}{T^4} = -\frac{b_2(T)}{2}\Phi^2 + b_4(T)ln(1 - 6\Phi^2 + 8\Phi^3 - 3\Phi^4), \tag{3.13}$$

$$\frac{\mathcal{U}_{FUKU08}}{bT} = -54e^{-a/T}\Phi^2 + ln(1 - 6\Phi^2 + 8\Phi^3 - 3\Phi^4), \tag{3.14}$$

with

$$b_2(T) = a_0 + a_1\left(\frac{T_0}{T}\right) + a_2\left(\frac{T_0}{T}\right)^2 + a_3\left(\frac{T_0}{T}\right)^3, \tag{3.15}$$

and

$$b_4(T) = b_4 \left(\frac{T_0}{T} \right)^3 . \tag{3.16}$$

The parameters $a, b, a_0, a_1, a_2, a_3, b_3$ and b_4 in Eqs. (3.12) to (3.14) are dimensionless free parameters. At $T = 0$, the Polyakov potential ($\mathcal{U}$) presented in these equations is equal to zero, resulting in the loss of the proposed phenomenology. The only exception occurs when we choose the DS10 potential (Dexheimer e Schramm 2010; Dexheimer *et al.* 2021), given as

$$\mathcal{U}_{DS10} = (a_0 T^4 + a_1 \mu^4 + a_2 T^2 \mu^2)\Phi^2 + \mathcal{U}_0(\Phi), \tag{3.17}$$

with

$$\mathcal{U}_0(\Phi) = a_3 T_0^4 \ln(1 - 6\Phi^2 + 8\Phi^3 - 3\Phi^4), \tag{3.18}$$

where μ is the chemical potential. When we search for the minimum of $\mathcal{U}$, we find the Polyakov loop and its complex conjugate, $\Phi^* = \left\langle 1/N_f Tr[\hat{L}^\dagger] \right\rangle$, i.e.

$$\frac{\partial \mathcal{U}(\Phi, \Phi^*, T)}{\partial \Phi} = \frac{\partial \mathcal{U}(\Phi, \Phi^*, T)}{\partial \Phi^*} = 0. \tag{3.19}$$

Our intention here is to preserve the confinement physics in the new model at $T = 0$ by incorporating the effects of the traced Polyakov loop Φ in the equations that define the constituent quark masses, as we show in the next section.

3.3 Parameters depending on the Polyakov Loop in the EQP model

From now, we closely follow the paper (Marzola *et al.* 2023). We first incorporate the Polyakov loop in the structure of the model, naming it as PEQP model. Then, we study its capability to describe symmetric quark matter and stellar matter. The inclusion of Φ in the equations of the EQP model is motivated as in (Mattos *et al.* 2019; Mattos *et al.* 2021), where the authors impose the vanishing of all couplings in the limit of $\Phi \to 1$, i.e., no interactions are expected anymore in the deconfined phase. Here we do the same by making the following replacements in the constants of the EQP model:

$$C \to C'(C, \Phi) = C(1 - \Phi^2), \tag{3.20}$$

and

$$D \to D'(D,\Phi) = D(1-\Phi^2). \tag{3.21}$$

As a consequence, the quark masses are now given by

$$m_i' = m_{i0} + m_I' = m_{i0} + \frac{D'(D,\Phi)}{\rho_b^{1/3}} + C'(C,\Phi)\rho_b^{1/3}. \tag{3.22}$$

By doing so, notice that one has $C' = D' = 0$ at $\Phi = 1$ and, consequently, $m_i' = m_{i0}$, i. e. the interaction vanishes when quarks are deconfined ($\Phi = 1$). Following, the chemical potentials relation reads as

$$\mu_i = \mu_i^* + \frac{1}{3}\frac{\partial m_I'}{\partial \rho_b}\frac{\partial \Omega_0}{\partial m_I'}, \tag{3.23}$$

and the system's new equations of state, at zero temperature, are rewritten as

$$P_{\text{PEQP}} = -\Omega_0 + \rho_b \frac{\partial m_I'}{\partial \rho_b}\frac{\partial \Omega_0}{\partial m_I'} - \mathcal{U}_0(\Phi), \tag{3.24}$$

and,

$$\epsilon_{\text{PEQP}} = \Omega_0 - \sum_i \mu_i^* \frac{\partial \Omega_0}{\partial \mu_i^*} + \mathcal{U}_0(\Phi), \tag{3.25}$$

in which the Polyakov Potential comes down to the latter term $\mathcal{U}_0(\Phi)$ expressed by Eq. (3.18). The original EQP model can be recovered by taking $a_3 = 0$, so $\mathcal{U}_0(\Phi) = 0$, as well as Φ. Therefore, $C' = C$, and $D' = D$. The term $\mathcal{U}_0$ is included in an ad hoc way to ensure $\Phi \neq 0$ solutions, obtained thorough $\partial \epsilon_{PEQP}/\partial\Phi = 0$ in the canonical ensemble for instance, and also to limit these solutions in the region of $\Phi < 1$, as discussed in (Mattos *et al.* 2021; Mattos *et al.* 2021).

3.4 Symmetric matter case

Once the PEQP model is built, the thermodynamical properties of the SU(3) system can be investigated. Firstly, we need to define all the parameters involved in the new model equations, such as the quark current masses (m_{i0}), a_3, T_0, C and $\sqrt{D}$. The quark current masses were already being defined following recent results provided by PDG (Workman e Others 2022) in Sec. 2.4 as $(m_{u0}, m_{d0}, m_{s0}) = (1.90, 4.67, 93.4)$ MeV. For the gluonic sector of the model, the parameters a_3 and T_0 from Eq. (3.18) are initially fixed as -0.4 (Dexheimer e Schramm 2010) and 190 MeV (Mattos *et al.* 2021;

Ratti *et al.* 2006), respectively, since they contribute to reproduce lattice data and information about the QCD phase diagram. However, the model that we are working on here is very different from the cited references, so this value for a_3 does not offer solutions of $\Phi \neq 0$, at least, not for symmetric matter. Because of that, a_3 will be treated as a free parameter so that we can explore its influence in providing satisfactory solutions to Φ. Finally, from the symmetric matter stability window in Fig. 2.1 the parameters C and $\sqrt{D}$ are chosen, with C within the range of $-0.8 \leq C \leq 0.2$ and $\sqrt{D}$ between $150 \leq \sqrt{D} \leq 195$ MeV. In our analysis the pair $(C, \sqrt{D}) = (0.2,\ 150\ \text{MeV})$ provides results related to more massive stars, which is why these values were chosen.

The original EQP model is constructed with the appeal that the thermodynamic consistency is respected, so we expect that even with the modifications done in the PEQP model it continues to obey the thermodynamic consistency conditions. The procedure to verify that this is the case is by taking the energy per baryon with ϵ given in Eq. (3.25) and plotting as function of the baryonic density for both EQP ($a_3 = 0$) and PEQP ($a_3 \neq 0$) models, as Fig. 3.1 shows.

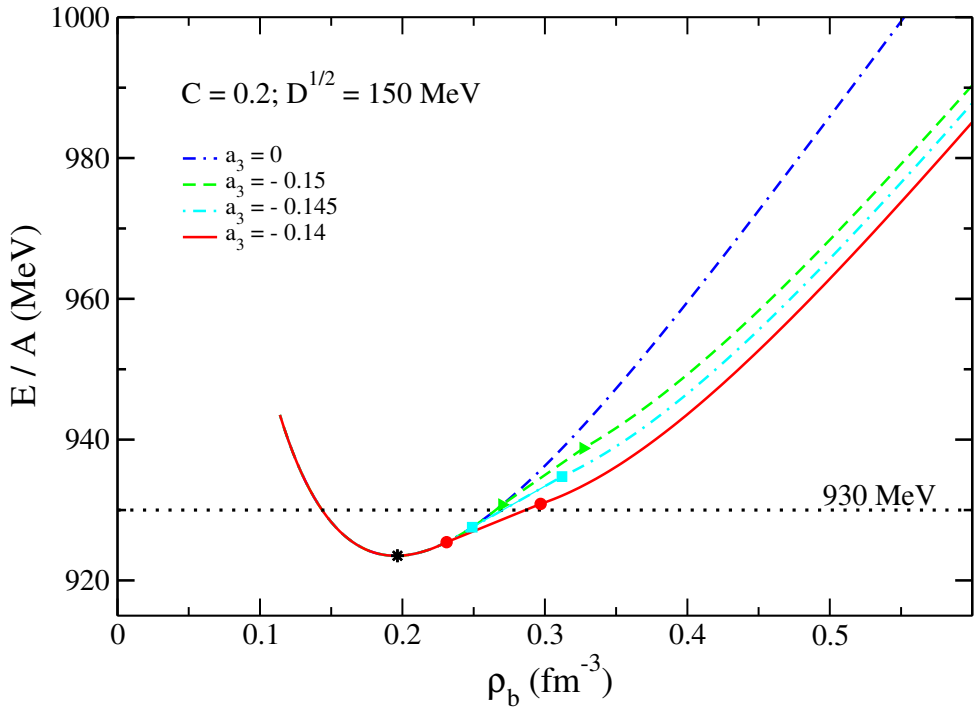

FIGURE 3.1 – Energy per baryon, $E/A = \epsilon/\rho_b$, as function of ρ_b for EQP ($a_3 = 0$) and PEQP ($a_3 \neq 0$) models.

In Sec. 2.5 we have established the necessary criteria for strange quark matter to be stable, i.e. the minimum of the energy per baryon needs to be lower or equal to 930 MeV. In the figure, the black dot indicates that this condition is confirmed since it is $<$ 930 MeV. As for the thermodynamic consistency, at this point pressure is zero, as requested by Eq. (2.13) condition, for both models. Notice that for the case of the PEQP

model, even for different values of $a_3 (a_3 \neq 0)$ the minimum of E/A is not modified by the emergency of $\Phi \neq 0$ solutions. This is an important result because it means that the symmetric matter stability window shown in Fig. 2.1 can be safely considered as the same one for the PEQP model at symmetric quark matter, and then we can rely on the pairs $(C, \sqrt{D})$ that produces stable SQM to go on through our investigations.

By doing so, we can step on the dynamics of deconfinement in $T = 0$, which can be achieved by analyzing the effect of the Polyakov potential $\mathcal{U}(\Phi)$. We already discussed that this term is responsible for non-null solutions of Φ, and as Eq. (3.18) shows, the parameter a_3 regulates this effect. From the thermodynamics point of view, this effect is properly observed by looking at the grand-canonical thermodynamic potential, $\Omega_{\text{PEQP}} = -P_{\text{PEQP}}$, where pressure is given by Eq.(3.24), as function of the traced Polyakov loop for the pair $C = 0.2$, $\sqrt{D} = 150$ MeV, for instance, in Fig. 3.2.

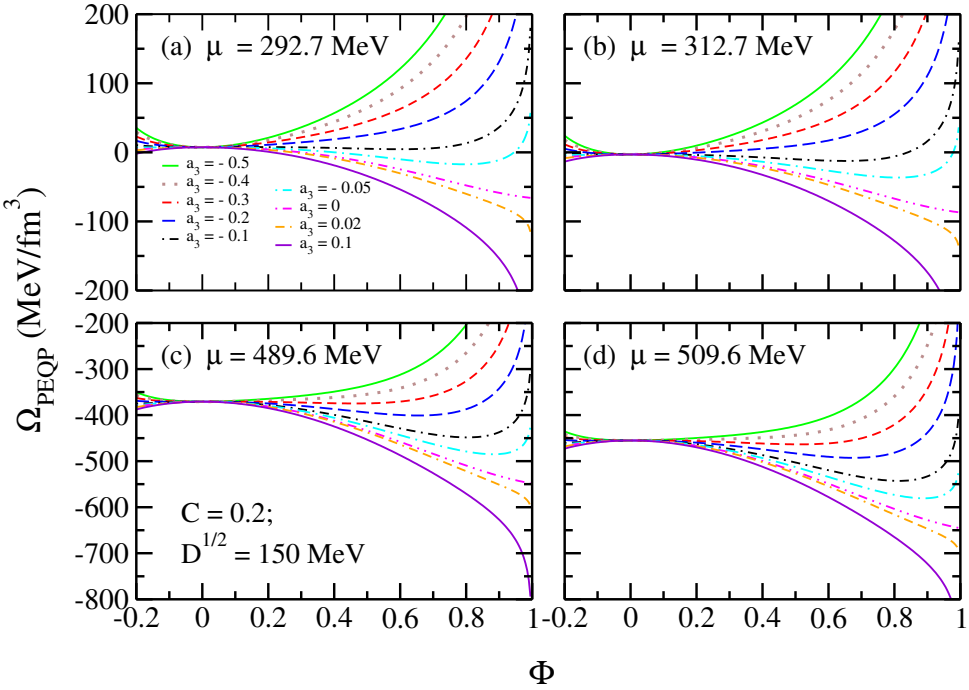

FIGURE 3.2 – Ω_{PEQP} as function of Φ for the pair $C = 0.2$, $\sqrt{D} = 150$ MeV for different values of μ, panels (a) to (d).

To generate the results present in this figure, Eq. (3.23) was rewritten in terms of the quarks Fermi momenta, $k_{Fi} = \sqrt{\mu_i^{*2} - m_i^2}$, and the quarks densities, $\rho_b = \sum_i \rho_i/3$, as follows:

$$\mu_i = \mu_i^* + \frac{1}{3}\frac{\partial m_I'}{\partial \rho_b}\frac{\partial \Omega_0}{\partial m_I'} = (k_{Fi}^2 + m_i^2)^{1/2} + f(\rho_u, \rho_d, \rho_s), \tag{3.26}$$

where we impose the symmetric matter condition of $\mu_u = \mu_d = \mu_s = \mu$, which results in

a system of three equations to determine ρ_i:

$$\mu = \begin{cases} \left[k_{Fu}(\rho_u)^2 + m_u(\rho_u,\rho_d,\rho_s)^2\right]^{1/2} + f(\rho_u,\rho_d,\rho_s), & (3.27) \\ \left[k_{Fd}(\rho_d)^2 + m_d(\rho_u,\rho_d,\rho_s)^2\right]^{1/2} + f(\rho_u,\rho_d,\rho_s), & (3.28) \\ \left[k_{Fs}(\rho_s)^2 + m_s(\rho_u,\rho_d,\rho_s)^2\right]^{1/2} + f(\rho_u,\rho_d,\rho_s), & (3.29) \end{cases}$$

with μ and a_3 as inputs, and $f(\rho_u,\rho_d,\rho_s)$ as the function that represents the term $\frac{1}{3}\frac{\partial m_I'}{\partial \rho_b}\frac{\partial \Omega_0}{\partial m_I'}$ in Eq. (3.26). This manipulation allows us to provide specific values for the common chemical potential, and Φ is now free to run as can be observed in the figure. For each chosen μ, in each panel, we can test different values of a_3 where some will produce a global minimum for $\Omega_{\rm PEQP}$ when $\Phi \neq 0$.

At a very particular value of the chemical potential, named here as $\mu_{\rm conf}$, some curves present two minima, meaning that the $\Omega_{\rm PEQP} \times \Phi$ curves play an important role for the confinement/deconfinement phase transition because the two minima characterize the transition from a confined system to a deconfined one. To explicitly illustrate it, we plot in Fig. 3.3 curves for $a_3 = -0.14$ and different values of μ.

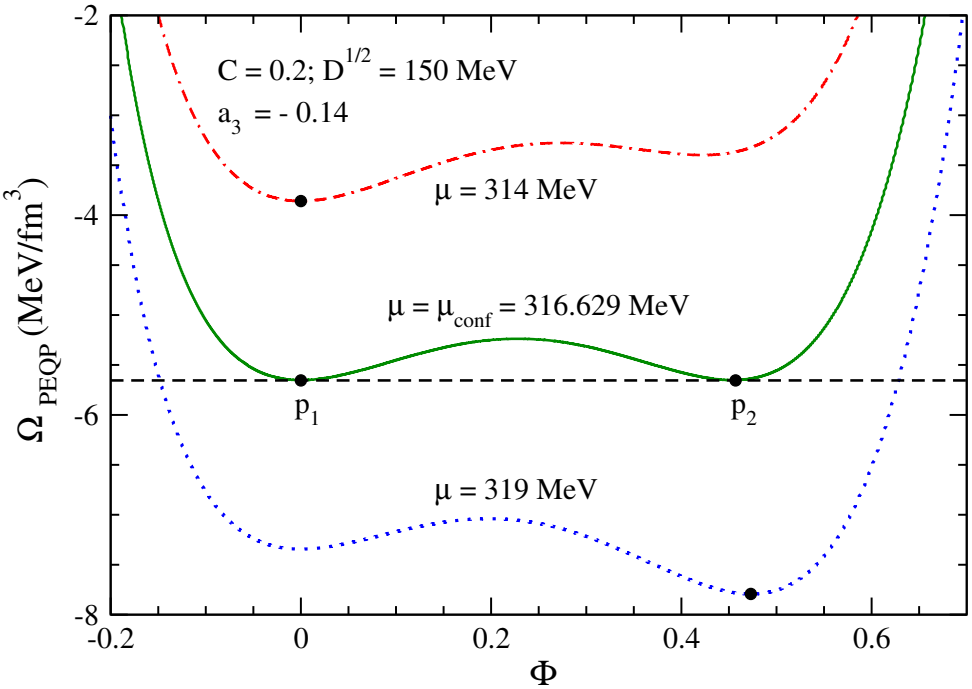

FIGURE 3.3 – $\Omega_{\rm PEQP}$ as function of Φ for three different values of μ.

Paying attention to the green curve, we identify that $\mu_{\rm conf} = 316.629$ MeV is the case where the two minima happen. If we slowly decrease μ, $\mu < \mu_{\rm conf}$ ($\mu = 314$ MeV for instance), it is only possible to obtain minima at $\Phi = 0$, indicating the confined phase (red curve). On the other hand, in the blue curve where μ is slowly increased, $\mu > \mu_{\rm conf}$ ($\mu = 319$ MeV for instance), the deconfinement phase is established, since a

minima for $\Phi \neq 0$ appears. At $\mu = \mu_{\text{conf}}$, the first order phase transition takes place, and the two minima emerge at $\Omega_{\text{PEQP}} \approx -5.7$ MeV/fm^3 (points p_1 and p_2 in Fig. 3.3). In (Masayuki e Koichi 1989), the same thermodynamic analysis is performed in a different context at finite temperature, where the authors explore how chiral symmetry restoration affects the thermodynamic quantities such as the energy density, pressure, and specific heat. The critical temperature for chiral symmetry restoration is a key parameter in their study, which is the temperature above which chiral symmetry is restored.

Back to our work, it is possible to verify the confinement/deconfinement transition exhibited by the PEQP model from another perspective, namely, by investigating the dependency of the traced Polyakov loop towards the chemical potential. Hence, the model's algorithm will run μ so that each value used as input has its correspondent Φ determined, where the ones that minimize $\Omega_{\text{PEQP}}(\mu, \Phi)$, will be selected. In other words, we select the Φ's that are solutions of $\partial\Omega_{PEQP}/\partial\Phi = 0$. The results are displayed in Fig. 3.4.

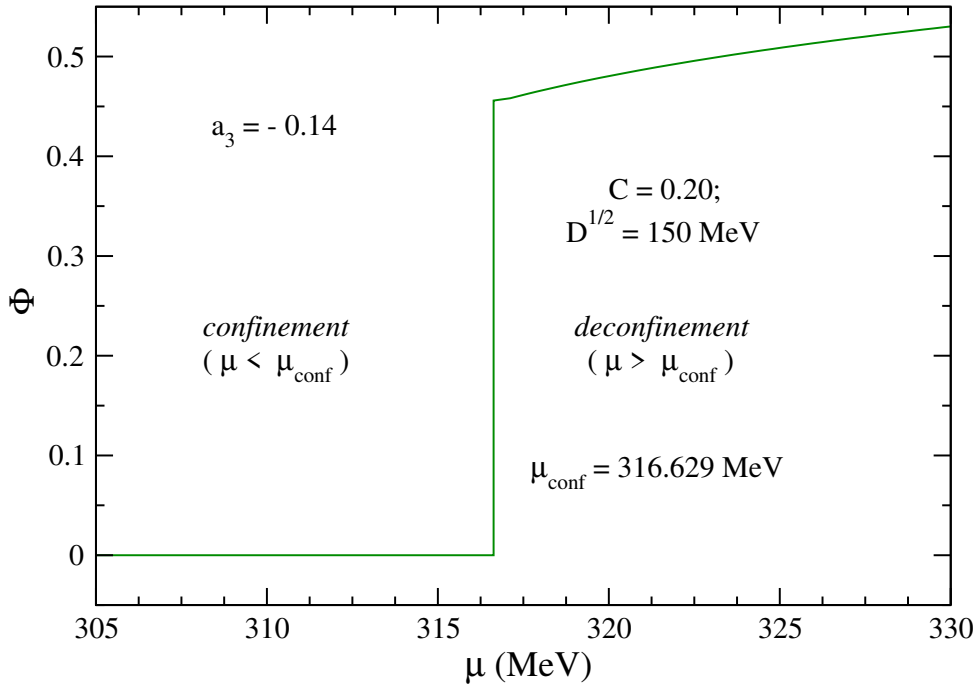

FIGURE 3.4 – Φ as a function of the common quark chemical potential.

Note in the figure that the discontinuity that appears in the values of the traced Polyakov loop, from $\Phi = 0$ to $\Phi \neq 0$, characterizes a first-order phase transition. This discontinuity delimits the thermodynamic phases of confinement, where $\mu < \mu_{\text{conf}}$ indicates the confinement region and when $\mu > \mu_{\text{conf}}$ the deconfinement one. With the Φ solutions in hand, Fig. 3.5 is able to be constructed, where Ω_{PEQP} is now evaluated as a function of μ.

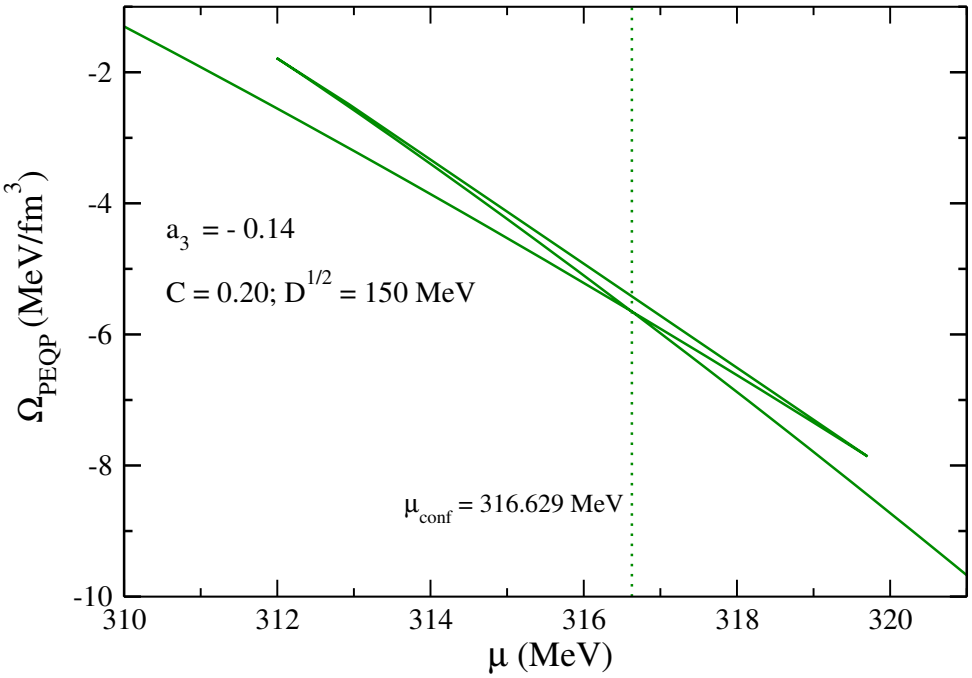

FIGURE 3.5 – Ω_{PEQP} as function of the common quark chemical potential.

As we saw in Fig. 3.3, μ_{conf} is a very sensible value that needs to be carefully investigated to be found. One way to accomplish this search is through the presented two minimum points of view. Another way is by looking for the crossing point in the curve of Ω_{PEQP} vs. μ (Fig. 3.5). Here, we identify μ_{conf} as being exactly 316.629 MeV, and for Ω_{PEQP} we find that it is ≈ -5.7 MeV/fm^3. These values are in agreement with the two minima method, which indicates that this second method of determining μ_{conf} by the grand canonical thermodynamic potential behavior as a function of μ is indeed another signature of the first-order phase transition exhibited by the model.

3.5 Stellar matter case

The motivation for applying the modifications in the EQP model, beyond the symmetric matter, is to look into the stellar matter behavior and analyze its features when working with compact stars (pure quarks or hybrid ones). On top of that, we are interested to know if the PEQP model is suitable enough to correspond positively to the observational data available about these objects. Therefore, in this section, we are going to analyze the effect of the traced Polyakov loop in a system composed of quarks and leptons (electrons) under charge neutrality and weak equilibrium conditions, which are the ones that describe systems like quark starts. Once again, we are relying on the PDG data mentioned in Sec. 2.4 to define the quark current masses for stellar matter as being $(m_{u0}, m_{d0}, m_{s0}) = (2.16, 5.15, 90)$ MeV.

From the stellar stability window (Fig. 2.2), we know that the presence of electrons gives us more possible values for the $(C, \sqrt{D})$ pair where SQM is stable. Hereafter, we take this set as being $C = 0.81$ and $\sqrt{D} = 127$ MeV. However, as done in the previous section, the stability window needs to be verified to see if it remains the same for the PEQP model stellar matter system. In Fig. 3.6 we have this analysis depicted.

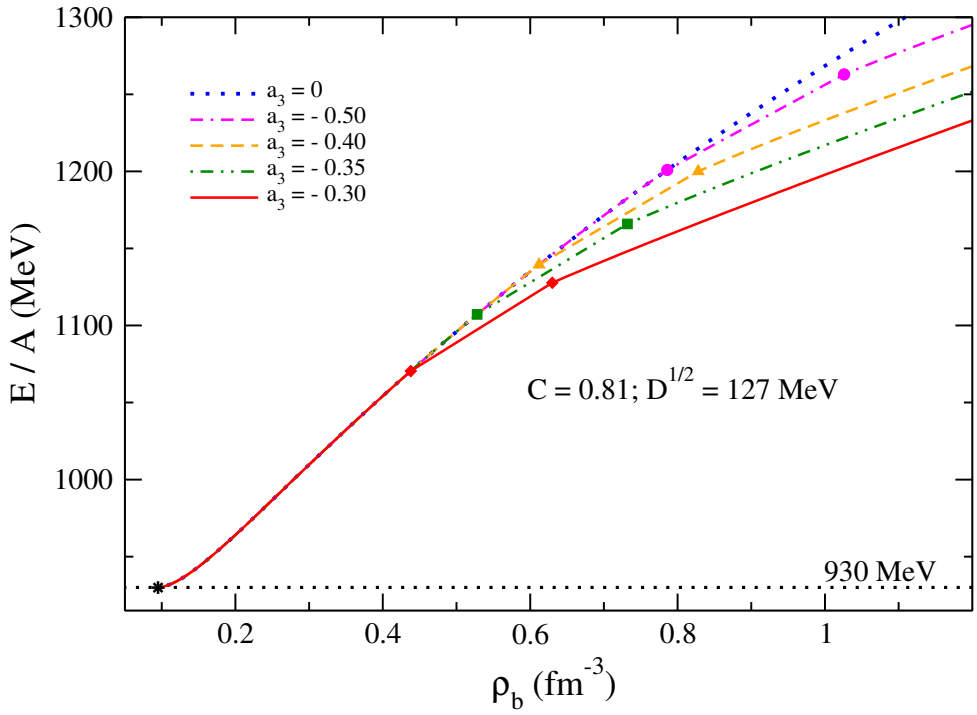

FIGURE 3.6 – Energy per baryon, $E/A = \varepsilon/\rho_b$, as function of ρ_b for EQP ($a_3 = 0$) and PEQP ($a_3 \neq 0$) models.

The figure shows the curves of the EQP ($a_3 = 0$) and PEQP ($a_3 \neq 0$) models for the energy per baryon as a function of the baryonic density. In the y-axis , $E/A = \varepsilon/\rho_b$, where ε is given by

$$\varepsilon = \epsilon_{\text{PEQP}} + \frac{\mu_e^4}{4\pi^2}. \tag{3.30}$$

The x-axis parallel line corresponds to 930 MeV, which is the limit value of the minimum energy per baryon for SQM to be stable. As we can see, the minimum of the energy per baryon of all curves are concentrated at the same point, represented by the black dot. The chart range is not favorable for us to see clearly that this value is lower than 930 MeV, but in fact it is, by being equal to 929.92 MeV. This means that the stellar stability window shown in Fig. 2.2 is a reliable source for us to choose the C and $\sqrt{D}$ parameters for the next applications of the PEQP model.

Following, to make it possible to identify the μ_{conf} regarding stellar matter, we need to

evaluate the grand canonical potential of the system Ω. This is done through

$$\Omega = -p = -P_{\text{PEQP}} - \frac{\mu_e^4}{12\pi^2}, \tag{3.31}$$

and the results are plotted in Fig. 3.7, where the typical structure of systems that present a first-order phase transition emerges, exactly as in the symmetric matter case. For reference, we also show the curve related to the original EQP model ($a_3 = 0$) in blue.

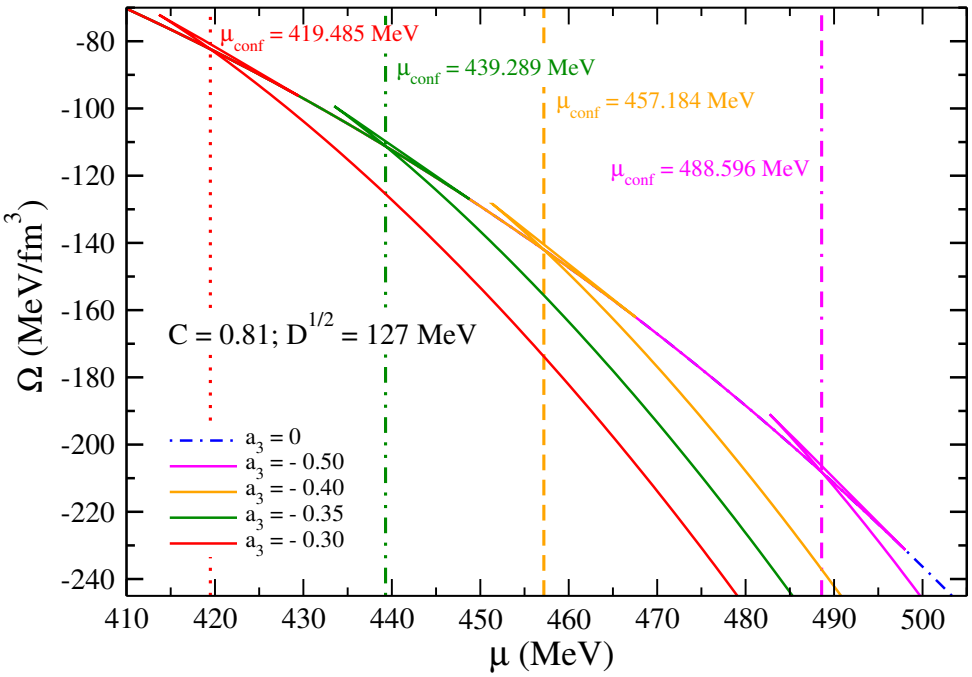

FIGURE 3.7 – Ω as a function of the common quark chemical potential for different values of a_3.

In the PEQP model, for each value of $a_3 \neq 0$ there is a corresponding value of Ω and μ_{conf} as Tab. 3.1 shows. Note that as a_3 decreases, lower values of Ω are obtained, and for the chemical potential related to the deconfinement phase transition the opposite happens, namely, it is higher when a_3 is lower.

a_3	$\Omega(MeV/fm^3)$	$\mu_{\text{conf}}(MeV)$
- 0.30	- 81.912	419.485
- 0.35	- 111.219	439.289
- 0.40	- 141.055	457.184
- 0.50	- 208.687	488.596

TABLE 3.1 – The grand canonical potential (Ω_{total}) and the confinement chemical potentials (μ_{conf}) according with the parameter a_3 for a stellar matter system.

Considering that quark stars are found at zero temperature and high density, we need

to verify the values predicted by the PEQP model for the baryonic density at the phase transition point, because quarks are expected to be asymptotically free at this regime. In Fig. 3.8 we have this analysis displayed. Here, the ratio of the baryonic density to the nuclear saturation density, taken here as $\rho_0 = 0.15$ fm^{-3}, is plotted against the chemical potential.

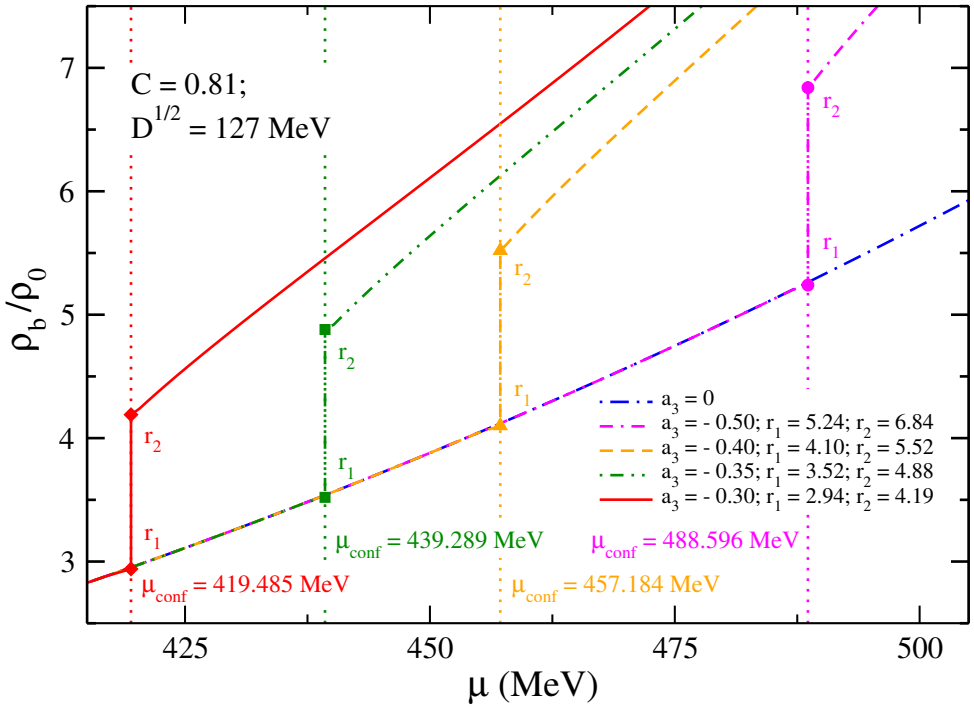

FIGURE 3.8 – ρ_b/ρ_0 as function of the common quark chemical potential for different values of a_3.

Looking at the figure, we are interested in identifying the points r_1 and r_2, because they represent the beginning and the end of the phase transition, respectively. Usually, ρ_b is expected to be at least 2 or 3 times higher than ρ_0. However, for the PEQP model, when we decrease the parameter a_3, ρ_b becomes from 2 to almost 7 times higher than ρ_0. The details are also given by Tab. 3.2 for better visualization. Notice that when $a_3 = -0.30$, ρ_b is 2.94 times higher than ρ_0 when the phase transition starts and equal to $4.19\rho_0$ at the final border of the co-existence phase. Now, when $a_3 = -0.50$, ρ_b is $5.24\rho_0$ at the phase transition beginning and $6.84\rho_0$ at the end. For $a_3 = 0$, when the original EQP model is restored, we can see that the (blue) curve is continuous, i.e. there are no deconfined phase transitions associated.

a_3	r_1	r_2
- 0.30	2.94	4.19
- 0.35	3.52	4.88
- 0.40	4.10	5.52
- 0.50	5.24	6.84

TABLE 3.2 – Ratio of the baryonic density to the nuclear saturation density, ρ_b/ρ_0 for the phase transition of the system.

Since the quark masses are written in terms of density, it is interesting to investigate its phase transition when the Polyakov loop is introduced in the new model. This investigation is presented in Fig. 3.9, where we take a single value of a_3 and observe the behavior of each quark mass as a function of the chemical potential.

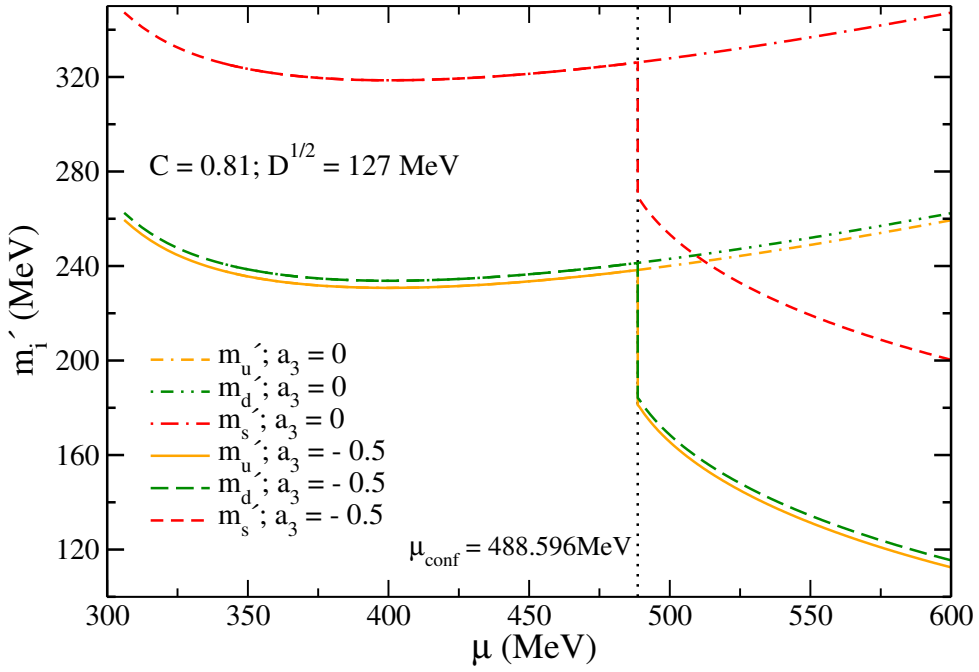

FIGURE 3.9 – Quark masses, calculated as in Eq. (3.22), as function of the common chemical potential for $a_3 = -0.50$ (PEQP model) and $a_3 = 0$ (EQP model).

From the expression of the quark masses, given by Eq. (2.32) in the EQP model, we can see that the term related to the parameter C will cause a drop on the quark masses and the latter term, related to the parameter $\sqrt{D}$, will be responsible for slowly increasing its mass. This can be confirmed by the curves of the quarks u, d, and s with $a_3 = 0$ in the figure. However, for the PEQP model, the quark masses are now written as in Eq. (3.22). When we compare both models, a significant reduction of the quark masses is caused by the inclusion of the traced Polyakov loop. This result indicates that the system is going

toward the direction of a similar chiral symmetry restoration, especially m_u and m_d since it is associated with the reduction of the constituent masses of the quarks.

Analyzing now the equations of state, we have them represented in Fig. 3.10, where the total energy density was obtained from Eq. (3.30), and the total pressure of the system from Eq. (3.31).

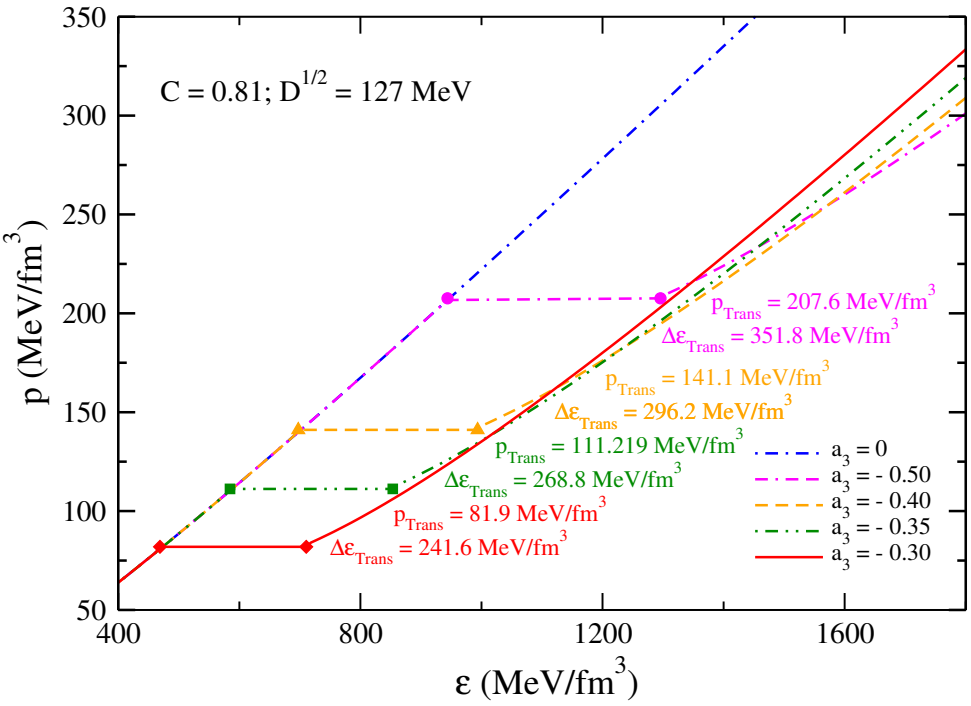

FIGURE 3.10 – Equation of state $p \times \varepsilon$ for different values of a_3.

As we can see from this figure, there is a plateau happening in the pressure simultaneously with an energy density gap. This is another clear consequence of the confinement/deconfinement phase transition. The transition pressure (p_{Trans}) and the energy density gap at the transition point ($\Delta\varepsilon_{\text{Trans}}$) are highlighted in the figure according with its correspondent value of a_3. When a_3 decreases we notice that p_{Trans} and $\Delta\varepsilon_{\text{Trans}}$ increase. In (Mattos *et al.* 2021), p_{Trans} and $\Delta\varepsilon_{\text{Trans}}$ were generated by a hadron-quark phase transition where this pattern was also detected. The PNJL0 model was applied in the quark sector of the transition in this referenced work.

Obtaining the EOS is an essential step in the compact stars study because they are the necessary ingredient to solve the Tolman-Oppenheimer-Volkoff (TOV) equations (Tolman 1939; Oppenheimer e Volkoff 1939). These equations are given by

$$\frac{dp(r)}{dr} = -\frac{[\varepsilon(r)+p(r)][m(r)+4\pi r^3 p(r)]}{r^2-2rm(r)} \tag{3.32}$$

$$\frac{dm(r)}{dr} = 4\pi r^2 \varepsilon(r), \tag{3.33}$$

for which the solution is constrained to $p(0) = p_c$ (central pressure) and $m(0) = 0$, with the conditions $p(R) = 0$ and $m(R) = M$ satisfied at the star surface. R is the radius of the respective quark star of mass M. From this procedure, we display the mass-radius diagrams for the quark stars in Fig. 3.11.

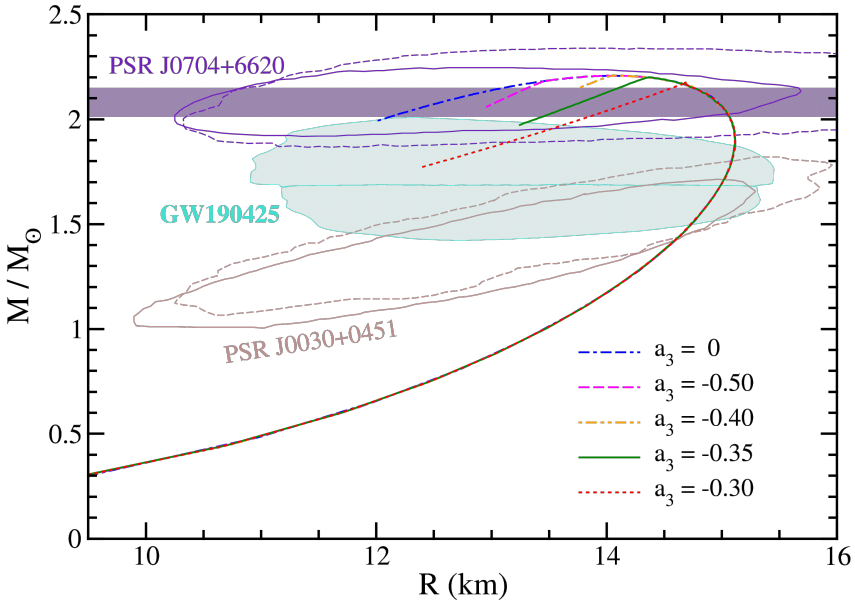

FIGURE 3.11 – Mass-radius diagrams constructed from the PEQP model for different values of a_3. The contours are related to data from the NICER mission, namely, PSR J0030+0451 (Riley *et al.* 2019; Miller *et al.* 2019) and PSR J0740+6620 (Riley *et al.* 2021; Miller *et al.* 2021), and the GW190425 event (Abbott *et al.* 2020), all of them at 90% credible level. The violet horizontal band is also related to the PSR J0740+6620 pulsar (Fonseca *et al.* 2021).

Usually, the curve representing a quark star family follows the behavior of the blue curve of the EQP model, where $a_3 = 0$. However, once we introduce the Polyakov loop to achieve the confinement/deconfinement phase transition in the PEQP model, we can notice the "cusp" followed by the decreasing linear branches emerging in the PEQP parameterization for quark stars of mass greater than two solar masses ($M_\odot$). This same feature was also observed in the hadron-quark phase transitions present in the hybrid stars analyzed in (Mattos *et al.* 2021) in which the quark sector was described by the PNJL0 model, that also contains the Polyakov loop in its structure. The first conclusion that

comes to mind about these linear branches, in both PEQP and PNJL0 models, is that they are composed by unstable stars, when we analyze the criterion $\partial M/\partial\varepsilon > 0$, that coincides with the curves built until the star with the maximum mass.

In order to verify the stability of these star configurations, we perform the specific response of the stars to radial oscillations (ARBAÑIL *et al.* 2023; Lenzi *et al.* 2023; Parisi *et al.* 2021; Pereira *et al.* 2018; Mariani *et al.* 2019; ARBAÑIL e Malheiro 2015; Sun *et al.* 2021; Jiménez e Fraga 2019). This is done through the solution of the following coupled equations

$$\frac{d\xi}{dr} = -\frac{1}{r}\left(3\xi + \frac{\Delta p}{\Gamma p}\right) - \frac{dp}{dr}\frac{\xi}{(p+\varepsilon)}, \tag{3.34}$$

and

$$\begin{aligned}\frac{d\Delta p}{dr} = {} & \xi\left[\omega^2 e^{\lambda-\nu}(p+\varepsilon)r - 4\frac{dp}{dr}\right] + \xi\left[\left(\frac{dp}{dr}\right)^2\frac{r}{p+\epsilon} - 8\pi e^{\lambda}(p+\varepsilon)pr\right] \\ & + \Delta p\left[\frac{dp}{dr}\frac{1}{p+\varepsilon} - 4\pi(p+\varepsilon)re^{\lambda}\right],\end{aligned} \tag{3.35}$$

with $e^{\lambda} = 1 - 2m(r)/r$, $d\nu/dr = -2(dp/dr)(p+\varepsilon)^{-1}$, and $\Gamma = (1+\varepsilon/p)(dp/d\varepsilon)$. ξ is the relative radial displacement, and Δp is the pressure perturbation, both quantities time dependent as $e^{i\omega t}$ in which ω is the eigenfrequency. If $\omega^2 > 0$ after the point of maximum mass, we can find stable stars in the linear branches of configurations such as those presented by the PEQP and PNJL0 models, where a first-order phase transition happens, but only if we consider slow phase transitions (ARBAÑIL *et al.* 2023; Lenzi *et al.* 2023; Parisi *et al.* 2021; Pereira *et al.* 2018). By this approach we can find the last stable star where $\omega = 0$ in the point of the mass-radius diagram.

Applying the method through all parameterizations of the PEQP model used to construct the mass-radius profiles we verified that they present $\omega^2 > 0$, when the slow phase transitions are considered. In other words, all of the curves presented in Fig. 3.11 for $a_3 \neq 0$ are stable under radial oscillations. Therefore, one verifies that a particular class of twin quark stars (stars with the same mass but different radii), namely, one of them composed by confined quarks, and the other one in which deconfined strongly interacting particles are found.

Still regarding Fig. 3.11, our results are compared with the recent observational astrophysical data provided by the NICER mission regarding the millisecond pulsars PSR J0030+0451 (Riley *et al.* 2019; Miller *et al.* 2019) and PSR J0740+6620 (Riley *et al.* 2021; Miller *et al.* 2021), and with data from the gravitational wave event named GW190425 (Abbott *et al.* 2020) analyzed by LIGO and Virgo Collaboration. Ad-

ditionally, we also display the PSR J0740+6620 data extracted from (Fonseca *et al.* 2021), that corresponds to $M = (2.08 \pm 0.07 M_{\odot})$ at 68.3% of credible level. Additionally, Tab. (3.3) displays the maximum masses, M_{max} $(M_{\odot})$, and its respective radius, R (km), found for each value of a_3. Observe that as a_3 decreases the quark star maximum mass increases, as well as its radius. Our findings point out to agreement between the results generated by the PEQP model and all observational data.

a_3	M_{max} $(M_{\odot})$	R (km)
- 0.30	2.18	14.69
- 0.35	2.20	14.37
- 0.40	2.21	14.06
- 0.50	2.21	14.13

TABLE 3.3 – Quark stars maximum masses and respective radius according with the parameter a_3.

4 Strange stars admixed with dark matter

As already discussed in this work, strange stars represent a type of compact stars composed of strange quarks and may be formed during the collapse of massive stars in supernova events, where densities are so high that quark matter becomes stable. These objects can provide insights into the equation of state of nuclear matter at extreme conditions, and challenge our understanding of the fundamental forces at play in the universe. That's because researchers are not capable yet to fully describe its detailed composition, structure, and dynamics. For that reason, the study of such objects involves different areas of physics like thermodynamics, quantum field theory, general relativity, nuclear reactions, etc. In that direction, there are currently studies with the proposal that dark matter (DM) (Bertone e Hooper 2018; Arbey e Mahmoudi 2021; Salucci 2019) could be present in compact stars.

The existence of DM is supported by the analysis of galaxies rotation curves, in which its rotational velocities do not decrease as expected with distance from the galactic center. Instead, they remain constant or even increase, suggesting the presence of unseen mass (Rubin Vera C. 1970). The gravitational lensing method also provides strong evidence because the gravitational field of massive foreground objects is responsible for bending the light from distant objects, which indicates that more mass is present than can be seen (only 10% to 20% is due to the visible mass of galaxy clusters) (Koopmans e Treu 2003; Massey *et al.* 2010). The anisotropy present in measurements of cosmic microwave background (CMB), especially the missions like WMAP (NASA 2001) and Planck (ESA 2009), show fluctuations that are consistent with a universe composed of dark matter (Adams *et al.* 1998; Pierpaoli 2004; Padmanabhan e Finkbeiner 2005; Aghanim *et al.* 2016; Hu e Dodelson 2002; Hu *et al.* 1997). Besides, the distribution of galaxies and galaxy clusters across the universe aligns with models that include dark matter to explain the observed large-scale structure (Springel *et al.* 2005). Due to these evidences, there is a consensus, at the present day, that the universe is composed of 68% of dark energy, 27% of DM, and 5% of ordinary matter. It is evident that the

universe exhibits a significant asymmetry between baryonic matter and antimatter, with observable matter far outnumbering antimatter. This phenomenon is often referred to as baryon asymmetry and is a critical element in understanding the early universe. There are mechanisms proposed to explain this asymmetry, such as Baryogenesis, where similar processes could also apply to dark matter, leading to a surplus of dark matter particles (Sakharov 1991).

Although many models treat DM as a symmetric component, meaning that for every dark matter particle, there is an antiparticle, in the asymmetric dark matter (ADM) scenario, dark matter particles are produced in a way that results in a net asymmetry. This could have occurred in the early universe, influenced by interactions and processes that distinguish between particles and antiparticles (PETRAKI e VOLKAS 2013). One of the processes is called Leptogenesis (Buchmüllera R. D. Pecceib 2006), where the decay of heavy leptons creates an imbalance in lepton and baryon numbers that can transfer to dark matter. Another one is the Affleck-Dine mechanism, which involves scalar fields that can generate an asymmetry in the number density of dark matter through their dynamics during inflation (Affleck e Dine 1985). The main point here is that repulsive self-interactions in asymmetric dark matter and small attractive interactions with baryonic matter would be possible.

To investigate the potential existence of strange stars admixed with dark matter we implement the two-fluid approach. One of the fluids is due to the "visible" matter described by the equiparticle quark model (EQP) without the Polyakov loop, and the other is the dark sector described by two different models: the fermionic and the bosonic one. The interaction between the "visible" and dark particles will be gravitational. Therefore, this chapter is divided as follows: the next section is dedicated to the formalism concerning the dark sector models, and in sequence, the calculations and results coming from this investigation are presented as well as the discussion. The recent astrophysical observational data will be responsible for checking the capability of the EQP model admixed with DM in satisfying these observational measurements as done in the previous section, with the inclusion of the compact star named HESS J1731-347".

4.1 Dark Matter models

In our approach, the dark sector will be described by a fermionic and a bosonic model. For the first one, we begin with a Lagrangian density that includes a kinetic term (Dirac Lagrangian density) for a single fermionic component, in addition to a vector meson coupled to the Dirac spinor (Xiang *et al.* 2014; Das *et al.* 2022; Thakur *et al.* 2024). The

expression reads as

$$\mathcal{L}_{\text{FDM}} = \bar{\chi}\left[\gamma_\mu(i\partial^\mu - g_V V^\mu) - m_\chi\right]\chi - \frac{1}{4}F_{\mu\nu}F^{\mu\nu} + \frac{1}{2}m_V^2 V_\mu V^\mu, \tag{4.1}$$

where $F_{\mu\nu} = \partial_\mu V_\nu - \partial_\nu V_\mu$ is the strength tensor of the vector meson. The quantities m_χ and m_V are the dark fermion mass and the mass of the dark vector meson, respectively. According to the authors in (Xiang *et al.* 2014), the dark scalar meson is not included in order to avoid one more free parameter to deal with, and for that reason, we followed the same procedure. This makes the model simpler to work with. Furthermore, by including a scalar particle, the attractive interactions would increase in the system, which would lead to lower final compact star masses. That's because the increase in its mass is directly related to repulsive interactions. Therefore, the dark scalar meson is not taken into account.

To calculate the energy density and pressure of the system, the mean-field approach is used, which is a typical procedure done in relativistic hadronic models with the same mathematical formulation for the Lagrangian density. Thus, the equations of state are given by

$$\mathcal{E}_{\text{FDM}} = \frac{1}{\pi^2}\int_0^{k_{F\chi}} dk\, k^2(k^2 + m_\chi^2)^{1/2} + \frac{1}{2}C_V^2\rho_\chi^2, \tag{4.2}$$

$$P_{\text{FDM}} = \frac{1}{3\pi^2}\int_0^{k_{F\chi}} dk\, \frac{k^4}{(k^2 + m_\chi^2)^{1/2}} + \frac{1}{2}C_V^2\rho_\chi^2, \tag{4.3}$$

with $C_V = g_V/m_V$ and $\rho_\chi = k_{F\chi}^3/(3\pi^2)$. The Fermi momentum of the dark particle is $k_{F\chi}$. Besides strange stars, neutron stars admixed with DM have also been the target of studies, where fermionic self-interacting dark matter is coupled to hadronic matter, as done in (Mariani *et al.* 2024), for instance.

Concerning the choice of fermionic and bosonic particles as dark particles, this occurs because the true nature of DM particles remains poorly understood, despite the efforts done through the last direct and indirect detection methods (Bauer *et al.* 2015). As a consequence, many possible candidates have been studied over the years, such as gravitinos, axinos, axions, sterile neutrinos, WIMPzillas, supersymmetric Q-balls, and mirror matter (Kusenko e Rosenberg 2013; Feng 2010). Since we are assuming that the dark sector in our study is composed of fermionic and bosonic particles, the latter one will be treated as the bosonic asymmetric dark matter model proposed in (Nelson *et al.* 2019; Rutherford *et al.* 2023). The authors define asymmetric dark matter as being composed of bosonic particles with repulsive self-interaction, in a MeV-GeV mass scale. Through scattering, two identical particles can self-interact by exchanging a gauge boson, i. e. a force carrier, which leads to attraction or repulsion between the particles. In our case, the

bosons exchange an eV-MeV mass-scale vector gauge boson (which also carries the Standard Model baryon number) resulting in a repulsive self-interaction. This vector gauge boson is responsible for generating the "dark asymmetry". In units of $\hbar = c = 1$, the action is given by

$$\mathcal{S}_{\text{BDM}} = -\int d^4x\sqrt{-g}\left(D^*_\mu\sigma^* D^\mu\sigma + m^2_\sigma\sigma^*\sigma + \frac{1}{2}m^2_\phi\phi_\mu\phi^\mu + \frac{1}{4}Z_{\mu\nu}Z^{\mu\nu} - g_B\phi_\mu J^\mu_B\right), \quad (4.4)$$

where g is the determinant of the metric, σ is the charged bosonic ADM field, σ^* is the anti-ADM field, m_σ is the mass of the bosonic ADM field, ϕ_μ is the vector boson field of the ADM mediator, m_ϕ is the mass of the vector boson field, $Z_{\mu\nu} = \nabla_{|\mu\phi_\nu|} = \nabla_\mu\phi_\nu - \nabla_\nu\phi_\mu$ is the field strength tensor of ϕ_μ, ∇_ν is the covariant derivative, g_B is the interaction strength of ϕ_μ with the Standard Model baryon number current J^μ_B, $D_\mu = \nabla_\mu + ig_\sigma\phi_\mu$, and g_σ is the interaction strength of σ with the ϕ_μ vector field. Only the necessary interactions are being considered: the ADM repulsive self-interactions, ADM minimal interaction with gravity, and ADM interaction with baryons (quarks in our case).

To simplify our calculations let's take some approximations into account: $g_B \leq 10^{-10}$ due to measurements of supernova SN1987A, where the energy radiated due to the possible production of ϕ_μ, from nucleon-nucleon Bremsstrahlung reactions in proto-neutron stars, must be consistent with the neutrino data of SN1987A (Rrapaj e Reddy 2016). Following, by assuming that $g_B << g_\sigma$, as discussed in (Nelson *et al.* 2019), the interaction between ADM and baryonic matter can be ignored, and the latter term of Eq. (4.4) can be discarded. The last one concerns neglecting the effects of gravity relative to the inverse length scales of neutron stars (Ivanytskyi *et al.* 2020), and for that we consider a flat spacetime.

If we take the gradient of the g_{tt} component of the metric, we can write the gradient as

$$\frac{dg_{tt}}{dr} = \frac{-2g_{tt}}{P+\epsilon}\frac{dP}{dr}, \quad (4.5)$$

where P = pressure, ϵ = energy density. From the stellar surface, we have that $g_{tt} = -1 + \frac{2GM}{Rc^2}$ and $P = 0$, where M = star total gravitational mass and R = star radius, which leads Eq. (4.5) to be

$$\frac{dg_{tt}}{dr} = \frac{-2GM}{c^2R^2}. \quad (4.6)$$

When the limit where $g_{tt} = 0$, $\frac{2GM}{Rc^2} = 1$, and we have that $dg_{tt}/dr < 1/R$. Considering the radius of a star as 10 km, such as the ones for compact stars, and a spherical layer of thickness $\delta r = 10^{-3}$ km, which is large enough to treat DM thermodynamically, we have

also had to ensure that

$$\frac{dg_{tt}}{dr}\delta r < \frac{\delta r}{R} = 10^{-4}. \tag{4.7}$$

Since the derivatives of the metric are small compared to the spatial scales of a compact star, we can approximate the spacetime as flat, leading us to the Lagrangian given by

$$\mathcal{L}_{\text{BDM}} = -\sqrt{-g}\left(D^*_\mu\sigma^* D^\mu\sigma - m^2_\sigma\sigma^*\sigma - \frac{1}{2}m^2_\phi\phi_\mu\phi^\mu - \frac{1}{4}Z_{\mu\nu}Z^{\mu\nu}\right). \tag{4.8}$$

By variations of the action and the approximations discussed, one can obtain the equations of motion as being

$$\left[D_\mu D^\mu - m^2_\sigma\right]\sigma = 0 \tag{4.9}$$

$$\left[D^*_\mu D^{*\mu} - m^2_\sigma\right]\sigma^* = 0 \tag{4.10}$$

$$\nabla_\mu Z^{\mu\nu} + ig_\sigma[\sigma^* D^\nu\sigma - (D^{*\nu}\sigma^*)\sigma] - m^2_\phi\phi^\nu = 0. \tag{4.11}$$

From the mean-field approximation, the stationary scalar field ansatz is given by

$$\sigma(r,t) = (Ae^{ikr} + Be^{-ikr})e^{-iwt}, \tag{4.12}$$

with A and B = real constants, k = the wave number, and ω = the eigen frequency of the spherically symmetric bound state of the scalar field. If the vector field is treated as a classical field, then $\phi_\mu = (\phi_0, 0)$, with ϕ_0 = constant. Applying the fields σ and ϕ_μ into the equations of motion, and letting $k = 0$, we find $\omega = g_\sigma\phi_0 \pm m_\sigma$. Considering that m_σ could be larger than $g_\sigma\phi_0$, we assume $\omega > 0$ and take the "+" solution. From the equation of motion of ϕ_μ and $\phi_\mu = (\phi_0, 0)$ we have that $m^2_\phi\phi_0 = 2g_\sigma m_\sigma\sigma^*\sigma$.

For the calculation of J^μ, let's take $J_0 = \rho_\sigma$, where ρ_σ = ADM number density, leading us to

$$J^\mu = \frac{i}{\sqrt{g}}\left(\sigma^*\frac{\partial\mathcal{L}_\sigma}{\partial\nabla_\mu\sigma^*} - \frac{\partial\mathcal{L}_\sigma}{\partial\nabla_\mu\sigma}\sigma\right) = -i(\sigma^*\nabla^\mu\sigma - (\nabla^\mu\sigma^*)\sigma) + 2g_\sigma\phi^\mu\sigma^*\sigma. \tag{4.13}$$

Since $J_0 = g_{0\nu}J^\nu$, and using the equation for ω, we can obtain $\rho_\sigma = 2\omega\sigma^*\sigma - 2g_\sigma\phi^\mu\sigma^*\sigma = 2m_\sigma\sigma^*\sigma \Rightarrow \phi_0 = \frac{g_\sigma}{m^2_\phi}\rho_\sigma$. The energy-momentum tensor is obtained as

$$T_{\mu\nu} = 2D^*_\mu\sigma^* D_\nu\sigma - g_{\mu\nu}\left(D^*_\rho\sigma^* D^\rho\sigma + m^2_\sigma\sigma^*\sigma\right) + m^2_\sigma\left(\phi_\mu\phi_\nu - \frac{1}{2}g_{\mu\nu}\phi_\rho\phi^\rho\right), \tag{4.14}$$

and it is used to find the equations of state for the bosonic DM model, which are given

by

$$\mathcal{E}_{\rm BDM} = m_\sigma \rho_\sigma + \frac{1}{2} C_{\sigma\phi}^2 \rho_\sigma^2, \tag{4.15}$$

$$P_{\rm BDM} = \frac{1}{2} C_{\sigma\phi}^2 \rho_\sigma^2, \tag{4.16}$$

with $C_{\sigma\phi} = g_\sigma / m_\phi$.

When analyzing bosonic DM inside compact stars, it is important to highlight that Black holes can be formed once a certain limit is reached (McDermott *et al.* 2012). For fermionic matter in its ground state, the Pauli exclusion principle counteracts gravity through the presence of degeneracy pressure. In contrast, bosonic systems lack the Fermi pressure, resulting in a lower limit for stability. However, this limit can be raised due to repulsive interactions, as indicated by Eq. (4.8). To satisfy this condition, we restrict the values of m_σ and $C_{\sigma\phi}$ to 10^{-2} MeV $\leqslant m_\sigma \leqslant 10^8$ MeV and 10^{-2} MeV$^{-1} \leqslant C_{\sigma\phi} \leqslant 10^3$ MeV^{-1}, respectively, in agreement to the findings of (Rutherford *et al.* 2023). For a deeper study of scalar fields, one can check (Khlopov *et al.* 1985). Other related bosonic dark matter models that interact with luminous matter, especially in the context of neutron stars, were examined in (Shakeri e Karkevandi 2024; Karkevandi *et al.* 2024).

4.2 Two-fluid approach

The goal of the study in this chapter is to analyze the characteristics arising from strange stars admixed with dark matter. For this purpose, the two-fluid approach is a suitable treatment, where the inter-fluid interaction uniquely comes from gravitational effects. This method treats the star as composed of two distinct fluids, allowing a detailed analysis of their respective contributions to the star's structure and stability. One fluid represents quark matter (identified as "visible" matter), while the other represents dark matter. Each fluid has its energy density $\mathcal{E}$ and pressure P, satisfying the conservation of energy-momentum separately. In other words, that is equivalent to having $P(r) = P_{\rm vis}(r) + P_{\rm DM}(r)$ and $\mathcal{E}(r) = \mathcal{E}_{\rm vis}(r) + \mathcal{E}_{\rm DM}(r)$, with r being the radial coordinate from the center of the star.

Usually, we make use of the TOV equations to obtain the mass and radius of the stars, but these equations are solved for a one-fluid only. For our study, it is necessary to develop TOV equations considering the two-fluid approach. Following what was done in (Xiang *et al.* 2014), we start from the star mass given by

$$M = \int_0^\infty 4\pi r^2 [\mathcal{E}_{\rm vis}(r) + \mathcal{E}_{\rm DM}(r)] dr, \tag{4.17}$$

which needs to be stationary concerning all variations of $\mathcal{E}_{\rm vis}(r)$ and $\mathcal{E}_{\rm DM}(r)$ to achieve the equilibrium of a particular stellar configuration when one has the uniform entropy per particle and the chemical composition of the "visible" and dark contribution in hands. At the same time, the energy densities must maintain the conservation of the quantities

$$N_{\rm vis} = \int_0^\infty 4\pi r^2 \rho_{\rm vis}(r) \left[1 - \frac{2Gm(r)}{r}\right]^{-1/2} dr, \tag{4.18}$$

$$N_{\rm DM} = \int_0^\infty 4\pi r^2 \rho_{\rm DM}(r) \left[1 - \frac{2Gm(r)}{r}\right]^{-1/2} dr, \tag{4.19}$$

where $m(r) = m_{\rm vis}(r) + m_{\rm DM}(r)$ is the total mass contained in the sphere of radius r. The visible matter mass is $m_{\rm vis}(r)$, and the dark matter mass is $m_{\rm DM}(r)$. These equations will keep the entropy per particle and the chemical composition unchanged. To ensure that is the case, the Lagrange multipliers λ and α are introduced, and the function variation for the given variation $\delta\mathcal{E}_{\rm vis}(r)$ and $\delta\mathcal{E}_{\rm DM}(r)$ is written as

$$\begin{aligned}
\delta M - \lambda\delta N_{\rm vis} - \alpha\delta N_{\rm DM} = &\int_0^\infty 4\pi r^2[\delta\mathcal{E}_{\rm vis}(r) + \delta\mathcal{E}_{\rm DM}(r)]dr \\
&- \lambda\int_0^\infty 4\pi r^2 \left[1 - \frac{2Gm(r)}{r}\right]^{-1/2} \delta\rho_{\rm vis}(r)dr \\
&- \lambda G\int_0^\infty 4\pi r^2 \left[1 - \frac{2Gm(r)}{r}\right]^{-3/2} \rho_{\rm vis}(r)\delta m(r)dr \\
&- \alpha\int_0^\infty 4\pi r^2 \left[1 - \frac{2Gm(r)}{r}\right]^{-1/2} \delta\rho_{\rm DM}(r)dr \\
&- \alpha G\int_0^\infty 4\pi r^2 \left[1 - \frac{2Gm(r)}{r}\right]^{-3/2} \rho_{\rm DM}(r)\delta m(r)dr,
\end{aligned} \tag{4.20}$$

with

$$\delta m(r) = \int_0^r 4\pi r'^2[\delta\mathcal{E}_{\rm vis}(r') + \delta\mathcal{E}_{\rm DM}(r')]dr'. \tag{4.21}$$

Notice that the integrands vanish outside $R + \delta R$ and the upper limit ∞ is used for convenience. With these variations, the entropy for "visible" and dark matter is supposed to remain unchanged, and we have that

$$\delta\left(\frac{\mathcal{E}_{\rm vis}(r)}{\rho_{\rm vis}(r)}\right) + P_{\rm vis}(r)\delta\left(\frac{1}{\rho_{\rm vis}(r)}\right) = 0, \tag{4.22}$$

$$\delta\left(\frac{\mathcal{E}_{\rm DM}(r)}{\rho_{\rm DM}(r)}\right) + P_{\rm DM}(r)\delta\left(\frac{1}{\rho_{\rm DM}(r)}\right) = 0, \tag{4.23}$$

thus

$$\delta\rho_{\rm vis}(r) = \frac{\rho_{\rm vis}(r)}{P_{\rm vis}(r)+\mathcal{E}_{\rm vis}(r)}\delta\mathcal{E}_{\rm vis}(r), \tag{4.24}$$

$$\delta\rho_{\rm DM}(r) = \frac{\rho_{\rm DM}(r)}{P_{\rm DM}(r)+\mathcal{E}_{\rm DM}(r)}\delta\mathcal{E}_{\rm DM}(r). \tag{4.25}$$

Applying Eq. (4.21) in Eq. (4.20), and interchanging the r and r' integrals, we find

$$\begin{aligned}\delta M - \lambda\delta N_{\rm vis} - \alpha\delta N_{\rm DM} = &\int_0^\infty 4\pi r^2\{1 - \frac{\lambda\rho_{\rm vis}(r)}{P_{\rm vis}(r)+\mathcal{E}_{\rm vis}(r)}\left[1-\frac{2Gm(r)}{r}\right]^{-1/2}\\ &- \lambda F_{\rm vis}(r) - \alpha F_{\rm DM}(r)\}\delta\mathcal{E}_{\rm vis}dr\\ &+\int_0^\infty 4\pi r^2\{1 - \frac{\alpha\rho_{\rm DM}(r)}{P_{\rm DM}(r)+\mathcal{E}_{\rm DM}(r)}\left[1-\frac{2Gm(r)}{r}\right]^{-1/2}\\ &- \lambda F_{\rm vis}(r) - \alpha F_{\rm DM}(r)\}\delta\mathcal{E}_{\rm DM}dr,\end{aligned} \tag{4.26}$$

with the quantities $F_{\rm vis}$ and $F_{\rm DM}$ being defined as

$$F_{\rm vis}(r) = G\int_0^\infty 4\pi r'\rho_{\rm vis}(r')\left[1-\frac{2GM(r')}{r'}\right]^{-3/2}dr', \tag{4.27}$$

$$F_{\rm DM}(r) = G\int_0^\infty 4\pi r'\rho_{\rm DM}(r')\left[1-\frac{2GM(r')}{r'}\right]^{-3/2}dr'. \tag{4.28}$$

From Eq. (4.26), $\delta M - \lambda\delta N_{\rm vis} - \alpha\delta N_{\rm DM}$ will vanish for all $\delta\mathcal{E}_{\rm vis}(r)$ and $\delta\mathcal{E}_{\rm DM}(r)$, if and only if,

$$1 - \frac{\lambda\rho_{\rm vis}(r)}{P_{\rm vis}(r)+\mathcal{E}_{\rm vis}(r)}\left[1-\frac{2Gm(r)}{r}\right]^{-1/2} - \lambda F_{\rm vis}(r) - \alpha F_{\rm DM}(r) = 0, \tag{4.29}$$

$$1 - \frac{\alpha\rho_{\rm DM}(r)}{P_{\rm DM}(r)+\mathcal{E}_{\rm DM}(r)}\left[1-\frac{2Gm(r)}{r}\right]^{-1/2} - \lambda F_{\rm vis}(r) - \alpha F_{\rm DM}(r) = 0, \tag{4.30}$$

which can be rewritten as

$$\frac{\rho_{\rm vis}(r)}{P_{\rm vis}(r)+\mathcal{E}_{\rm vis}(r)}\left[1-\frac{2Gm(r)}{r}\right]^{-1/2} + F_{\rm vis}(r) + \frac{\alpha}{\lambda}F_{\rm DM}(r) = \frac{1}{\lambda}, \tag{4.31}$$

$$\frac{\rho_{\rm DM}(r)}{P_{\rm DM}(r)+\mathcal{E}_{\rm DM}(r)}\left[1-\frac{2Gm(r)}{r}\right]^{-1/2} + F_{\rm DM}(r) + \frac{\lambda}{\alpha}F_{\rm vis}(r) = \frac{1}{\alpha}, \tag{4.32}$$

with

$$\frac{\lambda}{\alpha} = \frac{\rho_{\rm DM}(r)[P_{\rm vis}(r)+\mathcal{E}_{\rm vis}(r)]}{\rho_{\rm vis}(r)[P_{\rm DM}(r)+\mathcal{E}_{\rm DM}(r)]}, \tag{4.33}$$

which is obtained from the left-hand side of Eqs. (4.29) and (4.30) once they are equalized.

Now, let's take the derivative of both sides of Eq. (4.31), we have

$$\begin{aligned}
&\left\{\frac{\rho'_{\rm vis}(r)}{P_{\rm vis}(r)+\mathcal{E}_{\rm vis}(r)}-\frac{\rho_{\rm vis}(r)[P'_{\rm vis}(r)+\mathcal{E}'_{\rm vis}(r)]}{[P_{\rm vis}(r)+\mathcal{E}_{\rm vis}(r)]^2}\right\}\left[1-\frac{2Gm(r)}{r}\right]^{-1/2}\\
&+\frac{G\rho_{\rm vis}(r)}{P_{\rm vis}(r)+\mathcal{E}_{\rm vis}(r)}\left\{4\pi r[\mathcal{E}_{\rm DM}(r)+\mathcal{E}_{\rm vis}(r)]-\frac{m(r)}{r^2}\right\}\left[1-\frac{2Gm(r)}{r}\right]^{-3/2}\\
&-4\pi rG\rho_{\rm vis}(r)\left[1-\frac{2Gm(r)}{r}\right]^{-3/2}\\
&-4\pi rG\rho_{\rm vis}(r)\frac{P_{\rm DM}(r)+\mathcal{E}_{\rm DM}(r)}{P_{\rm vis}(r)+\mathcal{E}_{\rm vis}(r)}\left[1-\frac{2Gm(r)}{r}\right]^{-3/2}=0.
\end{aligned}\tag{4.34}$$

For uniform entropy per nucleon, the condition is given as

$$\frac{d}{dr}\left(\frac{\mathcal{E}_{\rm vis}(r)}{\rho_{\rm vis}(r)}\right)+P_{\rm vis}(r)\frac{d}{dr}\left(\frac{1}{\rho_{\rm vis}(r)}\right)=0,\tag{4.35}$$

which leads to

$$\rho'_{\rm vis}(r)=\frac{\rho_{\rm vis}(r)\mathcal{E}'_{\rm vis}(r)}{P_{\rm vis}(r)+\mathcal{E}_{\rm vis}(r)}.\tag{4.36}$$

If we take Eq. (4.36) and substitute in Eq. (4.34), we find the TOV equation for "visible" matter as being

$$\rho'_{\rm vis}(r)=-G[P_{\rm vis}(r)+\mathcal{E}_{\rm vis}(r)]\left[1-\frac{2Gm(r)}{r}\right]^{-1}\left\{4\pi r[P_{\rm vis}(r)+P_{\rm DM}(r)]+\frac{m(r)}{r^2}\right\}.\tag{4.37}$$

Similarly, we can calculate the TOV equation for dark matter as

$$\rho'_{\rm DM}(r)=-G[P_{\rm DM}(r)+\mathcal{E}_{\rm DM}(r)]\left[1-\frac{2Gm(r)}{r}\right]^{-1}\left\{4\pi r[P_{\rm vis}(r)+P_{\rm DM}(r)]+\frac{m(r)}{r^2}\right\}.\tag{4.38}$$

We can rewrite the TOV equations for "visible" and dark matter as follows

$$\frac{dP_{\rm vis}(r)}{dr}=-\frac{[\mathcal{E}_{\rm vis}(r)+P_{\rm vis}(r)]\,[m(r)+4\pi r^3P(r)]}{r\,[r-2m(r)]},\tag{4.39}$$

$$\frac{dP_{\rm DM}(r)}{dr}=-\frac{[\mathcal{E}_{\rm DM}(r)+P_{\rm DM}(r)]\,[m(r)+4\pi r^3P(r)]}{r\,[r-2m(r)]},\tag{4.40}$$

$$\frac{dm_{\rm vis}(r)}{dr}=4\pi r^2\mathcal{E}_{\rm vis}(r),\tag{4.41}$$

$$\frac{dm_{\rm DM}(r)}{dr}=4\pi r^2\mathcal{E}_{\rm DM}(r).\tag{4.42}$$

In these equations, one has DM = FDM (BDM) for fermionic (bosonic) dark matter. These equations are solved to model strange stars admixed with dark matter, and the procedure adopted here is: there are four initial conditions defined as $m_{\rm vis}(0) = m_{\rm DM}(0) = 0$, $P_{\rm vis}(0) = P^c_{\rm vis}$, and $P_{\rm DM}(0) = P^c_{\rm DM}$, where $P^c_{\rm vis}$ and $P^c_{\rm DM}$ are the central pressures related to "visible" and dark matter, respectively, given by the equations of state presented in the previous sections. For each set of initial conditions, the fourth-order Runge–Kutta method is used to obtain pressures and masses as functions of r. As for the the radii $R_{\rm vis}$ and $R_{\rm DM}$, we define them as quantities that lead to $P_{\rm vis}(R_{\rm vis})/P^c_{\rm vis} = 0$ and $P_{\rm DM}(R_{\rm DM})/P^c_{\rm DM} = 0$, within a certain tolerance. These radii are also useful to determine $M_{\rm vis} \equiv m_{\rm vis}(R_{\rm vis})$, and $M_{\rm DM} \equiv m_{\rm DM}(R_{\rm DM})$. Therefore, the total mass of the respective star is $M = M_{\rm vis} + M_{\rm DM}$, and its radius is $R = R_{\rm vis}$ if $R_{\rm vis} > R_{\rm DM}$, or $R = R_{\rm DM}$ if $R_{\rm DM} > R_{\rm vis}$. This latter case identifies dark matter halo configurations for the star of mass M and radius R. This mechanism is repeated for each point of the input equations of state, resulting in the final collected pairs (M, R) that form the mass-radius diagram.

In every star, a certain fraction of dark matter must be present in its composition, i.e., a fixed value of $F_{\rm DM} = M_{\rm DM}/M$. To satisfy this condition, first all the inputs for the TOV equations are constructed, namely $P^c_{\rm vis}$, $\mathcal{E}^c_{\rm vis}$, $P^c_{\rm DM}$ and $\mathcal{E}^c_{\rm DM}$ (although not used as initial conditions, the energy densities must also be provided since their relations with the pressures are utilized to replace $\mathcal{E}$'s by P's in the TOV equations). The "visible" matter equations of state (EOS) are straightforward, directly evaluated from Eq. (2.37). For both DM models, fermionic and bosonic, its EOS are connected with the ones from the "visible" sector through $\mathcal{E}_{\rm DM} = f\mathcal{E}_{\rm vis}$, where the energy density fraction, f, is a constant (Xiang *et al.* 2014) varying from 0 to 1. In the case of the bosonic DM model, this leads to an analytical expression for the dark boson density, given by

$$\rho_\sigma = \frac{m_\sigma}{C^2_{\sigma\phi}} \left(\sqrt{1 + \frac{2C^2_{\sigma\phi}}{m^2_\sigma} f\mathcal{E}_{\rm vis}} - 1 \right), \tag{4.43}$$

and, consequently, to a direct relation between dark pressure and quark energy density that reads as

$$P_{\rm BDM} = \frac{m^2_\sigma}{2C^2_{\sigma\phi}} \left(\sqrt{1 + \frac{2C^2_{\sigma\phi}}{m^2_\sigma} f\mathcal{E}_{\rm vis}} - 1 \right)^2. \tag{4.44}$$

Nevertheless, there are no analytical expressions linking the equations of state for quark matter and dark matter in the fermionic dark matter case. The free parameters of the dark sector used here are $m_\sigma = 15$ GeV (Rutherford *et al.* 2023), $C_{\sigma\phi} = 0.1$ MeV^{-1} (Rutherford *et al.* 2023), $m_\chi = 1.9$ GeV, and $C_V = 3.26$ fm. The last two values, inside the ranges 0.5 GeV $\leqslant m_\chi \leqslant$ 4.5 GeV (Calmet e Kuipers 2021) and

0.1 fm $\leqslant C_V \leqslant$ 5 fm (Xiang *et al.* 2014), were taken from (Thakur *et al.* 2024). As an illustration, we display BDM and FDM cases in Fig. 4.1 for fixed f.

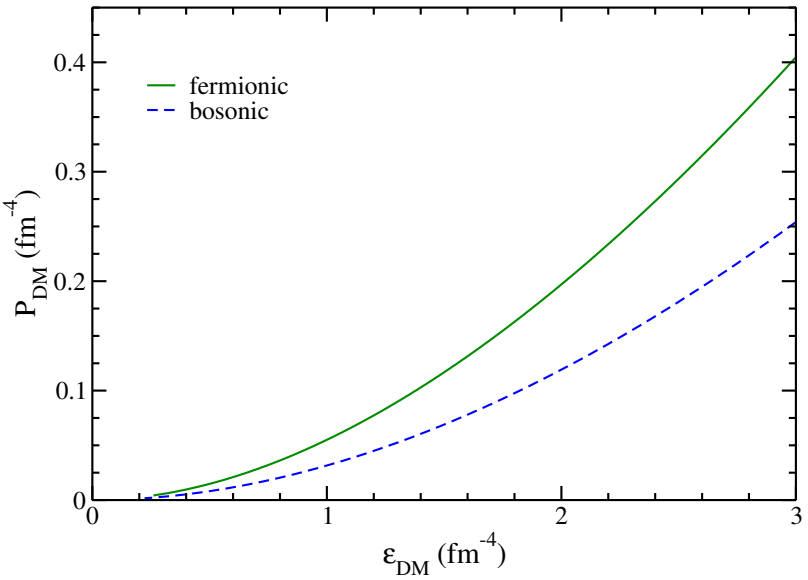

FIGURE 4.1 – Dark matter pressure as a function of its respective energy density for the fermionic and bosonic cases.

Note that for the selected set of parameters, the fermionic equation of state is stiffer than the BDM one, as expected. Given the relation $\mathcal{E}_{\rm DM} = f\mathcal{E}_{\rm vis}$, the two-fluid TOV equations are solved for a wide range of values for f. For each solution corresponding to a specific f, we evaluate $F_{\rm DM}$ and select only the solutions where the (M, R) pairs that meet the chosen value of $F_{\rm DM}$. The final outcome is a mass-radius diagram representing quark stars, each containing a fixed fraction of dark matter.

It is important to point out that the two-fluid approach requires a thorough analysis of the stability of the resulting compact quark-dark matter star, as detailed in (Barbat *et al.* 2024; Hippert *et al.* 2023). In a single-fluid system, the search for stable configurations involves examining the star's response to radial oscillations through a Sturm-Liouville problem for the relative radial displacement and the pressure perturbation, both of which depend on time via $e^{i\omega t}$, where ω is the eigenfrequency. Essentially, the solutions to the resulting differential equations indicate that stable stars are those for which $\omega^2 > 0$. Conversely, solutions with $\omega^2 < 0$ correspond to an exponentially growing perturbation, ultimately leading to the collapse of the compact star, as discussed in the previous chapter. For homogeneous stars case - those with a single phase - the location of the last stable configuration ($\omega = 0$) aligns with the maximum mass point in the mass-radius diagram, corresponding to the condition $\partial M/\partial \mathcal{E}^c = 0$.

In the two-fluid approach, the generalization indicates that, at the onset of unstable

configurations, the number of "visible" ($N_{\rm vis}$) and dark ($N_{\rm DM}$) particles remain constant under variations of $\mathcal{E}^c_{\rm vis}$ and $\mathcal{E}^c_{\rm DM}$. As noted in (Hippert *et al.* 2023; Barbat *et al.* 2024), it is analogous to diagonalizing the matrix $\partial N_i/\partial \mathcal{E}^c_j$ (i, j=VIS, DM) to identify its associated eigenvalues, which should be positive for stable stars configurations. However, as discussed in (Hong e Ren 2024), dark matter models with central pressures in the range of $P^c_{\rm DM} \lesssim 5.1$ fm^{-4} are expected to produce stars in a stable region. Here, both DM models, bosonic and fermionic, comply with this constraint. Moreover, the authors of (Liu *et al.* 2023; Liu *et al.* 2024) have noted in their calculations, based on prior studies (Leung *et al.* 2012; Leung *et al.* 2022), that the maxima of the fixed $F_{\rm DM}$ curves correspond to the last stable stars in the mass-radius diagram, similar to one-fluid systems. In our study, we adopt the same procedure and exclude points beyond the maximum. The resulting mass-radius diagrams for both models are presented in Fig. 4.2.

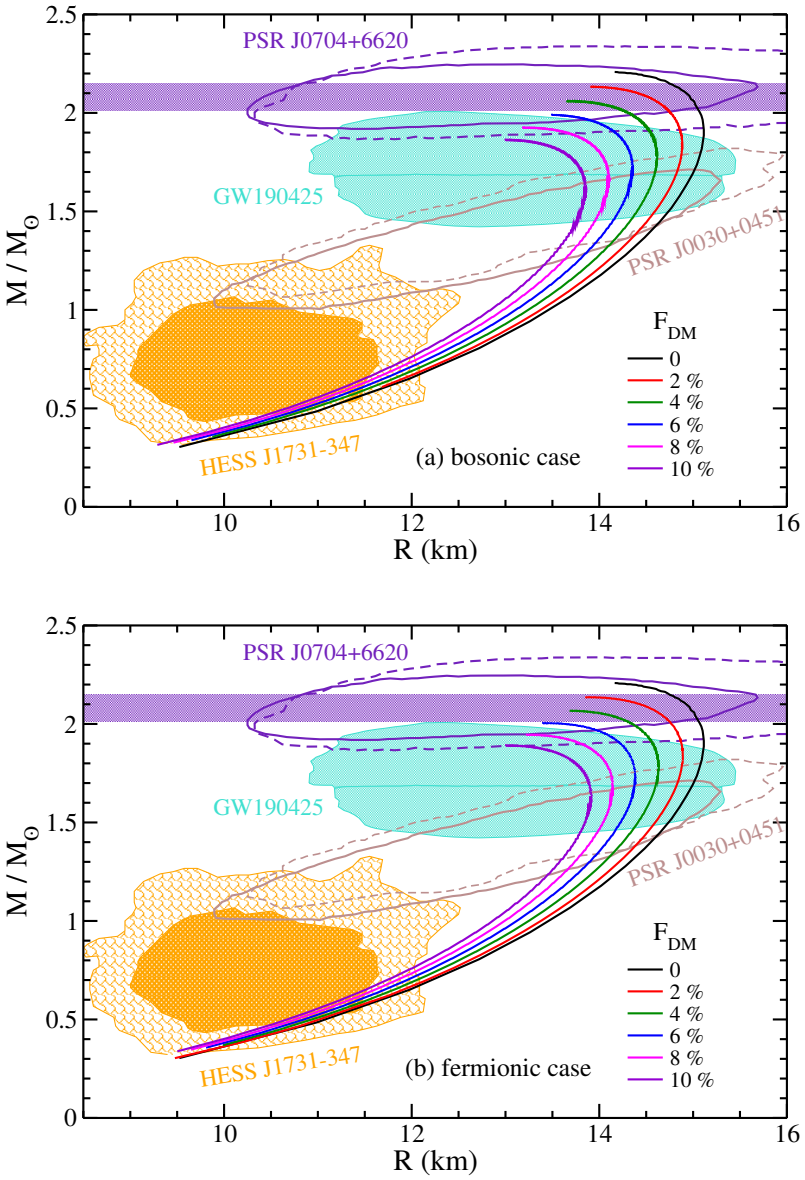

FIGURE 4.2 – Mass-radius relations for different fractions of dark matter in each strange stars. Results for (a) bosonic and (b) fermionic cases. The brown contours are related to data from the NICER mission, namely, PSR J0030+0451 (Riley *et al.* 2019; Miller *et al.* 2019) and PSR J0740+6620 (Riley *et al.* 2021; Miller *et al.* 2021), and blue ones are related to the GW190425 event (Abbott *et al.* 2020), all of them at 90% credible level. The orange contours are related to HESS J1731-347 measurement (DOROSHENKO *et al.* 2022). The violet horizontal lines are also related to the PSR J0740+6620 pulsar (Fonseca *et al.* 2021).

From this figure, it is clear that the maximum mass ($M_{\rm max}$) of each diagram decreases as the dark mass fraction increases. This trend aligns with previous studies that predict a reduction in stars configurations featuring a DM core (Nelson *et al.* 2019; Ellis *et al.* 2018; Ivanytskyi *et al.* 2020; Leung *et al.* 2011; Karkevandi *et al.* 2022). As an illustration, we plot $M_{\rm max}$ versus $F_{\rm DM}$ for both cases (BDM and FDM models) in Fig. 4.3.

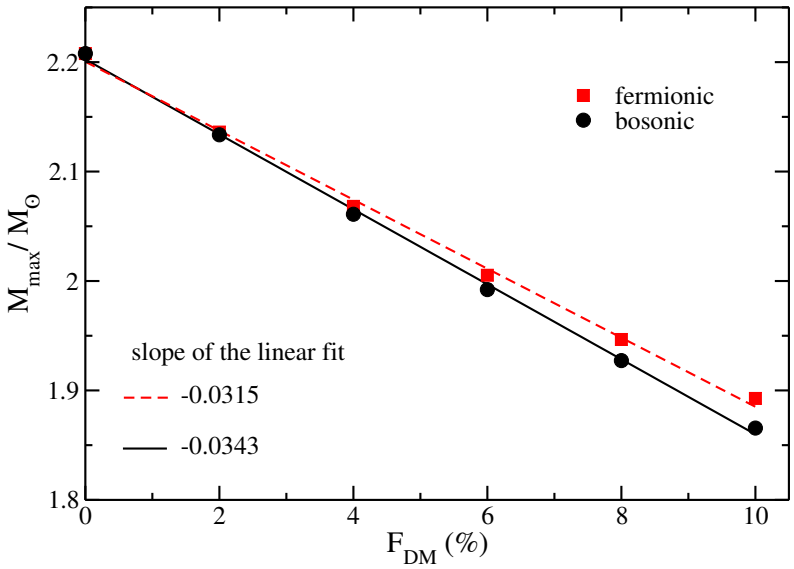

FIGURE 4.3 – Maximum total mass versus mass fraction for the strange-DM stars presented in Fig. 4.2.

It is noteworthy that there is a strong linear relationship between the maximum mass and the dark matter content. Consequently, the rate of decreasing $M_{\rm max}$ as a function of $F_{\rm DM}$ remains constant. This behavior is difficult to predict beforehand due to the complex structure of both the two-fluid equations and the equations of state employed as input - specifically, the EQP model for the "visible" sector and the fermionic/bosonic models for the dark one. We also provide the slope of the linear fit, which is -0.0343 for the bosonic and -0.0315 for the fermionic model; notably, both slopes are quite similar. Furthermore, these values are very close to -0.0362, a result obtained in (Mukhopadhyay e Schaffner-Bielich 2016) using a different quark model in the ordinary matter sector: the MIT bag model. In their dark sector, they employed a model consisting of fermionic particles with a mass of 100 GeV, which is more than 50 times greater than the mass used for the FDM model in our study. This similarity may suggest a potential universality in the linear decreasing trend of maximum mass in quark models mixed with dark matter.

In Fig. 4.3, the FDM model produces maximum masses slightly greater than the ones generated from the BDM model, a feature observed for the range of parameters investigated in our analysis. This indicates that the dark matter equations of state are stiffer for the fermionic case with fixed dark matter content compared to the bosonic description of the dark sector, as we have previously shown in Fig. 4.1. Although this particular figure was plotted for a fixed f, the input equations of state remain the same, so the curves produced for a constant value of $F_{\rm DM}$ are also identical.

Continuing with the characteristics related to Fig. 4.2, we emphasize that the differences between the complete mass-radius curves generated from the quark-FDM approach and the quark-BDM one are minimal. We attribute this effect to the dominance of the effective quark model over both the bosonic and fermionic dark matter models employed in our analysis. To illustrate this point, we display in Figs. 4.4 the profiles of the same star constructed by using both BDM and FDM models, with $M = 1.81 M_{\odot}$ and 10% of dark matter in its composition.

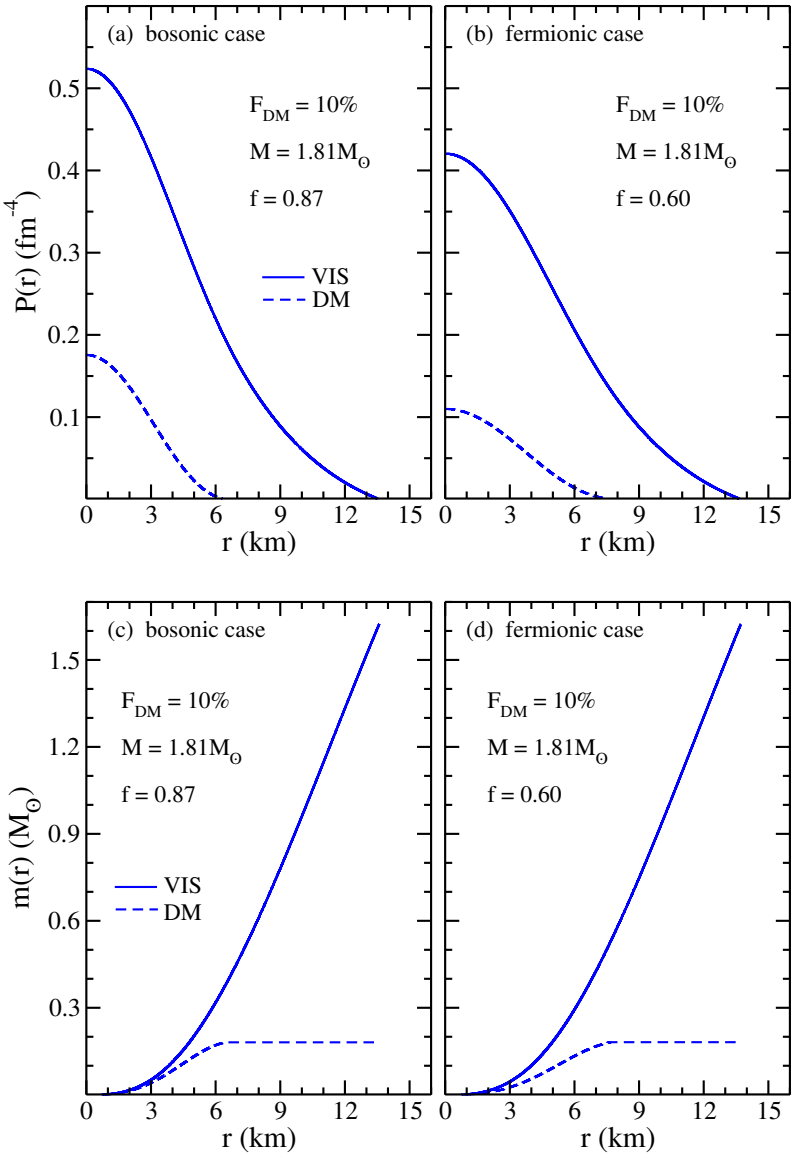

FIGURE 4.4 – Pressure (panels a and b) and enclosed mass (panels c and d) as functions of the radial coordinate for a mass fraction equal to 10% and total stellar mass of $M = 1.81 M_{\odot}$. Full (dashed) lines: visible (dark) matter. For the bosonic (fermionic) case in panel a (b), the energy density fraction is $f = 0.87$ (0.6).

From this example, we see that the radius of the star is $R = R_{\rm vis} \simeq 13.6$ (13.7) km,

since $R_{\rm vis} > R_{\rm DM}$ in this case, using the bosonic (fermionic) model for the dark sector. The primary change resulting from the switch between dark matter models is in the central pressure (at $r = 0$) in both sectors. However, $R_{\rm vis}$ remains nearly identical for both models, determining the final star's radius based on the criterion that R corresponds to the outermost radius between $R_{\rm vis}$ and $R_{\rm DM}$. This is not the case for stars that have a dark matter halo surrounding them. We can observe this effect in the example of $M = 1.86 M_{\odot}$ and $F_{\rm DM} = 10\%$, as shown in Fig. 4.5, particularly for the strange star constructed with the inclusion of bosonic dark matter. In this figure, we present two parametrizations of the

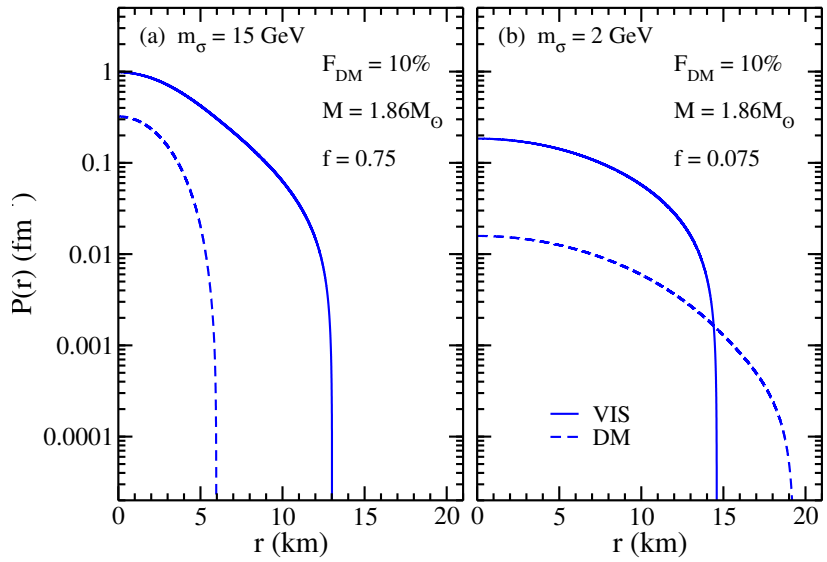

FIGURE 4.5 – Pressure as a function of radial coordinate for a mass fraction equal to 10% and total stellar mass of $M = 1.86 M_{\odot}$. Full (dashed) lines: visible (dark) matter. Strange star admixed with the bosonic dark matter with $m_\sigma = 15$ GeV (panel a) and $m_\sigma = 2$ GeV (panel b).

BDM model, specifically with different dark boson masses: $m_\sigma = 15$ GeV (standard value previously used) and $m_\sigma = 2$ GeV. Notice that reducing the dark particle mass leads to the condition $R_{\rm DM} > R_{\rm vis}$, consequently producing the formation of a DM halo. In this case, the radius of the final star changes from $R = R_{\rm vis} \simeq 13$ km to $R = R_{\rm DM} \simeq 19$ km. Since fermionic and bosonic models generate similar mass-radius diagrams for $m_\sigma = 15$ GeV and $m_\chi = 1.9$ GeV, the decrease in m_σ will create a more pronounced difference between the diagrams obtained from FDM model with $m_\chi = 1.9$ GeV with those from the BDM model with $m_\sigma = 2$ GeV, due to the emergence of DM halos in the latter. These features are compatible with findings in studies such as (Karkevandi *et al.* 2022), where the authors utilized the two-fluid approach with bosonic DM and in (Routaray *et al.* 2023) which applied a fermionic dark matter model to describe stellar matter. In both cases, the formation of DM halos is observed when the mass of the dark particles (whether bosons or fermions) is decreased. While those studies focus on neutron stars using hadronic models for the visible matter sector, our work examines strange stars, yet exhibits the

same effect.

Last but not least, we remark on the compatibility of our results with the recent observational astrophysical data from the NICER mission concerning the millisecond pulsars PSR J0030+0451 (Riley *et al.* 2019; Miller *et al.* 2019) and PSR J0740+6620 (Riley *et al.* 2021; Miller *et al.* 2021), as well as data from the gravitational wave event GW190425 (Abbott *et al.* 2020) analyzed by LIGO and Virgo Collaboration. This consistency is also seen with the PSR J0740+6620 data extracted from (Fonseca *et al.* 2021), which corresponds to a mass of $M = (2.08 \pm 0.07)M_{\odot}$ at 68.3% of credible level, along with the compact star designated as HESS J1731-347 (DOROSHENKO *et al.* 2022). These findings suggest possible scenarios in which strange stars can contain dark matter in their interiors.

5 Conclusion

The first proposal presented in this work brought us interesting results concerning the dynamics of the quarks phase transition at zero temperature. From a density-dependent quark model, with its thermodynamic consistency verified, we performed the introduction of the Polyakov loop (Φ) in its equations of state. By applying the recent values for current quark masses, all of them extracted from PDG, we were able to describe a system more similar to what is believed to exist.

For the symmetric matter case, we could analyze the confinement/deconfinement phase transition through different thermodynamic quantities, and also identify the particular chemical potential in which it happens. For the stellar matter case, we could also analyze the model predictions and quark stars more specifically. The asymptotic freedom of quarks at high densities was analyzed through the baryonic density, in which a discontinuity exactly at the transition point was identified, and the deconfined phase was found to be attained for values of ρ_b in a range of around 3 to 7 times the nuclear matter saturation density. In sequence, the quark masses analysis showed that the emergence of $\Phi \neq 0$ solutions led these quantities to a strong reduction, indicating a behavior similar to a chiral symmetry restoration of the system.

The EOS analysis of the PEQP model verified that the decreasing of the additional free parameter of the model increases the transition pressure plateau and the gap in the energy density presented by the confinement/deconfinement phase transition. For the mass-radius profiles themselves, the PEQP model was capable of generating quark stars with stable configurations that agree with the recent observational data provided by the NICER mission concerning the millisecond pulsars PSR J0030+0451 and PSR J0740+6620, and by the LIGO and Virgo Collaboration regarding the gravitational wave event named GW190425.

For the second proposal of this work, we explored the possible scenarios regarding the existence of strange quark stars that incorporate dark matter. We employed the equiparticle (EQP) model to describe strongly interacting matter, where the masses of the constituent quarks (u, d, s quarks) are affected by the medium through specific baryonic density-dependent functions. The parameters in these functions were selected based on

an analysis of the stability window of stellar matter, ensuring that they yield lower energy per baryon compared to iron nuclei.

The dark matter content of the system was examined through two distinct models: a fermionic model and a bosonic one. The fermionic model is described by a Lagrangian density in which the dark spinor experiences a repulsive interaction from a dark vector field. The equations of state in this model are determined by two free parameters: the dark fermion mass (m_χ), and the ratio of the vector interaction strength (g_V) to the vector field mass (m_V). We consider these quantities within the ranges of 0.5 GeV $\leqslant m_\chi \leqslant$ 4.5 GeV and 0.1 fm $\leqslant C_V = g_V/m_V \leqslant$ 5 fm. In the bosonic model, we adopt a version that neglects interactions between the dark boson and the quarks. Similar to the fermionic model, we incorporate a vector interaction, which is essential to prevent the star from collapsing due to the lack of degeneracy pressure. We derive the final equations for energy density and pressure, which also depend on two free parameters: the dark scalar mass (m_σ) and $C_{\sigma\phi} = g_\sigma/m_\sigma$, where g_σ is the interaction strength of the dark scalar field with the dark vector field. Here we consider values compatible with 10^{-2} MeV $\leqslant m_\sigma \leqslant 10^8$ MeV and 10^{-2} MeV$^{-1} \leqslant C_{\sigma\phi} \leqslant 10^3$ MeV^{-1}.

With the luminous and dark matter models established, we allowed both sectors to interact solely through gravity using a two-fluid approach. Our findings suggest that strange stars mixed with dark matter, characterized by a fixed dark matter fraction, could represent a viable scenario consistent with the astrophysical observational data previously mentioned with the inclusion of the measurement related to the compact star named HESS J1731-347. Additionally, we also identify stars that have dark matter halo configurations for smaller dark particle masses.

As for prospects, we are interested in continuing to work with the EQP and PEQP models to explore their capabilities in different scenarios that concern strange matter, such as hybrid stars and heavy ion collisions, for instance. To finish, let me address here that the work performed in chapter 3 was published as a paper in the Physical Review D (PRD 108, 083006). As for the work performed in chapter 4, the paper concerning its study was also submitted to a scientific journal with a good impact factor, and we are waiting for the response.

Bibliography

ABBOTT, B. P.; ABBOTT, R.; ABBOTT, T. D.; ACERNESE, F.; ACKLEY, K. *et al.* Gw170817: Observation of gravitational waves from a binary neutron star inspiral. **Phys. Rev. Lett.**, American Physical Society, v. 119, p. 161101, Oct 2017. Available at: https://link.aps.org/doi/10.1103/PhysRevLett.119.161101. 14

ABBOTT, B. P.; ABBOTT, R.; ABBOTT, T. D.; ACERNESE, F.; ACKLEY, K.; ADAMS, C. *et al.* Multi-messenger observations of a binary neutron star merger*. **The Astrophysical Journal Letters**, The American Astronomical Society, v. 848, n. 2, p. L12, oct 2017. Available at: https://dx.doi.org/10.3847/2041-8213/aa91c9. 14

ABBOTT, B. P.; ABBOTT, R.; ABBOTT, T. D.; ACERNESE, F.; ACKLEY *et al.* Gw170817: Measurements of neutron star radii and equation of state. **Phys. Rev. Lett.**, American Physical Society, v. 121, p. 161101, Oct 2018. Available at: https://link.aps-.org/doi/10.1103/PhysRevLett.121.161101. 14

ABBOTT, B. P.; ABBOTT, R.; ABBOTT, T. D.; ABRAHAM, S.; ACERNESE, F. *et al.* Gw190425: Observation of a compact binary coalescence with total mass 3.4 m. **The Astrophysical Journal Letters**, The American Astronomical Society, v. 892, n. 1, p. L3, mar 2020. Available at: https://dx.doi.org/10.3847/2041-8213/ab75f5. 14, 44, 45, 59, 63

ADAMS, J. A.; SARKAR, S.; SCIAMA, D. W. Cosmic microwave background anisotropy in the decaying neutrino cosmology. **Monthly Notices of the Royal Astronomical Society**, v. 301, n. 1, p. 210–214, 11 1998. ISSN 0035-8711. Available at: https://doi.org/10.1046-/j.1365-8711.1998.02017.x. 15, 47

AFFLECK, I.; DINE, M. A new mechanism for baryogenesis. **Nuclear Physics B**, v. 249, n. 2, p. 361–380, 1985. ISSN 0550-3213. Available at: https://www.sciencedirect.com-/science/article/pii/0550321385900215. 48

AGHANIM, N.; ARNAUD, M.; ASHDOWN, M.; AUMONT, J. e. a. Planck 2015 results - xi. cmb power spectra, likelihoods, and robustness of parameters. **Astronomy and Astrophysics**, v. 594, p. A11, 2016. Available at: https://doi.org/10.1051/0004-6361-/201526926. 15, 47

ALFORD, M. G.; SCHMITT, A.; RAJAGOPAL, K.; SCHÄFER, T. Color superconductivity in dense quark matter. **Rev. Mod. Phys.**, American Physical Society, v. 80, p. 1455–1515, Nov 2008. Available at: https://link.aps.org/doi/10.1103/RevModPhys.80-.1455. 12

ALKOFER, R.; SMEKAL, L. V. The infrared behaviour of qcd green's functions: Confinement, dynamical symmetry breaking, and hadrons as relativistic bound states. **Physics Reports**, v. 353, n. 5, p. 281–465, 2001. ISSN 0370-1573. Available at: https://www-.sciencedirect.com/science/article/pii/S0370157301000102. 13

ARBAÑIL, J. D. V.; MALHEIRO, M. Equilibrium and stability of charged strange quark stars. **Phys. Rev. D**, American Physical Society, v. 92, p. 084009, Oct 2015. Available at: https://link.aps.org/doi/10.1103/PhysRevD.92.084009. 45

ARBAÑIL, J. D. V.; RODRIGUES, L. S.; LENZI, C. H. Phase transition and stiffer core fluid in neutron stars: effects on stellar configurations, dynamical stability, and tidal deformability. **European Physical Journal C**, v. 83, n. 3, p. 211, mar. 2023. 45

ARBEY, A.; MAHMOUDI, F. Dark matter and the early universe: A review. **Progress in Particle and Nuclear Physics**, v. 119, p. 103865, 2021. ISSN 0146-6410. Available at: https://www.sciencedirect.com/science/article/pii/S0146641021000193. 14, 47

BACKES, B. C.; HAFEMANN, E.; MARZOLA, I.; MENEZES, D. P. Density dependent quark mass model revisited: Thermodynamic consistency, stability windows and stellar properties. **J. Phys. G**, v. 48, n. 5, p. 055104, 2021. 25

BARBAT, M. F.; SCHAFFNER-BIELICH, J.; TOLOS, L. Comprehensive study of compact stars with dark matter. **Phys. Rev. D**, American Physical Society, v. 110, p. 023013, Jul 2024. Available at: https://link.aps.org/doi/10.1103/PhysRevD.110.023013. 57, 58

BAUER, D.; BUCKLEY, J.; CAHILL-ROWLEY, M.; COTTA, R.; DRLICA-WAGNER, A.; FENG, J. L.; FUNK, S.; HEWETT, J.; HOOPER, D.; ISMAIL, A.; KAPLINGHAT, M.; KUSENKO, A.; MATCHEV, K.; MCKINSEY, D.; RIZZO, T.; SHEPHERD, W.; TAIT, T. M.; WIJANGCO, A. M.; WOOD, M. Dark matter in the coming decade: Complementary paths to discovery and beyond. **Physics of the Dark Universe**, v. 7-8, p. 16–23, 2015. ISSN 2212-6864. Available at: https://www.sciencedirect.com/science-/article/pii/S2212686415000059. 49

BERTONE, G.; HOOPER, D. History of dark matter. **Rev. Mod. Phys.**, American Physical Society, v. 90, p. 045002, Oct 2018. Available at: https://link.aps.org/doi/10.1103-/RevModPhys.90.045002. 14, 47

BERTONE, G.; HOOPER, D.; SILK, J. Particle dark matter: evidence, candidates and constraints. **Physics Reports**, v. 405, n. 5, p. 279–390, 2005. ISSN 0370-1573. Available at: https://www.sciencedirect.com/science/article/pii/S0370157304003515. 15

BODMER, A. R. Collapsed nuclei. **Phys. Rev. D**, v. 4, p. 1601 – 1606, 1971. 14, 17

BRAUN-MUNZINGER, P.; STACHEL, J. The quest for the quark–gluon plasma. **Nature**, v. 448, p. 302–309, 2007. ISSN 1476-4687. Available at: https://doi.org/10.1038-/nature06080. 12

BUBALLA, M. Njl-model analysis of dense quark matter. **Physics Reports**, v. 407, n. 4, p. 205–376, 2005. ISSN 0370-1573. Available at: https://www.sciencedirect.com/science-/article/pii/S037015730400506X. 28

BUCHMÜLLERA R. D. PECCEIB, T. Y. W. **Leptogenesis as the Origin of Matter**. Thesis (Doutorado) — Erwin Schrödinger International Institute for Mathematics and Physics, 2006. 48

CALMET, X.; KUIPERS, F. Theoretical bounds on dark matter masses. **Physics Letters B**, v. 814, p. 136068, 2021. ISSN 0370-2693. Available at: https://www.sciencedirect.com-/science/article/pii/S0370269321000083. 56

CHODOS, A.; JAFFE, R. L.; JOHNSON, K.; THORN, C. B. Baryon structure in the bag theory. **Phys. Rev. D**, American Physical Society, v. 10, p. 2599–2604, Oct 1974. Available at: https://link.aps.org/doi/10.1103/PhysRevD.10.2599. 13, 28

CHODOS, A.; JAFFE, R. L.; JOHNSON, K.; THORN, C. B.; WEISSKOPF, V. F. New extended model of hadrons. **Phys. Rev. D**, American Physical Society, v. 9, p. 3471–3495, Jun 1974. Available at: https://link.aps.org/doi/10.1103/PhysRevD.9.3471. 13, 28

CLOWE, D.; BRADAČ, M.; GONZALEZ, A. H.; MARKEVITCH, M.; RANDALL, S. W.; JONES, C.; ZARITSKY, D. A direct empirical proof of the existence of dark matter*. **The Astrophysical Journal**, v. 648, n. 2, p. L109, aug 2006. Available at: https:-//dx.doi.org/10.1086/508162. 14

DAS, A.; MALIK, T.; NAYAK, A. C. Dark matter admixed neutron star properties in light of gravitational wave observations: A two fluid approach. **Phys. Rev. D**, American Physical Society, v. 105, p. 123034, Jun 2022. Available at: https://link.aps.org/doi/10-.1103/PhysRevD.105.123034. 48

DEXHEIMER, V.; GOMES, R. O.; KLÄHN, T.; HAN, S.; SALINAS, M. Gw190814 as a massive rapidly rotating neutron star with exotic degrees of freedom. **Phys. Rev. C**, American Physical Society, v. 103, p. 025808, Feb 2021. Available at: https://link.aps-.org/doi/10.1103/PhysRevC.103.025808. 28, 32

DEXHEIMER, V. A.; SCHRAMM, S. Novel approach to modeling hybrid stars. **Phys. Rev. C**, American Physical Society, v. 81, p. 045201, Apr 2010. Available at: https://link.aps.org/doi/10.1103/PhysRevC.81.045201. 28, 32, 33

DOROSHENKO, V.; SULEIMANOV, V.; PÜHLHOFER, G.; ANDRESANTANGELOEA. A strangely light neutron star within a supernova remnant. **Nature Astronomy**, v. 6, p. 1444–1451, 12 2022. Available at: https://ui.adsabs.harvard.edu/abs/2022NatAs...6.1444D. 14, 59, 63

DRAGO, A.; PAGLIARA, G. Why can hadronic stars convert into strange quark stars with larger radii. **Phys. Rev. D**, American Physical Society, v. 102, p. 063003, Sep 2020. Available at: https://link.aps.org/doi/10.1103/PhysRevD.102.063003. 24

DUANE, S.; KENNEDY, A.; PENDLETON, B. J.; ROWETH, D. Hybrid monte carlo. **Physics Letters B**, v. 195, n. 2, p. 216–222, 1987. ISSN 0370-2693. Available at: https://www.sciencedirect.com/science/article/pii/037026938791197X. 13

ELLIS, J.; HÜTSI, G.; KANNIKE, K.; MARZOLA, L.; RAIDAL, M.; VASKONEN, V. Dark matter effects on neutron star properties. **Phys. Rev. D**, American Physical Society, v. 97, p. 123007, Jun 2018. Available at: https://link.aps.org/doi/10.1103/PhysRevD.97.123007. 59

EMERICK, A.; ZHAO, X.; RAPP, R. Bottomonia in the quark-gluon plasma and their production at rhic and lhc. **The European Physical Journal A**, v. 48, n. 5, 2012. Available at: https://doi.org/10.1140/epja/i2012-12072-y. 12

ESA. **Planck**. 2009. Available at: https://www.esa.int/Enabling_Support/Operations/Planck. 47

FENG, J. L. Dark matter candidates from particle physics and methods of detection. **Annual Review of Astronomy and Astrophysics**, Annual Reviews, v. 48, n. Volume 48, 2010, p. 495–545, 2010. ISSN 1545-4282. Available at: https://www.annualreviews.org/content/journals/10.1146/annurev-astro-082708-101659. 49

FERREIRA, M.; PEREIRA, R. C.; PROVIDÊNCIA, C. Quark matter in light neutron stars. **Phys. Rev. D**, American Physical Society, v. 102, p. 083030, Oct 2020. Available at: https://link.aps.org/doi/10.1103/PhysRevD.102.083030. 24

FONSECA, E.; CROMARTIE, H. T.; PENNUCCI, T. T.; RAY, P. S. *et al.* Refined mass and geometric measurements of the high-mass psr j0740+6620. **The Astrophysical Journal Letters**, The American Astronomical Society, v. 915, n. 1, p. L12, jul 2021. Available at: https://dx.doi.org/10.3847/2041-8213/ac03b8. 44, 46, 59, 63

FOWLER, G. N.; RAHA, S.; WEINER. Confinement and phase transitions. **Zeitschrift für Physik C Particles and Fields**, v. 9, p. 271–273, Jun 1981. Available at: https://doi-.org/10.1007/BF01410668. 13, 17

FRITZSCH, H.; GELL-MANN, M.; LEUTWYLER, H. Advantages of the color octet gluon picture. **Physics Letters B**, v. 47, n. 4, p. 365–368, 1973. ISSN 0370-2693. Available at: https://www.sciencedirect.com/science/article/pii/0370269373906254. 10

FUKUSHIMA, K. Chiral effective model with the polyakov loop. **Physics Letters B**, v. 591, n. 3, p. 277–284, 2004. ISSN 0370-2693. Available at: https://www.sciencedirect-.com/science/article/pii/S0370269304006203. 28

FUKUSHIMA, K. Phase diagrams in the three-flavor nambu–jona-lasinio model with the polyakov loop. **Phys. Rev. D**, American Physical Society, v. 77, p. 114028, Jun 2008. Available at: https://link.aps.org/doi/10.1103/PhysRevD.77.114028. 28, 31

GRIFFITHS, D. **Introduction to elementary particles.** [*S.l.*]: John Wiley Sons, 2008. ISBN 9783527406012. 10

GUNION, J.; VOGT, R. Determining the existence and nature of the quark-gluon plasma by upsilon suppression at the lhc. **Nuclear Physics B**, v. 492, n. 1, p. 301–337, 1997. ISSN 0550-3213. Available at: https://www.sciencedirect.com/science/article/pii-/S0550321397800375. 12

HANAUSKE, M.; SATAROV, L. M.; MISHUSTIN, I. N.; STÖCKER, H.; GREINER, W. Strange quark stars within the nambu–jona-lasinio model. **Phys. Rev. D**, American Physical Society, v. 64, p. 043005, Jul 2001. Available at: https://link.aps.org/doi/10-.1103/PhysRevD.64.043005. 24

HARRIS, J. W.; MÜLLER, B. The search for the quark-gluon plasma. **Annual Review of Nuclear and Particle Science**, v. 46, n. 1, p. 71–107, 1996. Available at: https://doi-.org/10.1146/annurev.nucl.46.1.71. 12

HATSUDA, T.; KUNIHIRO, T. Qcd phenomenology based on a chiral effective lagrangian. **Physics Reports**, v. 247, n. 5, p. 221–367, 1994. ISSN 0370-1573. Available at: https://www.sciencedirect.com/science/article/pii/0370157394900221. 28

HIPPERT, M.; DILLINGHAM, E.; TAN, H.; CURTIN, D.; NORONHA-HOSTLER, J.; YUNES, N. Dark matter or regular matter in neutron stars? how to tell the difference from the coalescence of compact objects. **Phys. Rev. D**, American Physical Society, v. 107, p. 115028, Jun 2023. Available at: https://link.aps.org/doi/10.1103/PhysRevD.107.115028. 57, 58

HOLLAND, K.; WIESE, U.-J. The center symmetry and its spontaneous breakdown at high temperatures. p. 1909–1944, 2000. Available at: https://doi.org/10.1142-/9789812810458_0040. 30

HONG, B.; REN, Z. Tracing quark and dark matter signals in neutron stars through inspiral stage gravitational waves. **Phys. Rev. D**, American Physical Society, v. 110, p. 023012, Jul 2024. Available at: https://link.aps.org/doi/10.1103/PhysRevD.110.023012. 58

HU, W.; DODELSON, S. Cosmic microwave background anisotropies. **Annual Review of Astronomy and Astrophysics**, Annual Reviews, v. 40, n. Volume 40, 2002, p. 171–216, 2002. ISSN 1545-4282. Available at: https://www.annualreviews.org/content/journals-/10.1146/annurev.astro.40.060401.093926. 15, 47

HU, W.; SUGIYAMA, N.; SILK, J. The physics of microwave background anisotropies. , v. 386, n. 6620, p. 37–43, mar. 1997. 15, 47

HUANG, K. **Quarks, Leptons and Gauge Fields**. [*S.l.*]: World Scientific, Singapore, 1992. 10

IVANYTSKYI, O.; SAGUN, V.; LOPES, I. Neutron stars: New constraints on asymmetric dark matter. **Phys. Rev. D**, American Physical Society, v. 102, p. 063028, Sep 2020. Available at: https://link.aps.org/doi/10.1103/PhysRevD.102.063028. 50

IVANYTSKYI, O.; SAGUN, V.; LOPES, I. Neutron stars: New constraints on asymmetric dark matter. **Phys. Rev. D**, American Physical Society, v. 102, p. 063028, Sep 2020. Available at: https://link.aps.org/doi/10.1103/PhysRevD.102.063028. 59

JIMÉNEZ, J. C.; FRAGA, E. S. Radial oscillations of quark stars from perturbative qcd. **Phys. Rev. D**, American Physical Society, v. 100, p. 114041, Dec 2019. Available at: https://link.aps.org/doi/10.1103/PhysRevD.100.114041. 45

KAPUSTA, J. I.; GALE, C. **Finite-Temperature Field Theory, Principles and applications**. [*S.l.*]: Cambridge University Press, 2006. 31

KAPUSTA J. I.; GALE, C. **Finite-temperature field theory: Principles and applications.** [*S.l.*]: Cambridge, University Press, 2011. (Cambridge Monographs on Mathematical Physics). ISBN 9780521173223, 9780521820820, 9780511222801. 30

KARKEVANDI, D. R.; SHAHRBAF, M.; SHAKERI, S.; TYPEL, S. Exploring the distribution and impact of bosonic dark matter in neutron stars. **Particles**, v. 7, n. 1, p. 201–213, 2024. ISSN 2571-712X. Available at: https://www.mdpi.com/2571-712X/7/1/11. 52

KARKEVANDI, D. R.; SHAKERI, S.; SAGUN, V.; IVANYTSKYI, O. Bosonic dark matter in neutron stars and its effect on gravitational wave signal. **Phys. Rev. D**, American Physical Society, v. 105, p. 023001, Jan 2022. Available at: https://link.aps.org/doi/10-.1103/PhysRevD.105.023001. 59, 62

KHLOPOV, M. Y.; MALOMED, B. A.; ZELDOVICH, Y. B. Gravitational instability of scalar fields and formation of primordial black holes. **Monthly Notices of the Royal Astronomical Society**, v. 215, n. 4, p. 575–589, 08 1985. ISSN 0035-8711. Available at: https://doi.org/10.1093/mnras/215.4.575. 52

KLEVANSKY, S. P. The nambu—jona-lasinio model of quantum chromodynamics. **Rev. Mod. Phys.**, American Physical Society, v. 64, p. 649–708, Jul 1992. Available at: https:-//link.aps.org/doi/10.1103/RevModPhys.64.649. 28

KOGUT, J. B. An introduction to lattice gauge theory and spin systems. **Rev. Mod. Phys.**, American Physical Society, v. 51, p. 659–713, Oct 1979. Available at: https://link-.aps.org/doi/10.1103/RevModPhys.51.659. 13

KOGUT, J. B. The lattice gauge theory approach to quantum chromodynamics. **Rev. Mod. Phys.**, American Physical Society, v. 55, p. 775–836, Jul 1983. Available at: https:-//link.aps.org/doi/10.1103/RevModPhys.55.775. 13

KOOPMANS, L. V. E.; TREU, T. The structure and dynamics of luminous and dark matter in the early-type lens galaxy of 0047–281 at z = 0.485*. **The Astrophysical Journal**, v. 583, n. 2, p. 606, feb 2003. Available at: https://dx.doi.org/10.1086/345423. 14, 47

KOUVARIS, C.; TINYAKOV, P. Can neutron stars constrain dark matter? **Phys. Rev. D**, American Physical Society, v. 82, p. 063531, Sep 2010. Available at: https://link.aps-.org/doi/10.1103/PhysRevD.82.063531. 15

KUSENKO, A.; ROSENBERG, L. J. **Snowmass-2013 Cosmic Frontier 3 (CF3) Working Group Summary: Non-WIMP dark matter**. 2013. Available at: https://arxiv.org/abs-/1310.8642. 49

LATTIMER, J. M.; PETHICK, C. J.; PRAKASH, M.; HAENSEL, P. Direct urca process in neutron stars. **Phys. Rev. Lett.**, American Physical Society, v. 66, p. 2701–2704, May 1991. Available at: https://link.aps.org/doi/10.1103/PhysRevLett.66.2701. 24

LENZI, C. H.; LUGONES, G.; VASQUEZ, C. Hybrid stars with reactive interfaces: Analysis within the nambu–jona-lasinio model. **Physival Review D**, v. 107, n. 8, p. 083025, 2023. 45

LENZI, C. H.; SCHNEIDER, A. S.; PROVIDÊNCIA, C.; MARINHO, R. M. Compact stars with a quark core within the nambu–jona-lasinio (njl) model. **Phys. Rev. C**, American Physical Society, v. 82, p. 015809, Jul 2010. Available at: https://link.aps.org/doi-/10.1103/PhysRevC.82.015809. 24

LEUNG, K.-L.; CHU, M.-C.; LIN, L.-M. Tidal deformability of dark matter admixed neutron stars. **Phys. Rev. D**, American Physical Society, v. 105, p. 123010, Jun 2022. Available at: https://link.aps.org/doi/10.1103/PhysRevD.105.123010. 58

LEUNG, S.-C.; CHU, M.-C.; LIN, L.-M. Dark-matter admixed neutron stars. **Phys. Rev. D**, American Physical Society, v. 84, p. 107301, Nov 2011. Available at: https://link.aps-.org/doi/10.1103/PhysRevD.84.107301. 59

LEUNG, S.-C.; CHU, M.-C.; LIN, L.-M. Equilibrium structure and radial oscillations of dark matter admixed neutron stars. **Phys. Rev. D**, American Physical Society, v. 85, p. 103528, May 2012. Available at: https://link.aps.org/doi/10.1103/PhysRevD.85.103528. 58

LIU, H.-M.; WEI, J.-B.; LI, Z.-H.; BURGIO, G.; SCHULZE, H.-J. Dark matter effects on the properties of neutron stars: Optical radii. **Physics of the Dark Universe**, v. 42, p. 101338, 2023. ISSN 2212-6864. Available at: https://www.sciencedirect.com/science-/article/pii/S2212686423001723. 58

LIU, H.-M.; WEI, J.-B.; LI, Z.-H.; BURGIO, G. F.; DAS, H. C.; SCHULZE, H.-J. Dark matter effects on the properties of neutron stars: Compactness and tidal deformability. **Phys. Rev. D**, American Physical Society, v. 110, p. 023024, Jul 2024. Available at: https://link.aps.org/doi/10.1103/PhysRevD.110.023024. 58

LOURENÇO, O.; DUTRA, M.; LENZI, C. H.; FLORES, C. V.; MENEZES, D. P. Consistent relativistic mean-field models constrained by gw170817. **Phys. Rev. C**, American Physical Society, v. 99, p. 045202, Apr 2019. Available at: https://link.aps.org/doi/10-.1103/PhysRevC.99.045202. 14

LOURENÇO, O.; DUTRA, M.; LENZI, C. H.; BISWAL, S. K.; BHUYAN, M.; MENEZES, D. P. Consistent Skyrme parametrizations constrained by GW170817. **European Physical Journal A**, v. 56, n. 2, p. 32, fev. 2020. 14

MARIANI, M.; ALBERTUS, C.; ALESSANDRONI, M. D. R.; ORSARIA, M. G.; PÉREZ-GARCÍA, M. Á.; RANEA-SANDOVAL, I. F. Constraining self-interacting fermionic dark matter in admixed neutron stars using multimessenger astronomy. **Monthly Notices of the Royal Astronomical Society**, v. 527, n. 3, p. 6795–6806, 11 2024. ISSN 0035-8711. Available at: https://doi.org/10.1093/mnras/stad3658. 49

MARIANI, M.; ORSARIA, M. G.; RANEA-SANDOVAL, I. F.; LUGONES, G. Magnetized hybrid stars: effects of slow and rapid phase transitions at the quarkâ€“hadron interface. **Monthly Notices of the Royal Astronomical Society**, v. 489, n. 3, p. 4261–4277, 09 2019. ISSN 0035-8711. Available at: https://doi.org/10.1093/mnras/stz2392. 45

MARZOLA, I.; DUARTE, S. B.; LENZI, C. H.; LOURENÇO, O. Quark confinement in an equiparticle quark model: Application to stellar matter. **Phys. Rev. D**, American Physical Society, v. 108, p. 083006, Oct 2023. Available at: https://link.aps.org/doi/10-.1103/PhysRevD.108.083006. 32

MASAYUKI, A.; KOICHI, Y. Chiral restoration at finite density and temperature. **Nuclear Physics A**, v. 504, n. 4, p. 668–684, 1989. ISSN 0375-9474. Available at: https:/-/www.sciencedirect.com/science/article/pii/037594748990002X. 37

MASSEY, R.; KITCHING, T.; RICHARD, J. The dark matter of gravitational lensing. **Reports on Progress in Physics**, v. 73, n. 8, p. 086901, jul 2010. Available at: https:/-/dx.doi.org/10.1088/0034-4885/73/8/086901. 14, 47

MATTOS, O. A.; FREDERICO, T.; LENZI, C. H.; DUTRA, M.; LOURENÇO, O. Pnjl model at zero temperature: The three-flavor case. **Phys. Rev. D**, American Physical Society, v. 104, p. 116001, Dec 2021. Available at: https://link.aps.org/doi/10.1103-/PhysRevD.104.116001. 15, 33, 44

MATTOS, O. A.; LOURENÇO, O.; FREDERICO, T. Confinement effects from a pnjl model at zero temperature regime. **J. Phys. Conf. Ser.**, IOP Publishing, v. 1291, n. 1, p. 012031, jul 2019. Available at: https://dx.doi.org/10.1088/1742-6596/1291/1/012031. 15, 28, 32

MATTOS, O. A.; LOURENÇO, O.; FREDERICO, T. Thermodynamical phases in a pnjl model at zero temperature. **The European Physical Journal C**, v. 81, n. 1, p. 1434–6052, jan 2021. Available at: https://doi.org/10.1140/epjc/s10052-021-08827-0. 15, 28, 32, 33, 43

MCDERMOTT, S. D.; YU, H.-B.; ZUREK, K. M. Constraints on scalar asymmetric dark matter from black hole formation in neutron stars. **Phys. Rev. D**, American Physical Society, v. 85, p. 023519, Jan 2012. Available at: https://link.aps.org/doi/10.1103-/PhysRevD.85.023519. 52

MCLERRAN, L. **Quarkyonic Matter and the Phase Diagram of QCD.** [*S.l.*]: World Scientific, 2009. 125–134 p. (Continous advances in QCD.). ISBN 978-981-283-865-0. 12

MCLERRAN, L. D.; SVETITSKY, B. Quark liberation at high temperature: A monte carlo study of su(2) gauge theory. **Phys. Rev. D**, American Physical Society, v. 24, p. 450–460, Jul 1981. Available at: https://link.aps.org/doi/10.1103/PhysRevD.24.450. 29

MENEZES, D. P. Modelling hadronic matter. **Journal of Physics: Conference Series**, IOP Publishing, v. 706, n. 3, p. 032001, apr 2016. Available at: https://dx.doi.org/10-.1088/1742-6596/706/3/032001. 12

MENEZES, D. P.; PROVIDÊNCIA, C.; MELROSE, D. B. Quark stars within relativistic models. **J. Phys. G: Nucl. Part. Phys.**, v. 32, n. 8, p. 1081, jun 2006. Available at: https://dx.doi.org/10.1088/0954-3899/32/8/001. 24

MILLER, M. C.; LAMB, F. K.; DITTMANN, A. J.; BOGDANOV, S. *et al.* Psr j0030+0451 mass and radius from nicer data and implications for the properties of neutron star matter. **The Astrophysical Journal Letters**, The American Astronomical Society, v. 887, n. 1, p. L24, dec 2019. Available at: https://dx.doi.org/10.3847/2041-8213/ab50c5. 14, 44, 45, 59, 63

MILLER, M. C.; LAMB, F. K.; DITTMANN, A. J.; BOGDANOV, S. *et al.* The radius of psr j0740+6620 from nicer and xmm-newton data. **The Astrophysical Journal Letters**, The American Astronomical Society, v. 918, n. 2, p. L28, sep 2021. Available at: https:/-/dx.doi.org/10.3847/2041-8213/ac089b. 14, 44, 45, 59, 63

MUKHOPADHYAY, P.; SCHAFFNER-BIELICH, J. Quark stars admixed with dark matter. **Phys. Rev. D**, American Physical Society, v. 93, p. 083009, Apr 2016. Available at: https://link.aps.org/doi/10.1103/PhysRevD.93.083009. 60

MUROYA, S.; NAKAMURA, A.; NONAKA, C.; TAKAISHI, T. Lattice QCD at Finite Density*): An Introductory Review. **Progress of Theoretical Physics**, v. 110, n. 4, p. 615–668, 10 2003. ISSN 0033-068X. Available at: https://doi.org/10.1143/PTP.110.615. 13

NAMBU, Y.; JONA-LASINIO, G. Dynamical model of elementary particles based on an analogy with superconductivity. i. **Phys. Rev.**, American Physical Society, v. 122, p. 345–358, Apr 1961. Available at: https://link.aps.org/doi/10.1103/PhysRev.122.345. 13, 28

NAMBU, Y.; JONA-LASINIO, G. Dynamical model of elementary particles based on an analogy with superconductivity. ii. **Phys. Rev.**, American Physical Society, v. 124, p. 246–254, Oct 1961. Available at: https://link.aps.org/doi/10.1103/PhysRev.124.246. 13, 28

NASA. **WMAP PRODUCES NEW RESULTS**. 2001. Available at: https://map.gsfc-.nasa.gov/news/. 47

NELSON, A. E.; REDDY, S.; ZHOU, D. Dark halos around neutron stars and gravitational waves. **Journal of Cosmology and Astroparticle Physics**, v. 2019, n. 07, p. 012, jul 2019. Available at: https://dx.doi.org/10.1088/1475-7516/2019/07/012. 49, 50, 59

OPPENHEIMER, J. R.; VOLKOFF, G. M. On massive neutron cores. **Phys. Rev.**, American Physical Society, v. 55, p. 374–381, Feb 1939. Available at: https://link.aps.org/doi-/10.1103/PhysRev.55.374. 43

PADMANABHAN, N.; FINKBEINER, D. P. Detecting dark matter annihilation with cmb polarization: Signatures and experimental prospects. **Phys. Rev. D**, American Physical Society, v. 72, p. 023508, Jul 2005. Available at: https://link.aps.org/doi/10.1103-/PhysRevD.72.023508. 15, 47

PARISI, A.; FLORES, C. V.; LENZI, C. H.; CHEN, C.-S.; LUGONES, G. Hybrid stars in the light of the merging event gw170817. **Journal of Cosmology and Astroparticle Physics**, IOP Publishing, v. 2021, n. 06, p. 042, jun 2021. Available at: https://dx.doi-.org/10.1088/1475-7516/2021/06/042. 45

PENG, G. Chiral condensates and size of the sigma term. **Nuclear Physics A**, v. 747, n. 1, p. 75–83, 2005. ISSN 0375-9474. Available at: https://www.sciencedirect.com/science-/article/pii/S0375947404010243. 23

PENG, G. X.; CHIANG, H. C.; ZOU, B. S.; NING, P. Z.; LUO, S. J. Thermodynamics, strange quark matter, and strange stars. **Phys. Rev. C**, American Physical Society, v. 62, p. 025801, Jun 2000. Available at: https://link.aps.org/doi/10.1103/PhysRevC.62-.025801. 22

PEREIRA, J. P.; FLORES, C. V.; LUGONES, G. Phase transition effects on the dynamical stability of hybrid neutron stars. **The Astrophysical Journal**, The American Astronomical Society, v. 860, n. 1, p. 12, jun 2018. Available at: https://dx.doi.org/10-.3847/1538-4357/aabfbf. 45

PEREIRA, R. C.; COSTA, P.; PROVIDÊNCIA, C. Two-solar-mass hybrid stars: A two model description using the nambu–jona-lasinio quark model. **Phys. Rev. D**, American Physical Society, v. 94, p. 094001, Nov 2016. Available at: https://link.aps.org/doi/10-.1103/PhysRevD.94.094001. 24

PETRAKI, K.; VOLKAS, R. R. Review of asymmetric dark matter. **International Journal of Modern Physics A**, v. 28, n. 19, p. 1330028, 2013. Available at: https://doi.org/10-.1142/S0217751X13300287. 48

PIERPAOLI, E. Decaying particles and the reionization history of the universe. **Phys. Rev. Lett.**, American Physical Society, v. 92, p. 031301, Jan 2004. Available at: https:/-/link.aps.org/doi/10.1103/PhysRevLett.92.031301. 15, 47

PLÜMER, M.; RAHA, S.; WEINER, R. Effect of confinement on the sound velocity in a quark-gluon plasma. **Physics Letters B**, v. 139, n. 3, p. 198–202, 1984. ISSN 0370-2693. Available at: https://www.sciencedirect.com/science/article/pii/0370269384912449. 13

POLYAKOV, A. Quark confinement and topology of gauge theories. **Nuclear Physics B**, v. 120, n. 3, p. 429–458, 1977. ISSN 0550-3213. Available at: https://www.sciencedirect-.com/science/article/pii/0550321377900864. 30

POLYAKOV, A. Thermal properties of gauge fields and quark liberation. **Physics Letters B**, v. 72, n. 4, p. 477–480, 1978. ISSN 0370-2693. Available at: https://www.sciencedirect-.com/science/article/pii/0370269378907372. 28

RANEA-SANDOVAL, I. F.; ORSARIA, M. G.; MALFATTI, G.; CURIN, D.; MARIANI, M.; CONTRERA, G. A.; GUILERA, O. M. Effects of hadron-quark phase transitions in hybrid stars within the njl model. **Symmetry**, v. 11, n. 3, 2019. ISSN 2073-8994. Available at: https://www.mdpi.com/2073-8994/11/3/425. 24

RATTI, C.; RÖßNER, S.; THALER, M.; WEISE, W. Thermodynamics of the pnjl model. **The European Physical Journal C**, v. 49, p. 1434–6052, Jan 2007. Available at: https:/-/doi.org/10.1140/epjc/s10052-006-0065-x. 28, 31

RATTI, C.; THALER, M. A.; WEISE, W. Phases of qcd: Lattice thermodynamics and a field theoretical model. **Phys. Rev. D**, American Physical Society, v. 73, p. 014019, Jan 2006. Available at: https://link.aps.org/doi/10.1103/PhysRevD.73.014019. 28, 31, 34

REINHARDT, G. **Field Quantization**. [*S.l.*]: Springer, 1996. 29

RILEY, T. E.; WATTS, A. L.; BOGDANOV, S.; RAY, P. S. *et al.* A nicer view of psr j0030+0451: Millisecond pulsar parameter estimation. **The Astrophysical Journal Letters**, The American Astronomical Society, v. 887, n. 1, p. L21, dec 2019. Available at: https://dx.doi.org/10.3847/2041-8213/ab481c. 14, 44, 45, 59, 63

RILEY, T. E.; WATTS, A. L.; RAY, P. S.; BOGDANOV, S. *et al.* A nicer view of the massive pulsar psr j0740+6620 informed by radio timing and xmm-newton spectroscopy. **The Astrophysical Journal Letters**, The American Astronomical Society, v. 918, n. 2, p. L27, sep 2021. Available at: https://dx.doi.org/10.3847/2041-8213/ac0a81. 14, 44, 45, 59, 63

ROBERTS, C. D.; WILLIAMS, A. G. Dyson-schwinger equations and their application to hadronic physics. **Progress in Particle and Nuclear Physics**, v. 33, p. 477–575, 1994. ISSN 0146-6410. Available at: https://www.sciencedirect.com/science/article/pii-/0146641094900493. 13

RÖSSNER, S.; RATTI, C.; WEISE, W. Polyakov loop, diquarks, and the two-flavor phase diagram. **Phys. Rev. D**, American Physical Society, v. 75, p. 034007, Feb 2007. Available at: https://link.aps.org/doi/10.1103/PhysRevD.75.034007. 28, 31

ROUTARAY, P.; MOHANTY, S. R.; DAS, H.; GHOSH, S.; KALITA, P.; PARMAR, V.; KUMAR, B. Investigating dark matter-admixed neutron stars with nitr equation of state in light of psr j0952-0607. **Journal of Cosmology and Astroparticle Physics**, IOP Publishing, v. 2023, n. 10, p. 073, oct 2023. Available at: https://dx.doi.org/10.1088-/1475-7516/2023/10/073. 62

RRAPAJ, E.; REDDY, S. Nucleon-nucleon bremsstrahlung of dark gauge bosons and revised supernova constraints. **Phys. Rev. C**, American Physical Society, v. 94, p. 045805, Oct 2016. Available at: https://link.aps.org/doi/10.1103/PhysRevC.94.045805. 50

RUBIN VERA C., F. W. K. J. Rotation of the andromeda nebula from a spectroscopic survey of emission regions. **Astrophysical Journal**, IOP Science, v. 159, p. 379, Feb 1970. Available at: https://articles.adsabs.harvard.edu//full/1970ApJ...159..379R-/0000403.000.html. 14, 47

RUTHERFORD, N.; RAAIJMAKERS, G.; PRESCOD-WEINSTEIN, C.; WATTS, A. Constraining bosonic asymmetric dark matter with neutron star mass-radius measurements. **Phys. Rev. D**, American Physical Society, v. 107, p. 103051, May 2023. Available at: https://link.aps.org/doi/10.1103/PhysRevD.107.103051. 49, 52, 56

RÖßNER, S. **Phases of QCD**. Thesis (Doutorado) — Technische Universität München, 2009. 28

SAKHAROV, A. D. Violation of cp invariance, c asymmetry, and baryon asymmetry of the universe. **Soviet Physics Uspekhi**, v. 34, n. 5, p. 392, may 1991. Available at: https://dx.doi.org/10.1070/PU1991v034n05ABEH002497. 48

SALUCCI, P. The distribution of dark matter in galaxies. **The Astronomy and Astrophysics Review**, v. 27, n. 1, p. 2, fev. 2019. 14, 47

SCHERTLER, K.; LEUPOLD, S.; SCHAFFNER-BIELICH, J. Neutron stars and quark phases in the nambu–jona-lasinio model. **Phys. Rev. C**, American Physical Society, v. 60, p. 025801, Jun 1999. Available at: https://link.aps.org/doi/10.1103/PhysRevC-.60.025801. 24

SHAKERI, S.; KARKEVANDI, D. R. Bosonic dark matter in light of the nicer precise mass-radius measurements. **Phys. Rev. D**, American Physical Society, v. 109, p. 043029, Feb 2024. Available at: https://link.aps.org/doi/10.1103/PhysRevD.109.043029. 52

SINGH, C. Signals of quark-gluon plasma. **Physics Reports**, v. 236, n. 3, p. 147–224, 1993. ISSN 0370-1573. Available at: https://www.sciencedirect.com/science/article/pii-/037015739390172A. 12

SOUZA, L. A.; DUTRA, M.; LENZI, C. H.; LOURENÇO, O. Effects of short-range nuclear correlations on the deformability of neutron stars. **Phys. Rev. C**, American Physical Society, v. 101, p. 065202, Jun 2020. Available at: https://link.aps.org/doi/10.1103/PhysRevC.101.065202. 14

SPRINGEL, V.; WHITE, S.; JENKINS, A. e. a. Simulations of the formation, evolution and clustering of galaxies and quasars. **Nature**, v. 435, p. 629–639, 2005. Available at: https://www.nature.com/articles/nature03597citeas. 47

SUN, T.-T.; ZHENG, Z.-Y.; CHEN, H.; BURGIO, G. F.; SCHULZE, H.-J. Equation of state and radial oscillations of neutron stars. **Phys. Rev. D**, American Physical Society, v. 103, p. 103003, May 2021. Available at: https://link.aps.org/doi/10.1103/PhysRevD.103.103003. 45

SUSSKIND, L. Lattice models of quark confinement at high temperature. **Phys. Rev. D**, American Physical Society, v. 20, p. 2610–2618, Nov 1979. Available at: https://link.aps.org/doi/10.1103/PhysRevD.20.2610. 28

SVETITSKY, B. Symmetry aspects of finite-temperature confinement transitions. **Physics Reports**, v. 132, n. 1, p. 1–53, 1986. ISSN 0370-1573. Available at: https://www.sciencedirect.com/science/article/pii/0370157386900141. 28

SVETITSKY, B.; YAFFE, L. G. Critical behavior at finite-temperature confinement transitions. **Nuclear Physics B**, v. 210, n. 4, p. 423–447, 1982. ISSN 0550-3213. Available at: https://www.sciencedirect.com/science/article/pii/0550321382901729. 28

TANABASHI, M.; HAGIWARA, K.; HIKASA, K.; NAKAMURA, K.; SUMINO, Y.; TAKAHASHI, F. e. a. Review of particle physics. **Phys. Rev. D**, American Physical Society, v. 98, p. 030001, Aug 2018. Available at: https://link.aps.org/doi/10.1103/PhysRevD.98.030001. 10

THAKUR, P.; MALIK, T.; DAS, A.; JHA, T. K.; PROVIDÊNCIA, C. Exploring robust correlations between fermionic dark matter model parameters and neutron star properties: A two-fluid perspective. **Phys. Rev. D**, American Physical Society, v. 109, p. 043030, Feb 2024. Available at: https://link.aps.org/doi/10.1103/PhysRevD.109.043030. 48, 57

TOLMAN, R. C. Static solutions of einstein's field equations for spheres of fluid. **Phys. Rev.**, American Physical Society, v. 55, p. 364–373, Feb 1939. Available at: https://link.aps.org/doi/10.1103/PhysRev.55.364. 43

VOGL, U.; WEISE, W. The nambu and jona-lasinio model: Its implications for hadrons and nuclei. **Progress in Particle and Nuclear Physics**, v. 27, p. 195–272, 1991. ISSN 0146-6410. Available at: https://www.sciencedirect.com/science/article/pii/0146641091900059. 28

WEINBERG, S. Non-abelian gauge theories of the strong interactions. **Phys. Rev. Lett.**, American Physical Society, v. 31, p. 494–497, Aug 1973. Available at: https://link.aps-.org/doi/10.1103/PhysRevLett.31.494. 10

WEISS, N. Wilson line in finite-temperature gauge theories. **Phys. Rev. D**, American Physical Society, v. 25, p. 2667–2672, May 1982. Available at: https://link.aps.org/doi-/10.1103/PhysRevD.25.2667. 30

WEN, X. J.; ZHONG, X. H.; PENG, G. X.; SHEN, P. N.; NING, P. Z. Thermodynamics with density and temperature dependent particle masses and properties of bulk strange quark matter and strangelets. **Phys. Rev. C**, American Physical Society, v. 72, p. 015204, Jul 2005. Available at: https://link.aps.org/doi/10.1103/PhysRevC.72.015204. 23, 24

WILSON, K. G. Confinement of quarks. **Phys. Rev. D**, American Physical Society, v. 10, p. 2445–2459, Oct 1974. Available at: https://link.aps.org/doi/10.1103/PhysRevD.10-.2445. 29

WITTEN, E. Cosmic separation of phases. **Phys. Rev. D**, v. 30, p. 272 – 285, 1984. 14, 17

WORKMAN, R. L.; OTHERS. Review of Particle Physics. **PTEP**, v. 2022, p. 083C01, 2022. 15, 25, 33

XIA, C. J.; PENG, G. X.; CHEN, S. W.; LU, Z. Y.; XU, J. F. Thermodynamic consistency, quark mass scaling, and properties of strange matter. **Phys. Rev. D**, American Physical Society, v. 89, p. 105027, May 2014. Available at: https://link.aps.org/doi/10-.1103/PhysRevD.89.105027. 13, 17

XIANG, Q.-F.; JIANG, W.-Z.; ZHANG, D.-R.; YANG, R.-Y. Effects of fermionic dark matter on properties of neutron stars. **Phys. Rev. C**, American Physical Society, v. 89, p. 025803, Feb 2014. Available at: https://link.aps.org/doi/10.1103/PhysRevC.89.025803. 48, 49, 52, 56, 57

YAKOVLEV, D.; KAMINKER, A.; GNEDIN, O.; HAENSEL, P. Neutrino emission from neutron stars. **Physics Reports**, v. 354, n. 1, p. 1–155, 2001. ISSN 0370-1573. Available at: https://www.sciencedirect.com/science/article/pii/S0370157300001319. 24

ZHANG, Y.; SU, R.-K. Quark mass density- and temperature-dependent model for bulk strange quark matter. **Phys. Rev. C**, v. 65, 2002. 17

FOLHA DE REGISTRO DO DOCUMENTO

1. CLASSIFICAÇÃO/TIPO	2. DATA	3. REGISTRO N°	4. N° DE PÁGINAS
TD	10 de dezembro de 2024	DCTA/ITA/TD-060/2024	80

5. TÍTULO E SUBTÍTULO:

Confinement and dark matter effects in an equiparticle quark model.

6. AUTOR(ES):

Isabella Aparecida Marzola

7. INSTITUIÇÃO(ÕES)/ÓRGÃO(S) INTERNO(S)/DIVISÃO(ÕES):

Instituto Tecnológico de Aeronáutica - ITA

8. PALAVRAS-CHAVE SUGERIDAS PELO AUTOR:

Strange quark matter, Phase transition, Dark matter, Nuclear physics

9.PALAVRAS-CHAVE RESULTANTES DE INDEXAÇÃO:

Matéria obscura; Transição de fase; Matéria de quark; Confinamento (Física de partículas); Física nuclear; Física.

10. APRESENTAÇÃO: **(X) Nacional ( ) Internacional**

ITA, São José dos Campos. Curso de Doutorado. Programa de Pós-Graduação em Física. Área de Física Nuclear. Orientador: Prof Dr. Odilon Lourenço da Silva Filho; coorientador: Prof. Sérgio José Barbosa Duarte (CPBF). Defesa em 28/11/2024. Publicada em 2024.

11. RESUMO:

In order to study quark matter under extreme conditions, such as high density and zero temperature, that are usually associated with compact objects (e.g strange stars), we explore two different scenarios throughout this work. In the first scenario we introduce the traced Polyakov loop into a thermodynamic consistent model with density dependent quark masses ($m'_{u,\,d,\,s}$). This implementation is responsible for quark confinement/deconfinement phase transition effects. By applying realistic values for the current quark masses, provided by the Particle Data Group, and by replacing the constants of the interacting part of $m'_{u,d,s}$ by functions of Φ, the symmetric and stellar quark matter systems become capable of achieving a first order phase transition structure, with Φ being the order parameter. From this improved model, we show that the system goes towards a similar chiral symmetry restoration behavior due to the emergence of a deconfined phase. Following, we perform an analysis concerning the mass-radius profiles of quark stars, where we are able to verify that the results found for the new model satisfy recent astrophysical observational data coming from the LIGO and Virgo Collaboration, and the NICER mission concerning the millisecond pulsars PSR J0030+0451, and PSR J0740+6620. The second scenario concerns the study of strange stars admixed with dark matter. Here we restrict ourselves into describing the "visible" matter through the previously mentioned quark model, but without the Polyakov loop. The dark sector itself is introduced into the system by two different approaches: the fermionic and the bosonic one, where we investigate the predictions of both models. For the fermionic model a spin 1/2 dark particle is considered, and for the bosonic model the particle is a dark scalar meson. In both models, there is the presence of a repulsive vector interaction, which is responsible for avoiding the collapse of the star due to the lack of the degeneracy pressure in the bosonic model. Our findings for the two new systems suggest that stable strange star configurations are consistent with data from PSR J0030+0451, PSR J0740+6620, NICER, and HESS J1731-347. Additionally, we identify stars with dark matter halo configurations for lower dark particle masses.

12. GRAU DE SIGILO:

(X) OSTENSIVO ( ) RESERVADO ( ) SECRETO